Tampere University

Mathieu Poppe

Modeling the battery parameters that affect the fault current of a feeding BESS in LV grids

Master of Science Thesis
Electrical Engineering
Faculty of Information Technology and Communication Sciences (ITC)
Examiner 1: Prof. Sami Repo
Examiner 2: MSc. Lasse Peltonen
December 2022

Abstract

Mathieu Poppe: Modeling the battery parameters that affect the fault current of a feeding BESS in LV grids
Master of Science Thesis
Tampere University
Master's Degree Programme in Electrical Engineering
December 2022

The popularity of renewable energy makes the use of battery energy storage systems (BESS) in the grid very attractive. BESS can support the intermittent power output of renewable energy sources. BESS can also provide a support during and after grid failure and even provide black-start capability in case of a blackout. Li-ion batteries are mainly used for these BESS because of their high energy density.

In this thesis, the parameters affecting on the fault current of the battery in a BESS are modeled. In most studies around BESS, the inverter has gotten more attention than the battery part. However, the battery part behaves different than a simple DC voltage source. It is evaluated to what extent the behaviour of the battery affects the fault current fed by a BESS. The focus is on the open-circuit voltage (OCV) and internal resistance (R_{int}) of the battery. The state of charge (SoC), operating temperature, C-rate and state of health (SoH) of the battery affect this voltage and resistance. The behavior of the inverter is also taken into account to get a realistic BESS model. The developed model uses only data available in the manufacturer's datasheets and information from existing studies.

Today, a general fault model already exists for conventional generators, e.g., synchronous generators, but for inverter-based distributed energy resources (IBDER), e.g. BESS, there is not yet a generally accepted model for fault current calculations. There is a great need for simplified fault current models in the industry. These fault models are needed to get the overall dynamic fault response. One possible application is the sizing of overcurrent protection devices. If a BESS feeds in island mode, the available fault current will often be smaller due to the sensitive components that can handle less fault current than robust synchronous or asynchronous machines. These robust generators can provide high short-circuit currents for a short amount of time.

The BESS model is incorporated into a simulation software program, here Matlab Simulink, to perform simulations.

Keywords: BESS, fault current, modeling, overcurrent protection, OCV, R_{int}, SoC, SoH, operating temperature, C-rate

Preface

This thesis is the final work of the Master's degree in Electrical Engineering and was carried out in Tampere, Finland, at Hervanta campus of Tampere University. I would like to express my sincere thanks to Tampere University.

A special thanks goes to professor Sami Repo who gave me the opportunity to deepen my knowledge of battery energy storage systems. In addition, I would like to thank Lasse Peltonen for the guidance throughout this thesis, sharing his knowledge in inverter-based energy sources with me and for his helpful comments during the writing process.

Finally, I would like to thank my girlfriend and family, who have supported me throughout my studies and during this international exchange.

Tampere, 19 December 2022

Mathieu Poppe

Contents

List of Figures

List of Tables

List of Symbols And Abbreviations

AC	Alternating current
BESS	Battery energy storage system
BMS	Battery management system
C	Capacitance [F]
CES	Community energy storage
CO_2	Carbon dioxide
C-rate	Charge and discharge rate
DC	Direct current
DoD	Depth of discharge
EIS	Electrochemical Impedance Spectroscopy
EMF	Electromotive force [V]
ESS	Energy storage system
EV	Electric vehicle
f	Frequency
FRT	Fault-ride-through
HV	High voltage
I	Current [A]
I_{DC}	Current at the DC side [A]
I_k	RMS uninterrupted short-circuit current [A]
$I_{k"}$	RMS initial symmetrical short-circuit current [A]
I_p	Peak short-circuit surge current [A]
I_f	Fault current [A]
IBDER	Inverter-based distributed energy resource
KPI	Key performance indicator
L	Inductance [H]
Li-ion	Lithium-ion
LCO	Lithium Cobalt Oxide
LFP	Lithium iron phosphate
LMO	Lithium manganese oxide
LTO	Lithium titanium oxide
LV	Low voltage
LVRT	Low voltage ride-through
MV	Medium voltage
NCA	Nickel cobalt aluminium
NMC	Nickel manganese cobalt
NiMH	Nickel metal hydride
OCV	Open-circuit voltage [V]
p.u.	Per unit (times the nominal value)
P	Active power [W]
PC	Peukert coefficient
PCS	Power conversion system
PRBS	Pseudo random binary sequence
PV	Photovoltaic
PWM	Pulse width modulation
Q_b	Battery capacity [Ah]

R	Resistance [Ω]
R_{int}	Internal resistance [Ω]
R^2	R-squared
RMSE	Root-mean-square error
t	Time [s]
TCV	Temperature coefficient of voltage
SoC	State of charge
SoH	State of health
SSR	Sum of Squares Residual
SST	Sum of Squares Total
V	Voltage [V]
ΔV	Voltage difference [V]
V_{DC}	DC terminal voltage battery [V]
UPS	Uninterruptible power supply
X	Reactance [Ω]
Z	Impedance [Ω]
τ	Time constant [s]
ω	Frequency [Hz]

1 Introduction

1.1 Introduction to energy storage and motivation

Energy storage has become indispensable over the years, just think of smartphones, laptops, electric vehicles (EV), etc., and nowadays also as grid storage due to the increase of renewable energy sources and rising energy prices. In *figure 1.1*, the schematic representation of an energy storage system in an electricity supply system is given.

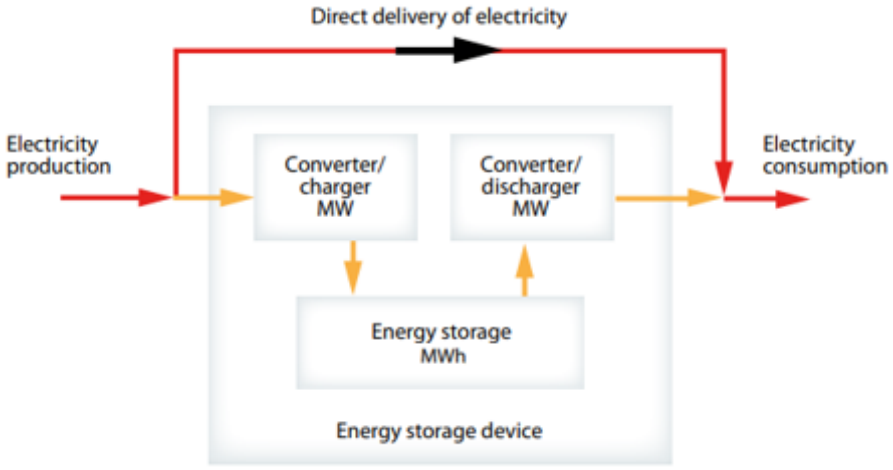

Figure 1.1 *Schematic representation of an energy storage system [8]*

Electricity is produced by power plants and consumed by consumers, but some of the produced energy also goes to an energy storage system where it is stored. With energy storage, excessive energy can be used at another time and it can increase reliability.

The most used type of battery is the Li-ion battery. These are rechargeable batteries, also called secondary batteries.

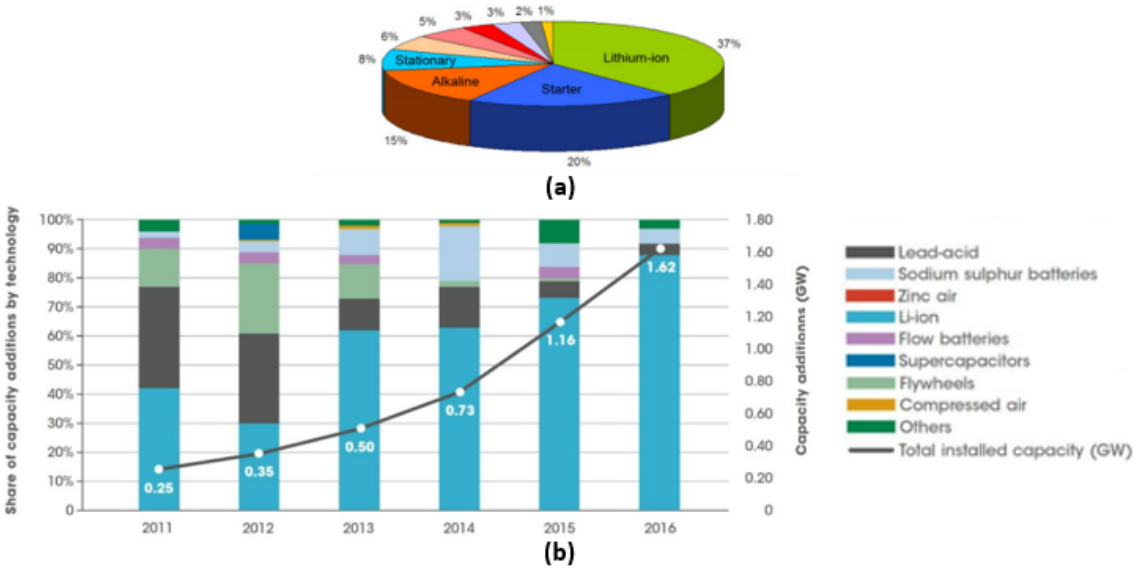

Figure 1.2 *Proportions of used batteries (a) In general [22] (b) For grid storage [27]*

In *figure 1.2a*, it can be seen that Li-ion batteries are the most used in general, but for grid storage, Li-ion batteries are even more dominant. In *figure 1.2b*, the increase in installed battery power is represented and the vast majority of the newly installed BESS consist of Li-ion batteries. This curve shows the progression until 2016, but today the dominance of Li-ion has become even stronger [41].

The main reasons for the dominance are its high energy density and low self-discharge. This type of battery is being used in UPS-systems, EV, BESS, etc. However, different types of Li-ion batteries are used for these different applications, as they differ in their key performance indicators (KPI) *(figure 1.3)*.

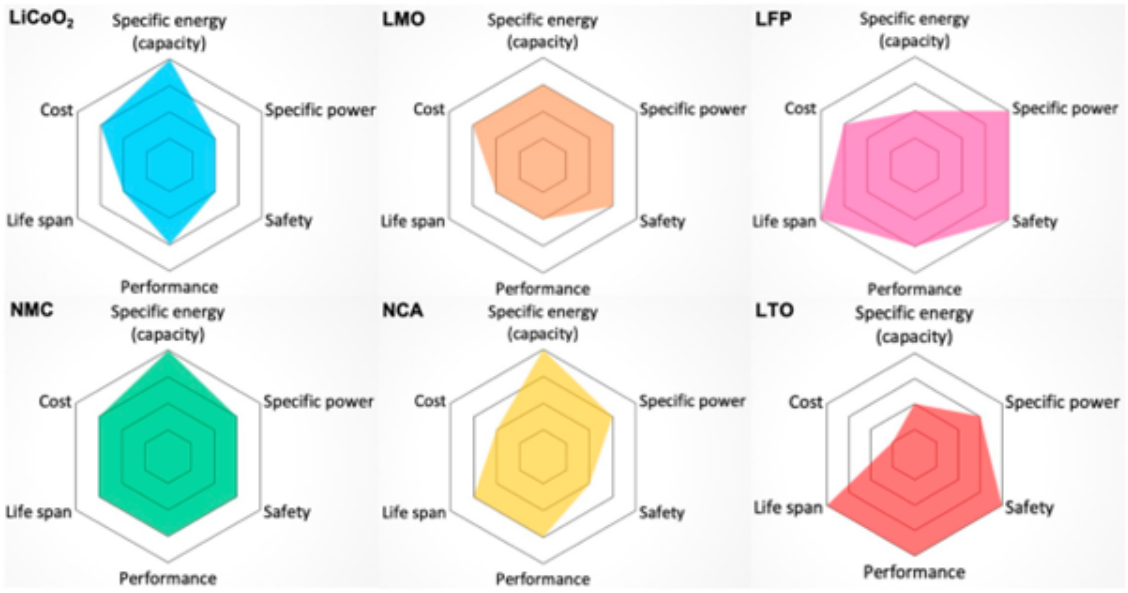

Figure 1.3 *Different types of Li-ion batteries and the KPI [50]*

This figure shows how Li-ion batteries differ in performance. Based on this, one can choose which type of Li-ion battery is best for a particular purpose. For customer devices, i.e. home batteries, safety and affordability are top priorities. Home batteries should also have a long life span. For that reason, LFP batteries are typically used as home batteries. In contrast, BESS for grid applications are more likely to use NMC batteries because they have high specific energy (capacity) and they are safe, compared to other high-energy batteries like NCA cells. Cost is less important here. [26] is a good resource to find out what type of Li-ion battery is used for which application.

BESS can be used for individual customers e.g. to interface with their photovoltaic (PV) panels, but current developments in smart grids are also beginning to look at community energy storage (CES). These are BESS implemented in LV distribution grids to power a number of homes in a neighbourhood. This type of energy storage provides more control, quality, stability and reliability and is therefore beneficial to both customers and utilities.

In *figure 1.4*, the working principle of a BESS supporting an LV grid is given. There are two different operating modes: on-grid and off-grid. On-grid is the 'normal' operating mode. If the main grid fails, the battery can take over and supply the loads off-grid. This off-grid mode is also called the island mode because the battery is making an island on itself without the presence of the external utility power grid. The transition to active low voltage distribution networks made the (intentional) islanding scenario, in case of disturbance in the main grid, more common throughout the years [13].

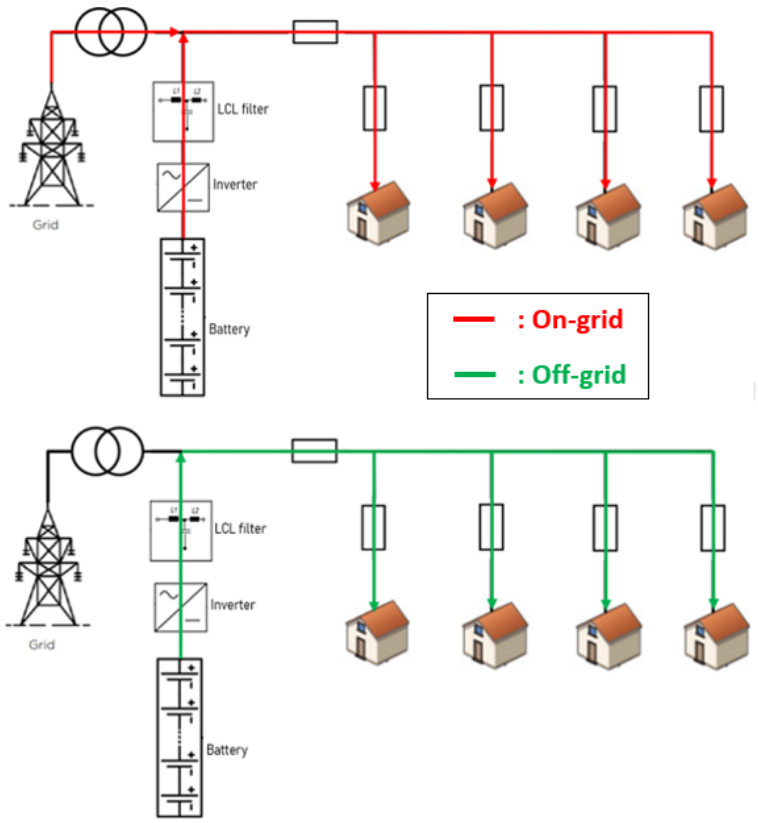

Figure 1.4 *Operating modes LV grid with BESS*

The BESS its performance and behaviour get affected by many different parameters. The parameters of battery models vary in function of the operation condition of the battery. BESS modeling helps us to understand the behaviour and improve its performance and efficiency. None of these BESS models represents the exact behaviour, but approximations can be made with equivalent models. Fault current models can be made to predict the fault current behaviour in order to improve fault detection systems of BESS.

The use of BESS is constantly increasing. Different from synchronous generators, there are no generally accepted short-circuit models for BESS yet. There is a strong need in the industry for these types of models, which makes it interesting as a master's thesis topic.

1.2 Research objective and question

The objective of this thesis is to develop a BESS model and with that comes some research questions. The main research question is:

What are the parameters that effect the fault current of the BESS?

In other words, a BESS model is made to determine the RMS fault current behaviour with the battery as fault current source. This model contains the battery and the inverter. The main focus is on the battery, specifically on its electromotive force (EMF)/open-circuit voltage (OCV) and internal resistance, because there parameters mainly define the fault current response. The purpose is to study the dynamic fault response and which one of the components is limiting the fault current under different operating conditions. The restricting component determines the maximum overcurrent capability of the BESS. This is a simplified model to give the user an idea of what the fault current will be in particular situations.

Different types of batteries can be used for grid storage, so next question should be raised:

- Can a general fault current model be developed for all Li-ion BESS?

All factors used in the model should be derivable from information provided by the manufacturer, e.g. technical datasheets. Next question follows:

- Can the fault current fed by a BESS be modeled only using information from the manufacturer's datasheet?

This thesis should provide an answer to the above-mentioned research questions.

1.3 Methodology and scope of the thesis

The first part of the thesis is the literature survey. The creation of the model is based on information from theory or experimental measurements from previous studies. A BESS is an inverter-based distributed energy resource (IBDER). However, they can be used in DC grids as well, so without inverters, but that is out of scope here. To determine a BESS model, technical specifications on the characteristics of batteries and inverters are needed. Because Li-ion batteries are the most used *(figure 1.2)*, its characteristics were the reference for creating the battery model. Furthermore, the model is based on already existing battery and inverter models.

As shown in *figure 1.4*, the BESS can operate grid-connected and in island mode. The voltage at the point of common coupling (PCC) and fault impedance dictate the magnitude of the fault current if the PCC is the fault location. The voltage at the PCC depends on the operating mode. These modes can be divided into four categories:

1. **Main grid is feeding:** The voltage difference between the main grid and PCC depends on the impedance of the feeder
2. **Main grid + grid-feeding BESS:**
   (a) BESS in grid-feeding mode is feeding active power. The amount of power increases the voltage at the PCC compared to scenario 1, resulting in a higher voltage at PCC and therefore a higher fault current
   (b) BESS in grid-feeding mode is feeding active power. This active power has no significant impact on the PCC voltage. The fault current is the same as in scenario 1
3. **Main grid + grid-supporting BESS:** BESS in grid-supporting mode, feeding parallel with the main grid, supports voltage as much as possible at PCC. Fault current is often the highest in this mode
4. **Islanded BESS:**
   (a) Grid-forming inverter of BESS regulates the voltage at PCC and can keep the voltage at the desired level during the fault, e.g. 1.00 p.u., so full fault current can be fed. The inverter can have a higher reference value for the voltage when operating in island mode (e.g. 1.02 p.u.), so the fault current can be the highest in this mode as well, assuming that the BESS's reference voltage is 1.00 p.u. when operating parallel with the main grid
   (b) Grid-forming inverter of BESS regulates the voltage at PCC, but fault current is restricted because the inverter cannot provide enough current

The main question is *'What will be the voltage reference value that has a direct influence on the fault current level?'*. It is stated that the fault current can be the highest when the BESS is supporting the voltage at the PCC when feeding parallel with the grid, but the fault current can also

be the highest when operating in island mode. Although the fault current may be highest in island mode, the fault current is most likely the lowest in island mode because of the limited capability of the BESS due to battery and inverter limitations.

With all previous information, a BESS model is created for fault calculations in LV grids. Some assumptions are made for this purpose:

- The fault is an **external fault**, on AC level.
- The studied time frame is **0-5 s**, since the fault should be eliminated after this period.
- The battery is operating in **discharge mode** at the time of the fault.
- In most datasheets of standalone BESS, the DC/DC converter is not included. Since the BESS will not be coupled to e.g. PV panels or an LVDC grid is not under investigation here, the DC/DC converter is excluded in the BESS model.
- Both the battery and the inverter can be the restrictive element for the available fault current, but the main focus is on the **battery**. The limitations, imposed by the manufacturer, determine whether or not the inverter can supply current to the fault. In this thesis, the emphasis is not on inverter control, hence inverter control is considered to a limited extent.

The next step is to analyze this model in Matlab Simulink. Simulations are done in order to approximate the RMS fault current fed by the BESS. A single-phase fault is modeled, but the principle is the same for a two-phase or three-phase fault looked from the DC-side. The fault current is generally the smallest for single-phase faults. Here factors affecting the fault current capability of the BESS is considered, so the type of fault is less relevant. These faults can occur in different modes of operating *(figure 1.4)*. As already mentioned, the focus is on the BESS operating in island mode (off-grid), so this operating mode is simulated. It can be evaluated later if the BESS model can also serve for grid-connected applications. The fault current affecting parameters of the BESS are varied.

2 Literature survey

Creating a BESS model requires background information on BESS. This chapter discusses the components of a BESS and its fault current characteristics.

2.1 Introducing principles

2.1.1 Working principle of a Li-ion cell

A Li-ion battery cell is an electrochemical energy storage device. A battery stores chemical energy and converts it to electrical energy.

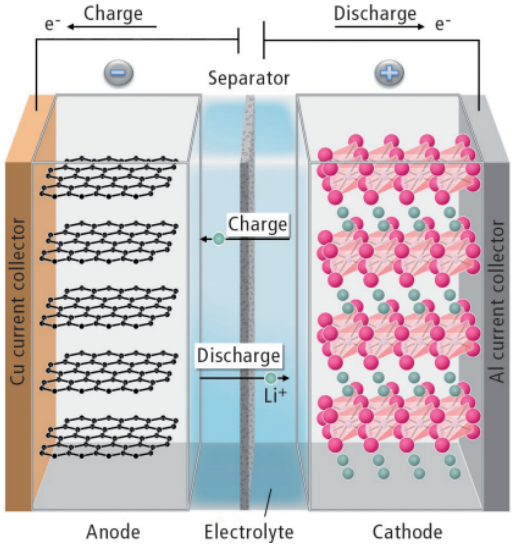

Figure 2.1 *Functional principle Li-ion battery cell [77]*

In *figure 2.1*, the working principle of a Li-ion cell is represented. The potential electrical energy is stored in two electrodes: the anode and the cathode. The positive cathode consists of an aluminium current collector and, in most commercial batteries, a metal oxide. The most common used metal oxides for Li-ion batteries are $LiCoO_2$ (LCO), $LiMn_2O_4$ (LMO), $LiNi_{0.33}Mn_{0.33}Co_{0.33}O_2$ (NMC) and $LiFePO_4$ (LFP) [31]. The negative anode consists of a copper current collector and a carbon material, typically graphite [31]. An electrolyte between the electrodes, usually a liquid or polymer, makes ionic and electronic conductivity possible. During both charging and discharging of the battery cell, a chemical redox reaction occurs that has an ionic and electronic component [18]. This chemical reaction starts at the electrode of the migrating material where an oxidation reaction takes place [23]. As a result, a number of positive ions and an equal number of electrons are formed. The number of positive ions and electrons depends on the chosen migrating material. It is wanted that the positive ions flow through the electrolyte, but that the electrons flow to an external circuit. For that reason, a separator is needed. This separator ensures ionic conductivity and electrical isolation, preventing a direct short circuit between the electrodes. The separator let the positive ions through but forces the electrons to flow through an external circuit. This is possible due to the smaller electrical resistance of the electrons compared with the separator. The positive ions and electrons recombine again at the other electrode, which is known as a reduction reaction. When the electrons and positive ions can move in both ways, the process is reversible. When the process is reversible, the batteries are rechargeable, which is the case for Li-ion batteries.

The concentration is on the discharge mode of a battery. During discharge, the positive charged Li^+ ions move from the negative anode to the positive cathode through the separator. The electrons flow from the anode to the cathode through the external circuit, resulting in current. The electromotive force (EMF) or OCV is the voltage difference between the electrodes. When (re)charging a Li-ion battery, the opposite reaction happens. The positive electrode is losing electrons and the negative electrode is gaining electrons. Here the terms "positive electrode" for the cathode and "negative electrode" for the anode are actually no longer correct, but in battery terminology, these terms are commonly assigned like this.

The battery has internal resistance due to the used materials in the cell that have resistance. The internal resistance can be divided into ohmic and polarization resistance. Ohmic resistance is the resistance of the used material, such as the current collector, electrode and electrolyte. Polarization resistance is the transition resistance between the electrodes and the electrolyte.

2.1.2 Batteries in series and parallel

Integrating batteries into the grid means that they must be able to provide a significant voltage and current. A Li-ion battery typically has a voltage of 3.6V. Knowing that the low-voltage grid has a voltage of 400V (3Φ AC), this is a remarkably low voltage. To increase voltage and current, batteries are connected in series and parallel, respectively.

The principle of connecting batteries in series is depicted in *figure 2.2*. Connecting batteries in series increases the total voltage, but also the total internal resistance of the battery pack.

$$\begin{cases} R_{series} = R_1 + R_2 + ... + R_n \\ V_{oc,series} = V_{oc,1} + V_{oc,2} + ... + V_{oc,n} \end{cases} \tag{2.1}$$

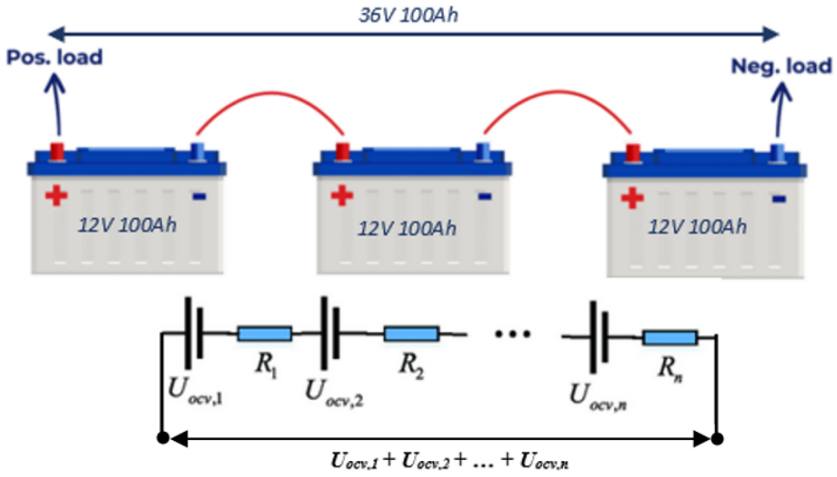

Figure 2.2 *Example batteries in series*

The principle of connecting batteries in parallel is depicted in *figure 2.3*. Connecting batteries in parallel increases the (dis)charge capacity and, in other words, allows them to feed more current. Connecting batteries in parallel reduces internal resistance.

$$\begin{cases} R_{parallel} = (\frac{1}{R_1} + \frac{1}{R_2} + ... + \frac{1}{R_n})^{-1} \\ I_{parallel} = I_1 + I_2 + ... + I_n \end{cases} \tag{2.2}$$

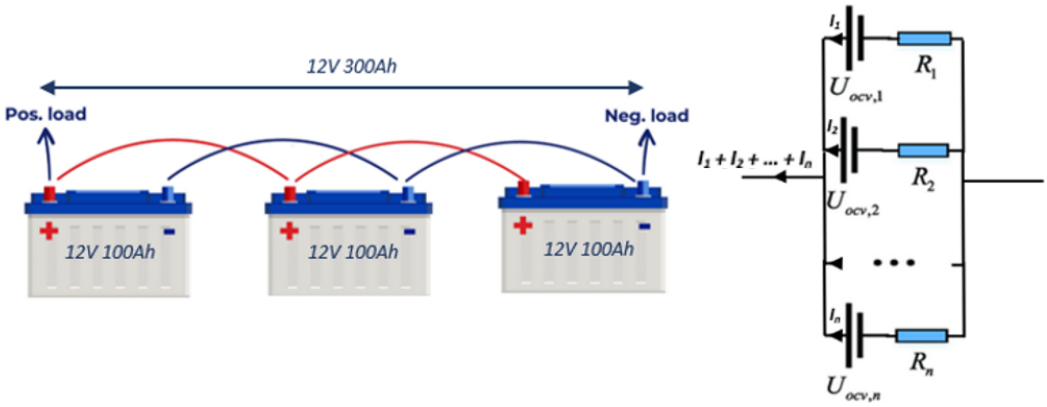

Figure 2.3 *Example batteries in parallel*

2.1.3 Representation BESS

The simplified representation of the fault current circuit fed by a BESS is illustrated in figure *figure 2.4*.

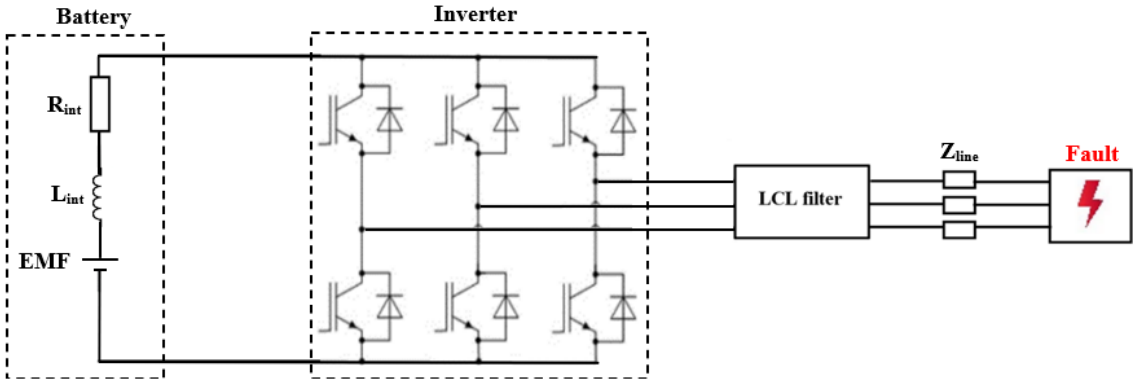

Figure 2.4 *Simplified representation of BESS fault current*

The battery has an internal resistance R_{int}. The battery has an internal inductance L_{int} as well. The inductance causes the transient behavior of the current. To convert the DC battery voltage to AC, there is a three-phase inverter with IGBTs as switching components. The current flows through the lines, which have impedance Z_{line}, to the fault. The fault can also have a particular impedance Z_{fault}. The battery acts here as a generator. Initially, dynamic behaviour occurs, the so-called transient response. For example, the larger the inductance of the battery circuit, the slower the fault current rises. After the dynamic behaviour of the fault current, steady-state fault currents are obtained.

2.1.4 Potential application

An application of the BESS model developed in the thesis is to evaluate the behaviour of a BESS during fault event. This is a mandatory part when sizing the fuses of battery-supported LV grids. The fault current is usually smaller if only the BESS is feeding. The BESS in island mode is illustrated in *figure 2.5*. When the utility grid is feeding, the fault current can be 10-50 times the full load current. In this case, the protection fuse should interrupt the fault immediately. When working in island mode, the available fault current is usually only 2-5 times the full load current [37].

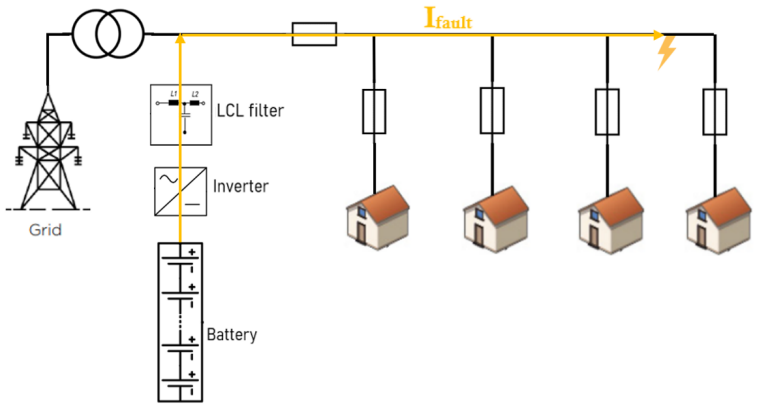

Figure 2.5 *BESS in island feeding fault current*

The characteristics of the fuse protection are such that the fault currents are quickly interrupted in grid-connected mode, but when working in island mode they react much slower. A possible 'solution' to get this fault current high enough is oversizing the BESS. This is an expensive and so unwanted solution. There is also a low current limit for these fuses, so they do not burn when feeding the load currents in normal operation. With the BESS model, a good estimation of the fault current can be made in order to size the fuse protection properly.

To motivate the purpose of this research, an example of an inverter-based resource, such as a BESS, feeding a fault in both grid-connected mode and island mode is given in [3]. Note that this is a particular example, this is not what happens in general. The used grid is given in *figure 2.6*. Faults are simulated in two different places C1 and C2. The results are illustrated in *figure 2.7*. Faults are simulated in two different places C1 and C2. The results are illustrated in *figure 2.7*.

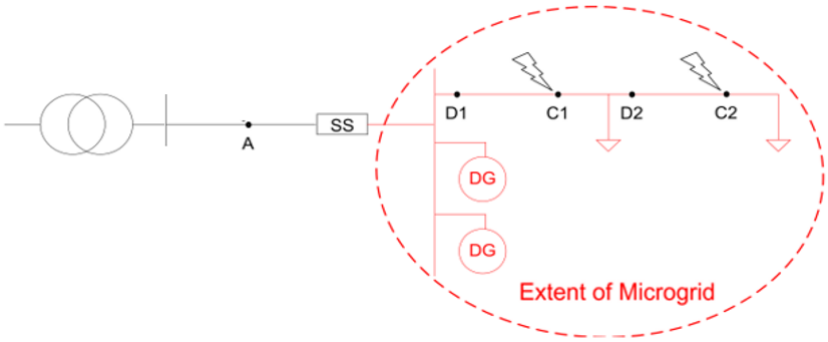

Figure 2.6 *Example of a grid with IBDER [3]*

(a)

	3ϕ fault at $C1$			3ϕ fault at $C2$		
	$I_a[A]$	$I_b[A]$	$I_c[A]$	$I_a[A]$	$I_b[A]$	$I_c[A]$
$D1$	811.6	812.2	811.3	430	431.2	430
$D2$	0	0	0	424.8	425.9	424.6

(b)

	3ϕ fault at $C1$			3ϕ fault at $C2$		
	$I_a[A]$	$I_b[A]$	$I_c[A]$	$I_a[A]$	$I_b[A]$	$I_c[A]$
$D1$	817.8	818.5	817.4	433.8	434.4	433.6
$D2$	0	0	0	428.3	429.13	428.0

(c)

	3ϕ fault at $C1$			3ϕ fault at $C2$		
	$I_a[A]$	$I_b[A]$	$I_c[A]$	$I_a[A]$	$I_b[A]$	$I_c[A]$
$D1$	66.24	66.24	66.24	66.29	66.31	66.23
$D2$	0.014	0.007	0.004	65.49	65.48	65.45

(d)

	3ϕ fault at $C1$			3ϕ fault at $C2$		
	$I_a[A]$	$I_b[A]$	$I_c[A]$	$I_a[A]$	$I_b[A]$	$I_c[A]$
$D1$	132.68	132.69	132.65	132.68	132.69	132.67
$D2$	0.02	0.01	0	131.48	131.52	131.50

Figure 2.7 *Fault simulation results (a) Grid-connected and one IBDER feeding (b) Grid-connected and two IBDER feeding (c) Island mode and one IBDER feeding (d) Island mode and two IBDER feeding [3]*

It can be noted that the location of the fault does not affect the fault current. This is because the inverter(s) feeds their maximum current in both situations and these are limited to their maximum value. Consequently, the fault current is independent of the impedance in the grid in this specific case.

When the IBDER operate in island mode, switch SS is open. It can be seen that when operating grid-connected, meaning that both the grid and the IBDER are feeding, the fault current is much higher than when only the IBDER feed. This research also addresses the problem of these low fault currents: the fault remains undetected by the protection in some cases. This research also addresses the problem of these low fault currents, the fault remains undetected by the protection in some cases. The circuit breakers in this example are situated on positions D1 and D2 in *figure 2.6*. The trip curves are shown in *figure 2.8*.

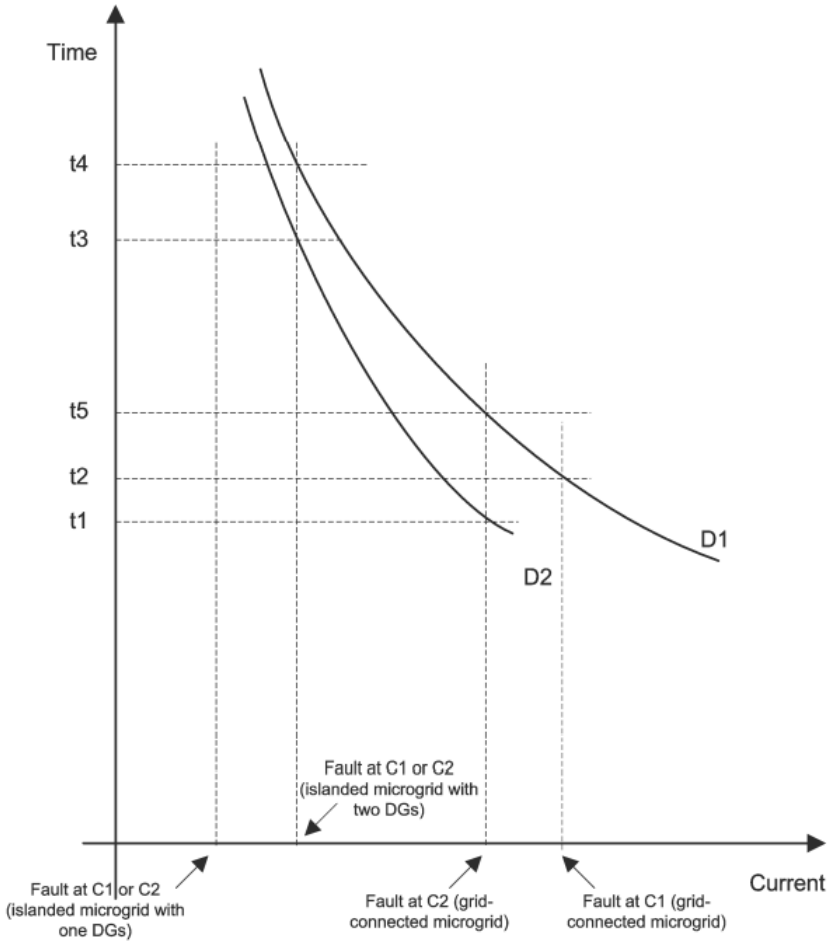

Figure 2.8 *Impact IBDER on inverse time/current characteristic curves [3]*

When working grid-connected, the fault current is higher and the protection trips fastest. When working with two IBDER, the protection waits longer to trip, as can be seen in *figure 2.8*. The lower fault current delays the response of the overcurrent protection because this situation already seems closer to nominal load situation. The fault current is not high enough for rapid cut-off. When only one IBDER is feeding the fault current, the overcurrent protection does not trip. The fault current remains undetected, so the protection won't cut the current.

In Finland, LV installations (< 1kV) are carried with fuses defined in standard series SFS 6000 [71]. The burning time of these fuses is up to 5 s, so the BESS should supply the fault current for at least 5 s. The conditions of the fuses can be found in the SFS-EN 60269-1 standard [4]. In

figure 2.9, the maximum currents are given for which the particular fuses should definitely operate within 5 s. These are defined in the standard SFS-EN 60269-1. Note that these are the currents for a single phase and not the three-phase currents.

Fuse size [A]	I_{max} (5s) [A]	Fuse size [A]	I_{max} (5s) [A]	Fuse size [A]	I_{max} (5s) [A]
16	65	**80**	425	**400**	2840
20	85	**100**	580	**500**	3800
25	110	**125**	715	**630**	5100
32	150	**160**	950	**800**	7000
40	190	**200**	1250	**1000**	9500
50	250	**250**	1650	**1250**	13000
63	320	**315**	2200		

Figure 2.9 *Maximum fuse current for 5 s burning time [4]*

Figure 2.10 illustrates an example of the time-current characteristic curves of fuses.

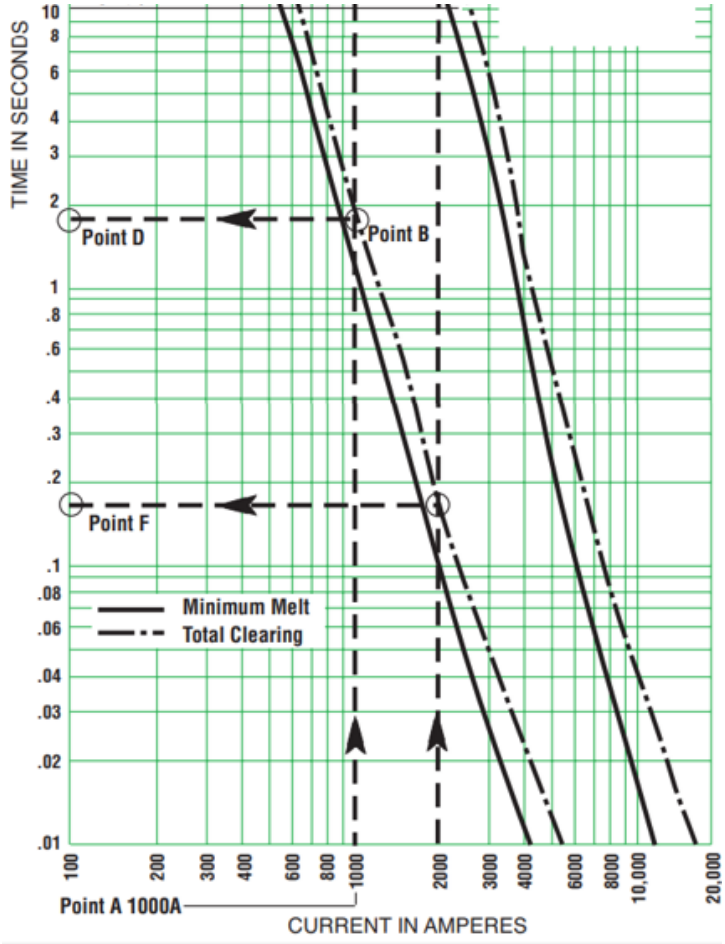

Figure 2.10 *Example characteristic curves fuses [2]*

The fuses have a 'minimum melt'-curve and a 'total clearing'-curve. The minimum melt is less relevant in this study since certainty is desired that the fuse burns. The currents in the curves indicate the RMS currents and not the peak currents.

2.1.5 Generator fault current

In this thesis, the dynamic behaviour of the fault current is investigated, divided into different 'steady-state' periods. With this is meant that the dynamic behaviour of the BESS is not outlined using electromagnetic simulations, but the BESS fault current is investigated at different time periods. In synchronous machines, the fault current can be divided into three distinctive periods based on the physical properties of the machine: the subtransient, transient and steady-state fault current. Note that the BESS does not have these distinctive periods. In the technical datasheet of a synchronous generator, the subtransient, transient and steady-state reactances are given. Using these reactances, the fault currents can be calculated for these 3 different stages of the fault current [6].

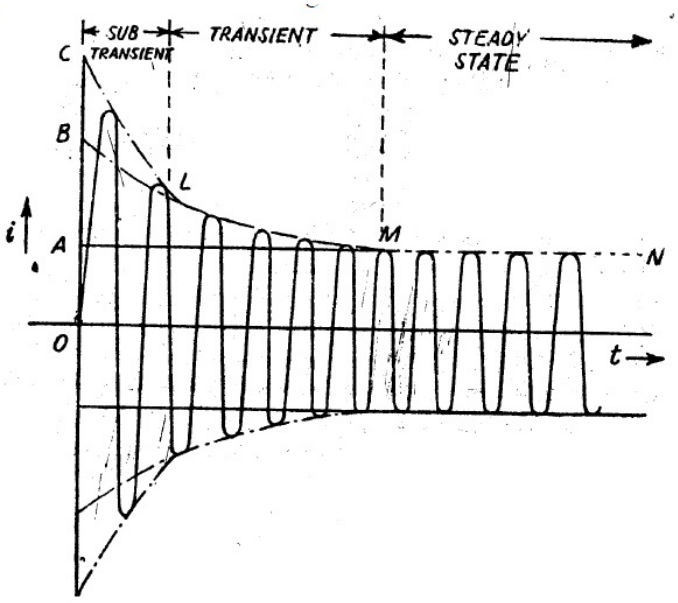

Figure 2.11 *Short-circuit characteristics synchronous generator [12]*

The subtransient current I", transient current I' and steady-state current I can be calculated with the following equations, respectively:

$$I" = \frac{E_a}{X"_d} = \frac{|OC|}{\sqrt{2}} \tag{2.3}$$

$$I' = \frac{E_a}{X'_d} = \frac{|OB|}{\sqrt{2}} \tag{2.4}$$

$$I = \frac{E_a}{X_d} = \frac{|OA|}{\sqrt{2}} \tag{2.5}$$

E_a is the induced electromagnetic force [V] and $X"_d$, X'_d and X_d are respectively the subtransient, transient and steady-state reactance. |OC|, |OB| and |OA| represent the peak values of the current and can be deduced from *figure 2.11*.

The short-circuit current is not constant during the subtransient or transient period, as depicted in *figure 2.11*, there is a decay during these periods, but the fault current calculations using the given reactances from the manufacturers' datasheets do provide a good reference of the RMS fault current.

In synchronous generators, the physical laws determine the fault current, but for BESS, controllers will have a big influence on the fault current.

2.2 Fault current characteristics of lithium-ion batteries

This section describes the fault current characteristics of these Li-ion batteries. In some cases, for which the simplest approach of a battery is enough, a battery can be modeled as an ideal DC voltage source, but batteries are not ideal DC voltage sources. The internal resistance of a battery is negligible in many cases because of the much greater impedance of the load relative to the internal resistance of the battery. However, for fault current studies, a battery cannot be modeled as an ideal DC voltage source. A "perfect" short circuit has no impedance so that would mean that the fault current fed by a battery is infinite. This is not the case. The internal resistance of the battery should be approximated as accurately as possible to model the fault current in a realistic manner. The fault current of a battery can be calculated by using Ohm's law:

$$I_f = \frac{V_{oc}}{R_{int} + R_f} \tag{2.6}$$

Here is I_f the fault current, V_{oc} the open-circuit voltage, R_{int} the internal resistance of the battery and R_f the fault resistance.

Note that all the discussed parameters are deduced from different studies that may date back several years. Batteries today are increasingly optimized, so the profile of the internal resistance may already be different for today's manufactured batteries. However, the principles do not change.

2.2.1 Open-circuit voltage

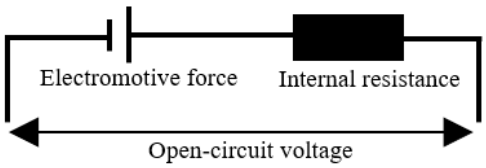

Figure 2.12 *Open-circuit voltage*

The OCV of a battery is a characteristic parameter that defines the electrical potential between the positive terminal (cathode) and the negative terminal (anode). Sometimes the OCV is also called EMF, although it is not a force. *Figure 2.12* represents an oper-circuit with infinite impedance, so the current is zero. When the current is zero, OCV is equal to EMF. When the current is flowing, the voltage at the terminals is no longer the OCV, but the terminal voltage. Elements that affect this parameter are the chemical compositions of electrodes and electrolyte, thermodynamic entropic effects, mechanical stress, microscopic distortions, etc. These elements can vary by the SoC, temperature, discharge current and cycle age [20].

State of charge

This open-circuit voltage varies depending on how much the battery is charged. One can call this effect **chemical depletion**. This principle can be explained using the Nernst equation [81]:

$$E = E_0 - \frac{R \cdot T}{n \cdot F} \cdot ln(Q) \tag{2.7}$$

Q is the reaction coefficient in this equation. The reaction that happens in a battery can be represented by the following reaction form:

$$aA + bB \rightleftharpoons cC + dD$$

Q can be calculated for this reaction.

$$Q = \frac{[C]^c[D]^d}{[A]^a[B]^b} \tag{2.8}$$

$[X]^x$ indicates the concentration of the material in the battery. When discharging, the reaction starts from chemical elements $[C]^c$ and $[D]^d$. As a Li-ion battery discharges, the concentration of the material decreases and chemical elements $[A]^a$ and $[B]^b$ are less concentrated, resulting in the reaction coefficient $Q > 1$. A more detailed explanation can be found in [81]. If all the material of the battery were solid, the OCV would remain approximately constant, since there is no change in concentration, but that is not the case in Li-ion batteries. When the battery is charged and discharged, the concentration changes and consequently the OCV is SoC dependent.

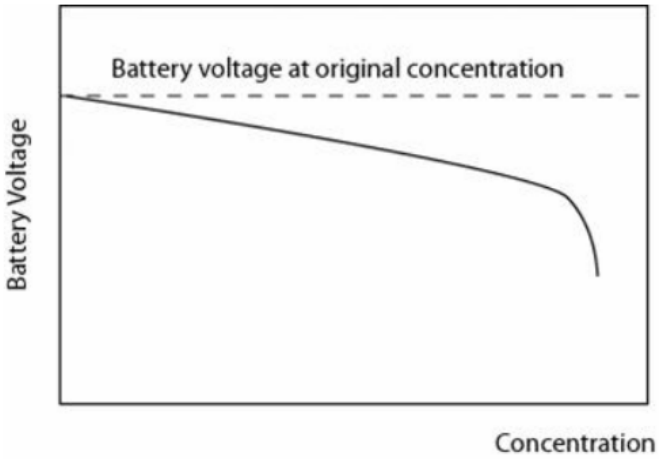

Figure 2.13 *OCV vs. concentration battery [46]*

As the battery discharges, the concentration decreases and consequently the OCV decreases (*figure 2.13*). Note that both EMF and terminal potential difference decrease when discharging the battery, but they are not the same, although both are expressed in the unit [V]. EMF is the provided amount of energy per coulomb of charge passing through the cell. Due to the internal resistance, the terminal voltage will drop more than the EMF when operating.

The OCV-SoC curves of Li-ion batteries are presented *figure 2.14*. These curves apply to new, resting batteries at a temperature of 298.15 K. They differ depending on their chemical properties.

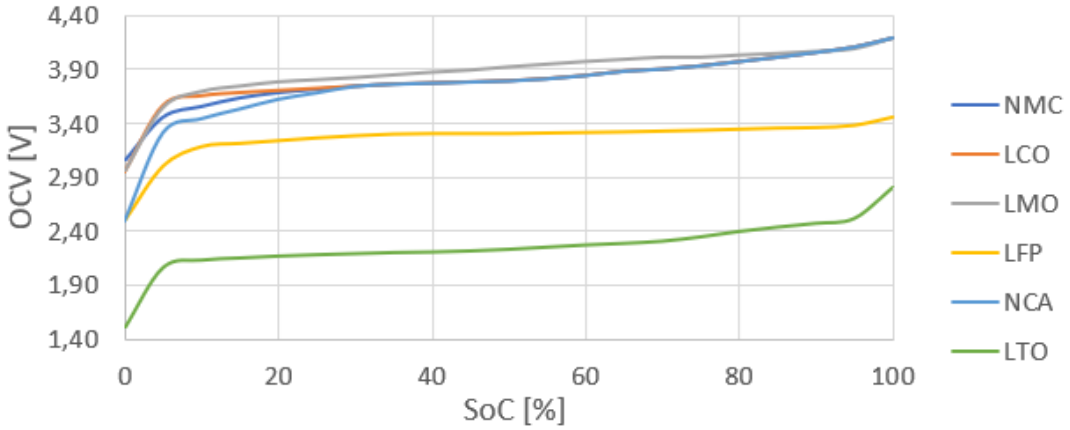

Figure 2.14 *OCV-SoC curves Li-ion batteries [9] [51] [66]*

These are the typical OCV-SoC curves of Li-ion batteries, but variations are possible depending on what voltage the manufacturer states the battery is considered to be fully charged and fully discharged. In general, the OCV of the batteries decreases with decreasing SoC. As the battery loses ions, the OCV drops. This means that the OCV is decreasing during discharge.

The battery stops charging and discharging at particular voltage values. The battery must operate within these OCV ranges, but charging to an even higher OCV and discharging to an even lower OCV is theoretically possible. The reasons this is not done are the following:

- **Maximum operating voltage:** When the battery is being charged, a point will be reached where the electrolyte begins to break down and consequently the voltage begins to rise sharply. This damages the battery and is therefore unwanted. Hence, the voltage is cut off.
- **Minimum operating voltage:** When the battery is being discharged, the concentration of the electrolyte decreases and resistance is strongly increasing. Discharging beyond this limit would harm the battery as a result of heat generation.

The resulting capacity in the battery is indicated as SoC or DoD. The relationship between DoD and SoC is described by the following equation:

$$DoD = 100\% - SoC \tag{2.9}$$

To determine the SoC of a rechargeable battery, the OCV-method can be used [74]. This method calculates the SoC based on its relation with the OCV. The OCV-method is accurate in steady-state but is less accurate due to the OCV dependence on temperature and ageing. Besides, the SoC determination takes a long time and accurate voltage measurements are required. For that reason, Coulomb counting is commonly used [63].

$$SoC(t) = SoC(t_0) + \int_{t_0}^{t} \eta \cdot \frac{I(t)}{Q_b}\, dt \tag{2.10}$$

In this formula $SoC(t_0)$ is the initial SoC, η the efficiency during charging or discharging, I the charge or discharge current and Q_b the battery capacity. This method is preferred because it is easy and low-cost.

When determining the SoC-OCV curves of batteries, it is important to consider the operating mode: charging or discharging. There is hysteresis between OCV for charge and discharge [19].

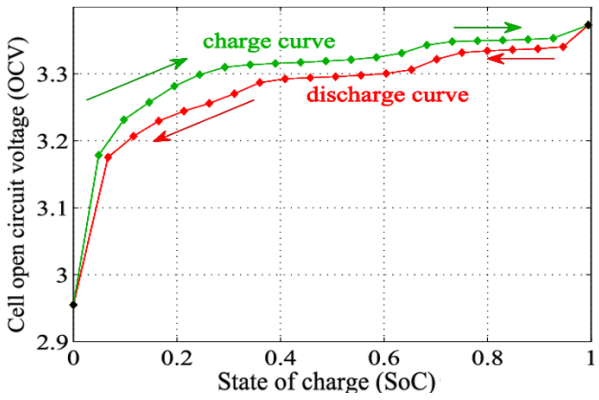

Figure 2.15 *Hysteresis OCV-SoC curve charge and discharge mode [73]*

The hysteresis, presented in *figure 2.15*, is the result of thermodynamical entropic effects, mechanical stress and microscopic distortions within the active electrodes [34]. For Li-ion batteries, the difference is minimal and commonly neglected. In this thesis, only discharge mode is considered.

Operating temperature

Temperature is another affecting factor in the OCV-SoC curves. Batteries are electrochemical storage systems. Temperature plays a major role in chemical reactions, and it is no different with batteries. However, there is no simple relationship between temperature and the EMF of electrochemical cells, as they depend on what happens internally [56]. The behaviour of Li-ion batteries is considered here. These are less temperature dependent than lead-acid batteries, but not negligible for fault calculations. The effect of temperature on OCV can be expressed as the temperature coefficient of voltage (TCV). This principle is represented in *figure 2.16*.

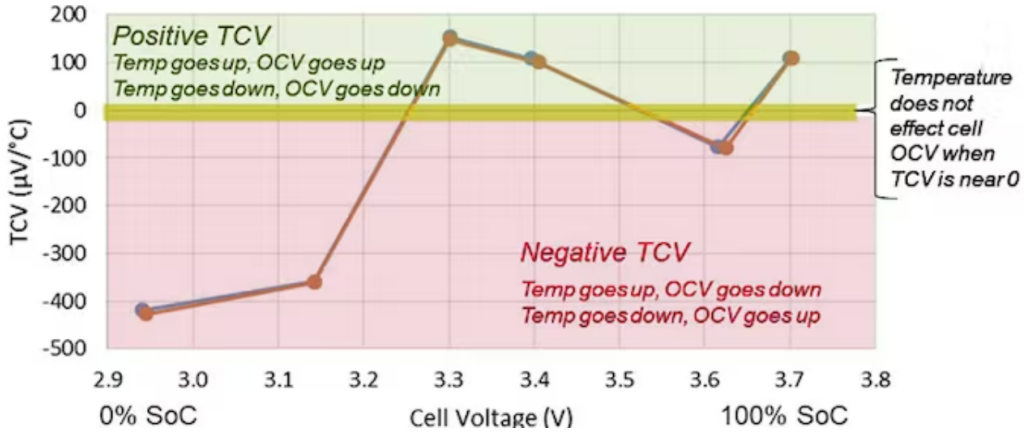

Figure 2.16 *Temperature coefficient of voltage of a Li-ion cell [19]*

Only when the battery is almost fully discharged, e.g. below 20%, the change in OCV becomes significant. A positive TCV means the OCV increases with increasing temperature and a negative TCV means the OCV decreases with increasing temperature. The magnitude of the TCV in *figure 2.16* cannot be generalized for all battery cells. The effect of temperature can be reviewed for the entire OCV-SoC curve. The OCV-SoC curves for different temperatures is shown in *figure 2.17*.

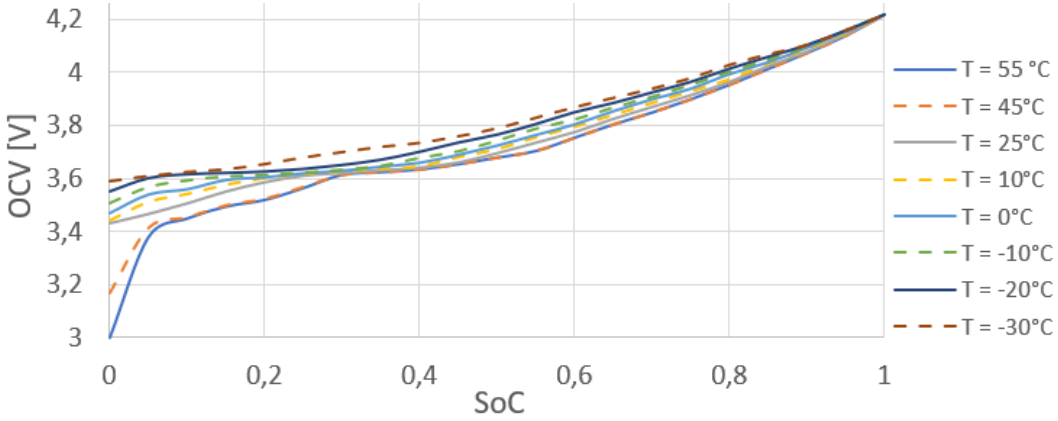

Figure 2.17 *OCV-SoC curve with temperature dependency NMC battery [76]*

Figure 2.17 applies to NMC batteries but is similar for all Li-ion batteries [75]. At low SoC, the OCV varies significantly. As can be seen in *figure 2.17*, the voltage drop per °C is larger when the battery SoC is low. Increasing temperatures cause the OCV to drop because of the negative TCV. The lower the voltage, the more negative the TCV becomes, meaning that the effect of higher temperatures is amplified.

Discharge current

It has been explained that the OCV-SoC curves differ for charge and discharge mode (*figure 2.15*). To discuss the effect of discharge current, EMF is a the better term since current cannot flow in an open circuit, but it has been clarified previously that OCV and EMF are the same for a battery. It is important to distinguish this parameter when the battery is actually not connected to a circuit, so open-circuit, and when the battery is charging or discharging to a load.

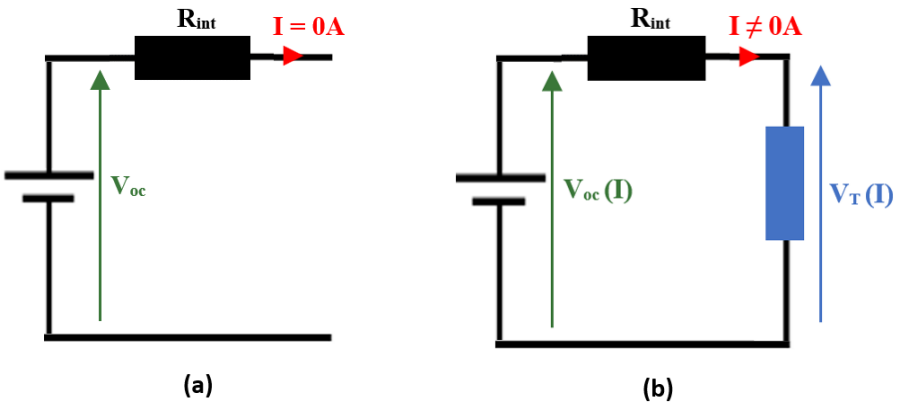

Figure 2.18 *Open-circuit voltage (a) No load (b) With load*

In *figure 2.18*, the difference between the no-load state and the loaded state of the battery is depicted. When there is no load, no current is flowing so OCV is not affected by the current. When a load is connected and the current is flowing, the OCV-SoC curve shifts up or down depending on the operating mode. Adding energy, i.e. charging, shifts the curve up and extracting energy, i.e. discharging, shifts the curve down. When discharging at high currents, a phenomenon called **migration bottleneck** can occur [49]. This means that ions cannot migrate quickly enough from one electrode to another and clogging is caused, resulting in a decrease in OCV. The downshift of the OCV-SoC curve as a function of the discharge current is illustrated in *figure 2.19*.

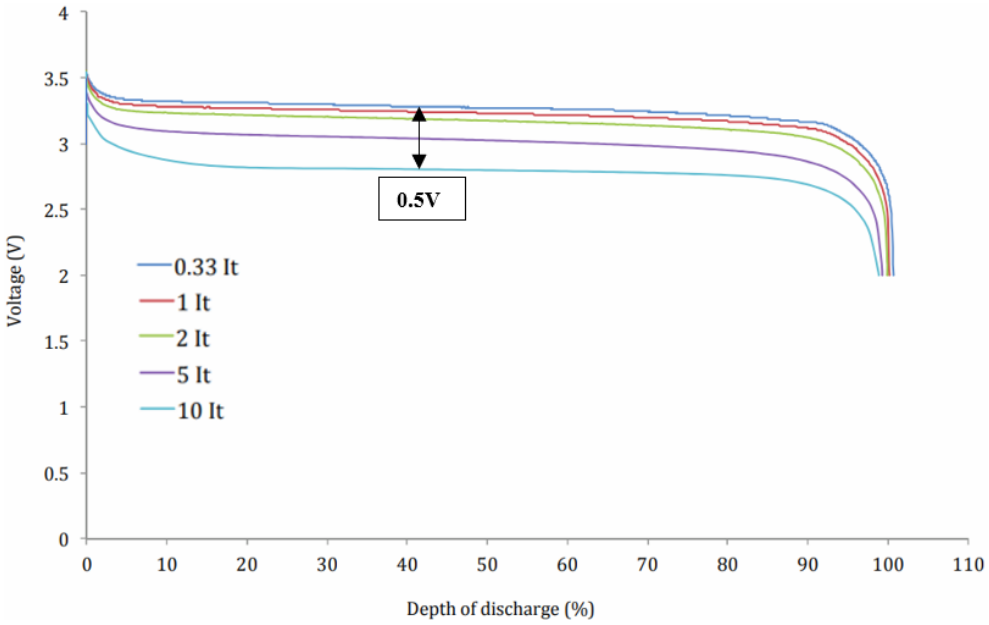

Figure 2.19 *Shifting OCV-SoC curve in discharge mode of LFP battery [35]*

I_t is the discharge current that a battery can feed for an hour. Therefore, the current is given as a C-rate. This is the ratio at which the battery charges or discharges and is calculated as follows:

$$I_c = \frac{I}{Q_b} \tag{2.11}$$

I_c is the C-rate, I the discharge current [A] and Q_b the nominal capacity of the battery [Ah]. It can be seen that the larger the discharging current, the more the curve shifts downwards. The shifting of the curve can be considered to have a linear relation with the discharge rate. The total voltage shift from 0.3C to 10C is 0.5V, which means that the voltage shifts approximately 1.5% per 1C ($= \frac{0.5V}{3.3V \cdot 10}$). This particular example is for an LFP battery, but this behaviour is similar for all Li-ion batteries. Note that both OCV and terminal voltage are current dependents, but their dependence is not the same. The terminal voltage drops additionally by the resistive losses due to the internal resistance of the battery.

Cycle age

After charging and discharging a battery multiple times, the battery becomes damaged. Both the material and the chemical reactions of the battery deteriorate. As the rechargeable battery ages, i.e. after more charge-discharge cycles, the OCV of Li-ion batteries changes significantly at low SoC [75]. Studies revealed that the amount of Li-ions, which are responsible for the transport of electrical charge, between the electrodes had decreased on the cathode and had permanently attached themselves to the anode [21].

The OCV-SoC curves of NMC batteries are presented in *figure 2.20* for a new Li-ion battery and an aged Li-ion battery.

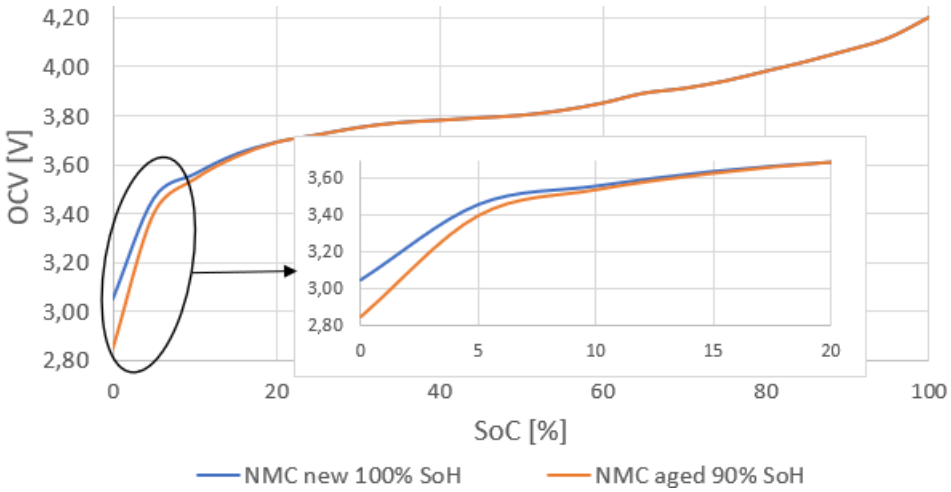

Figure 2.20 *OCV-SoC curves of a Li-ion battery for different SoH [75]*

In this figure, cycle age is specified by the SoH. The SoH can be calculated based on the residual capacity of the battery:

$$SoH = \frac{Q_{cur}}{Q_{new}} \cdot 100\% \tag{2.12}$$

With Q_{cur} being the residual capacity of the battery in its current state and Q_{new} being the maximal capacity of a new battery. For new BESS, the BMS usually monitors this SoH.

At an SoC $< 20\%$, the OCV is smaller for aged batteries. The lower OCV when the battery is almost discharged is the result of Li-ions sticking to the anode. As the battery discharges further, a larger decrease in OCV is noticeable compared to the new battery (*figure 2.21*).

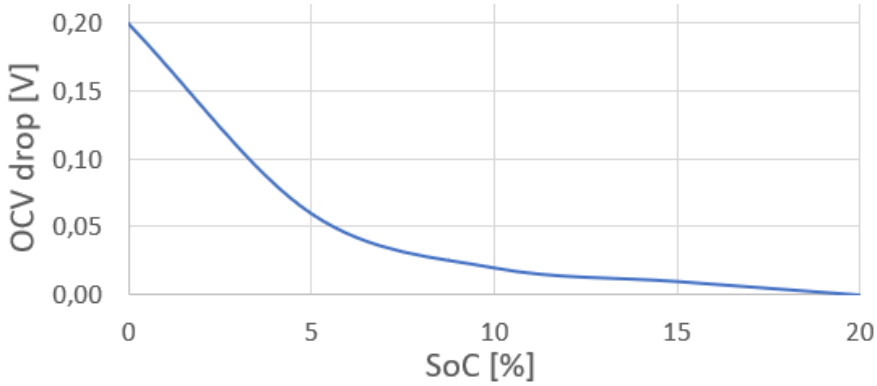

Figure 2.21 *Decrease in OCV due to ageing*

OCV determination

BESS have typically a BMS that can measure the OCV. This is different from the terminal voltage, so internal resistance compensation is needed. However, the OCV-SoC curves are rarely provided by BESS manufacturers, so there are two options for determining these curves:

- If the type of battery is given, take the typical OCV-SoC curves and multiply by the number of batteries n in the BESS, assuming that all batteries behave the same.

$$V_{oc,tot}(SoC) = n \cdot V_{oc}(SoC) \tag{2.13}$$

  Where $V_{oc,tot}(SoC)$ is the OCV of the whole BESS, n is the number of batteries in series and $V_{oc}(SoC)$ is the OCV of a single battery.

- Measure the OCV with a DC voltmeter [45]

2.2.2 Internal resistance

In here, the battery's impedance is termed internal resistance. An ideal battery would be one with no internal resistance, but practically this does not exist. The internal resistance of a battery is present due to the resistance of components in the battery and ionic elements (e.g. chemical reaction rate). In this way, the internal resistance can be divided into the ohmic and polarization resistance, as indicated in 2.1.1.

- **Ohmic resistance:** internal structure of the battery, electrical contact between the active electrode materials and the current collectors, homogeneity of the active material, etc.
- **Polarization resistance:** composition of the electrolyte

The battery is represented as a DC voltage source with a resistance in series. How this parameter varies, depends on what happens between the anode and cathode of the battery. The internal resistance is affected by SoC, operating temperature, discharge current and cycle age [20].

This parameter is usually provided in the technical datasheet of the manufacturer and is the primary indicator for evaluating battery quality. The internal resistance used to vary much more as a function of the parameters mentioned above, but with current developments in battery technology, mainly by the EV industry, the internal resistance is lower and already varies less.

State of charge

The SoC of the battery has also an effect its internal resistance. When the battery is almost fully charged, a state is reached where the electrolyte breaks down. This can be considered a slightly unstable conductive state, because there are too many ions, causing the internal ohmic resistance to be higher. As the battery discharges, the conductive state becomes more stable, but the ion concentration of the electrolyte reduces. This reduction in concentration makes the battery less conductive and causes the internal resistance to increase at lower SoC, both ohmic and polarization resistance [78]. *Figure 2.22* shows the relation between the R_{int} and the SoC. The fully discharged and charged SoC are considered to be generally the same. For example, for an NMC battery, the battery is fully discharged and charged at an OCV of 3.0 V and 4.2 V, respectively.

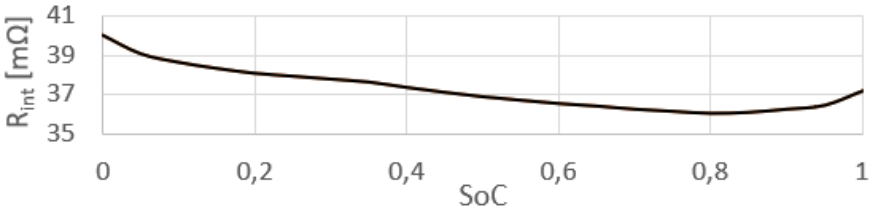

Figure 2.22 *R_{int} vs. SoC Li-ion battery [32]*

The internal resistance peaks when the battery is almost fully charged and discharged. At an SoC of $\approx 80\%$, the internal resistance reaches its optimum, i.e. least resistance.

Operating temperature

Before the EV era, the temperature had a very strong effect on internal resistance and differs for batteries with different chemical compositions and capacities [52]. In today's batteries, the battery's internal resistance is less dependent on the operating temperature when operating within the right temperature frame. As a result of the common use of NMC batteries in EVs, recently developed NMC batteries are less temperature dependent than, e.g., LFP batteries.

The internal resistance of the battery opposes the flow of electrons. As the temperature increases, the particles get more kinetic energy and the electrons become more mobile, resulting in an increase of current and a decrease in internal resistance [10]. However, at some temperatures, the internal resistance may rise again because higher temperatures cause the atoms to vibrate more, resulting in more collisions with electrons. More collisions between atoms and electrons mean more friction, resulting in an increase in electrolyte resistance and therefore internal resistance. The R_{int} vs. temperature curve, depicted in *figure 2.23*, is obtained.

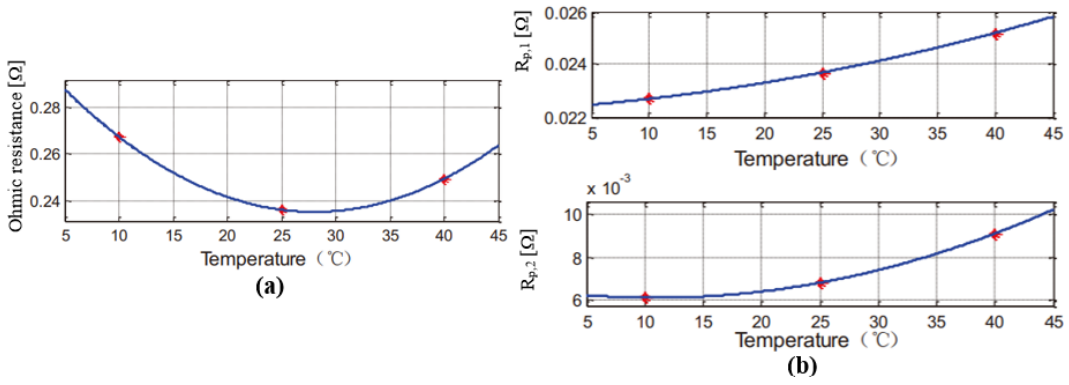

Figure 2.23 *R_{int} vs. temperature Li-ion battery (a) Ohmic resistance (b) Polarization resistance [39]*

This is a general approach for all Li-ion batteries. Operating at high temperatures is also unwanted because there is a risk that the electrodes will melt, resulting in more resistance and more losses. Batteries get more damage operating at higher temperatures. It is desired to work in the right temperature range of the battery to maximize efficiency. More information about the temperature progression is outlined in 2.2.4.

Discharge current

Internal resistance is a determinant factor of the discharge current, but the magnitude of discharge current also affects internal resistance. A higher current means also that there are more collisions between atoms and electrons, resulting in more friction. When there is more friction, it becomes harder for the electrons to flow so internal resistance increases. If this effect prevails, the internal resistance increases at higher currents as depicted in *figure 2.24*.

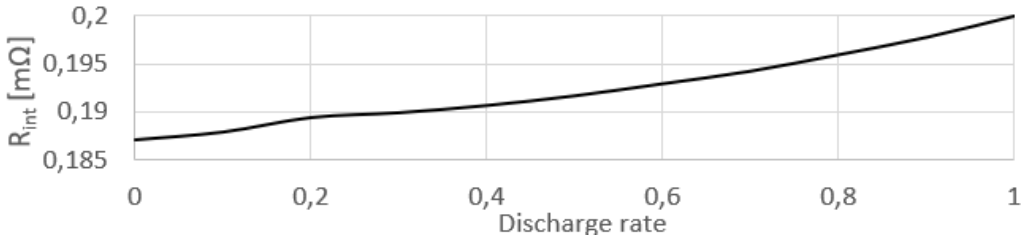

Figure 2.24 *R_{int} as a function of discharge current: prevail friction [42]*

In this curve, the operating temperature is 25°C. When the temperature is higher, the atoms vibrate more and consequently there are more collisions and friction. At higher temperatures, the atoms are even more mobile, so the 'friction effect' will be stronger. This is the curve in normal operating mode, i.e. discharge rates between 0C and 1C. The relation between R_{int} and discharge rate looks linear. However, when discharging at very high currents, e.g. 10-15C, the current might trigger other phenomena, e.g. depletion of the surface concentration of the battery. Consequently, the relation between R_{int} and I can become exponential rather than linear.

On the other hand, current causes the battery to heat up according to Joule's law.

$$q_{joule} = I_b^2 \cdot R_{int} \tag{2.14}$$

More fault current I_b flowing through the internal resistance of the battery R_{int} results in more heat dissipation q_{joule}. A higher temperature causes the electrons in the battery medium to be more mobile. This results in less internal resistance. This effect can prevail over the friction effect, as depicted *figure 2.25*.
This effect will prevail mainly when the temperature is low because the internal resistance is usually highest then. This results in more Joule heat (see *equation (2.14)*). There is less friction because the atoms are vibrating less. However, this is the effect of temperature rather than discharge current. The temperature reponse goes beyond Joule heat and is discussed further in 2.2.4.

The relationship between discharge current and internal resistance can be separated into two parts: 'the friction part' and 'the mobility part'. As of the moment high current flows, there are more electrons and consequently more friction and resistance. This effect takes place almost instantaneously, i.e. within 5 s, and doesn't change significantly over time. The friction effect is stronger at higher temperatures, because of the more vibrating atoms. The increase in mobility due to heating occurs as a function of time. Joule heat is in [W] or [J/s] so more heat is created every second. The effect is weaker when the battery operates at an already higher temperature.

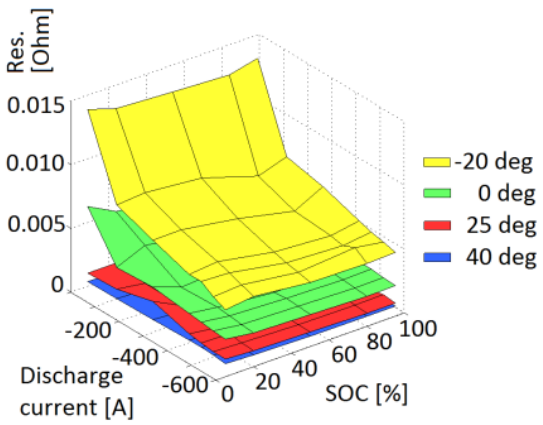

Figure 2.25 *R_{int} 30Ah NMC Li-ion cell as a function of operating temperature and SoC for various discharge currents: prevail mobility [65]*

To give an idea of the overall effect of the discharge current depending on what the battery temperature is, the curve in *figure 2.26* can be constructed. $\Delta R_{int}(I)$ is the variation in internal resistance as a result of discharge current.

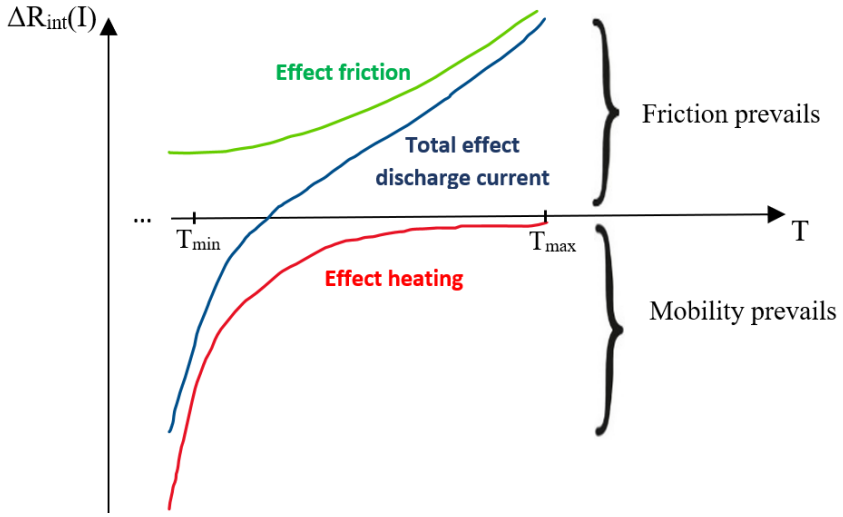

Figure 2.26 *Discharge current dependence of internal resistance: overall principle*

The impact of discharge current over a period of, e.g., 30 s is illustrated. This 30s is an arbitrary value but indicates that this is not the instantaneous equivalent effect. T_{min} and T_{max} are typically ≈ -20°C and 60°C. In general, the 'mobility part' due to heating will dominate at lower temperatures and the 'friction part' at higher temperatures.

Cycle age

As the material and chemicals of the battery are aging, they deteriorate and the internal resistance increases. The internal resistance can be divided into two components in series: the ohmic resistance and the polarization resistance [79]. It is the ohmic resistance that increases with the age of the battery. The polarization resistance, on the other hand, remains approximately constant. Battery ageing affects the resistance of the used materials and chemicals. For example, when charging and discharging a battery, the battery experiences mechanical stress between the electrodes. This mechanical stress causes the distance between the electrodes to increase.

By considering the battery as a conductor, the formula '$R = \rho \cdot \frac{l}{A}$' can be applied. This means that the internal resistance increases with the distance between electrodes, resulting in slower reactions.

The curve for a Li-ion battery with an operating temperature of 40°C, 4C charging and discharging current and 100 % DoD variation is depicted in *figure 2.27*. For the values of ohmic resistance and polarization resistance, arbitrary values were taken, meaning that the proportion of ohmic resistance and polarization resistance is not considered.

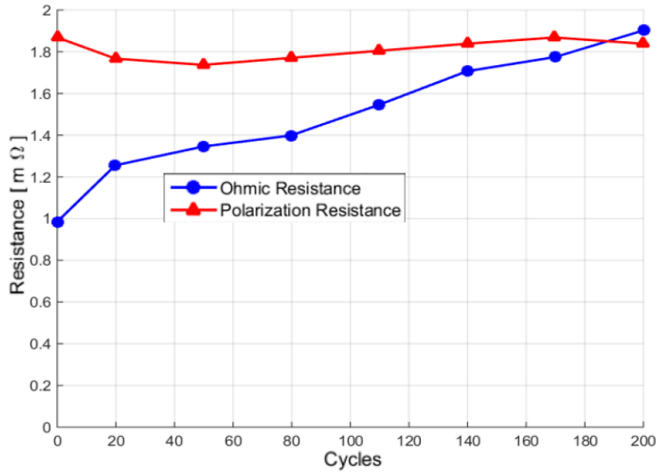

Figure 2.27 *Internal resistance as a function of cycle age [79]*

Cycle age has a significant effect on internal resistance, specifically on the ohmic resistance, but the increase in resistance also depends on DoD variations, operating temperature and C-rate when charging and discharging the battery. If the cycle is carried out at a higher current, temperature or deeper discharge, the battery is more damaged and consequently, the internal ohmic resistance rises faster, see *figure 2.28*.

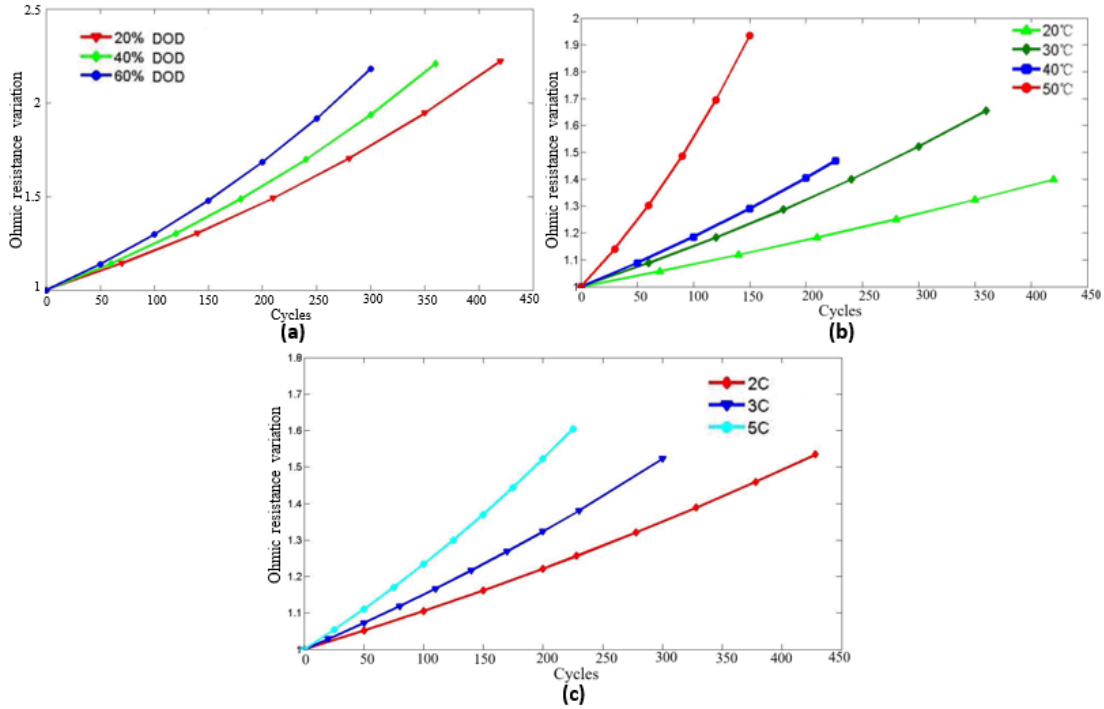

Figure 2.28 *Parameters affecting on internal resistance increase by cycle age [79]*

Figure 2.28a represents the increase of ohmic resistance as a function of cycle age for different DoD variations, *figure 2.28b* for different operating temperatures and *figure 2.28c* for different C-rates. As such, it is difficult to predict what the internal resistance will be after a particular number of cycles without assuming that the battery will operate under certain conditions during these cycles.

The parameter cycle age is often replaced by the parameter SoH. SoH is related to the capacity of the battery, see *formula (2.12)*, but it can also be calculated via the internal resistance:

$$SoH = \frac{R_{new}}{R_{int}} \cdot 100\% \tag{2.15}$$

With R_{new} being the internal resistance of a new battery. The SoH can be determined with *equation (2.12)*, but there are still two unknown parameters in *equation (2.15)*: R_{new} and R_{int}. The internal resistance of a battery itself is given as '$< ...m\Omega$' by the manufacturer, so for that reason, it is assumed to be the end-of-life resistance, R_{eol}. If this parameter is known, the internal resistance of a new battery R_{int} can be determined:

$$R_{new} = R_{eol} \cdot \frac{Q_{eol}}{Q_{new}} \tag{2.16}$$

Where Q_{new} is the capacity of a new battery and Q_{eol} is the end-of-life capacity of the battery. The internal resistance is inversely proportional to the residual battery capacity, whose cycle characteristics are usually given by the manufacturer, e.g. [5]. R_{int} can now be determined using *equation (2.15)*.

Internal resistance determination

The term internal resistance is used in this thesis, but if the exact dynamic behaviour of the battery is determined, one can talk back to impedance. Internal impedance can be measured in different ways. A reference value can be given by the manufacturer. Some different methods of measuring this impedance are introduced in this paragraph. Measurement methods can range from simple and cheap to complex and expensive, but also more accurate.

The simplest method is the DC load method, presented in *figure 2.29*. Two measurements are needed: the OCV and terminal or closed circuit voltage across an external load.

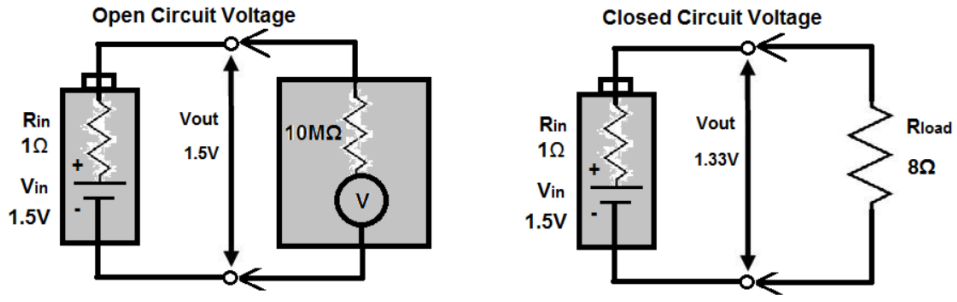

Figure 2.29 *Ohmic measurement of internal battery resistance*

The voltage difference ΔV is needed to calculate the resistance:

$$\Delta V = V_{oc} - V_{load} \tag{2.17}$$

Assuming that the OCV current is zero, the resistance can be calculated using Ohm's law:

$$R_{int} = \frac{\Delta V}{I_{load}} \tag{2.18}$$

Inaccuracies in this method can occur if the discharge current dependence of OCV and R_{int} are not taken into account. One possibility is to perform this test in a fraction of a second, using a switch, so that the effect of current has not yet been pushed through. This method can also involve inaccuracies since the battery has transient behaviour in voltage and current due to inductance and capacitance, respectively. Another possibility is to take into account the shifting of the OCV, as stated in 2.2.1, and determine the discharge current dependence of the internal resistance by performing this measurement with different loads.

If the exact behaviour of the battery is needed, Electrochemical Impedance Spectroscopy (EIS) is commonly used [15]. This can be done in a laboratory but is an expensive, complex and time-consuming process. Alternative measurement methods have already been developed, such as pseudo-random binary sequence (PRBS). This method is less time-consuming and easier to integrate into the BMS, but accuracy is compromised [15].

A battery model is developed using the parameters from the manufacturer's technical datasheet. If nothing is given of internal resistance and it cannot be determined from datasheet information, it must be measured. Depending on the desired accuracy of the model, internal impedance can be measured using the simple DC load method to exact impedance determination with EIS. Because it is assumed here that the least amount of information is provided, EIS or other time-consuming, complex and/or expensive measurement methods are not considered. If measurements must be performed, it is assumed that only a volt-, ampere- and resistance meters are available to the user.

2.2.3 Transient behavior

Inductance

When a fault occurs, the peak current is not immediately obtained. The inductance of the battery influences the transient behaviour of the fault current, as it counteracts current changes.

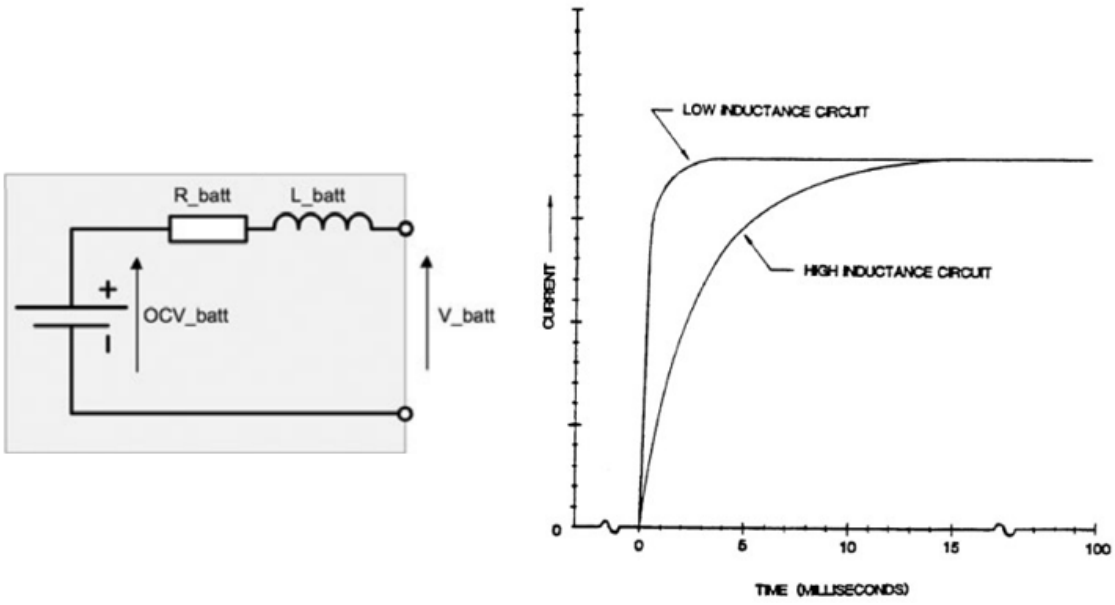

Figure 2.30 *Battery fault current as RL-circuit [48]*

The IEEE standard 1375-1998 [48] states that a battery short-circuit can be seen as an RL-circuit (*figure 2.30*). The inductance ensures that the increase in current is slower and so the peak is later reached. The duration of the transient period is approximately 5τ. The time constant τ of an RL circuit can be calculated using the next equation:

$$\tau = \frac{L}{R} \tag{2.19}$$

The current rises to its peak value within 5-15 ms, depending on the exact inductance of the battery [48]. Note this is the specific curve of lead-acid batteries, but according to the standard, this rise time applies to all stationary batteries. In [82] the L and R of a Li-ion battery are determined in a given state using EIS. It is also found that 5τ, calculated using *formula (2.19)*, is less than 15 ms. Unlike resistance, there is almost no temperature dependence on inductance.

Inductance can be added to the model for the transient behaviour of the battery. This will rather serve for fast-response overcurrent protections that should interrupt the current after, e.g., 30 ms.

Capacitance

The battery has some capacitance as well that counteracts voltage changes. The capacitance is in parallel with the polarization resistance. The manufacturers do not provide separate values for ohmic and polarization resistance, so this parameter is difficult to model without measurements. If the full transient behavior of the battery is studied, measurements must be performed to determine the ohmic and polarization resistance. In an earlier mentioned study [39], a Thevenin model was created for Li-ion batteries. In this study, the fast transient capacitance has an order of magnitude of 10^3-10^4 is in parallel with a 10^{-1}-10^{-2} polarization resistance. In series with those RC elements, there is a resistance with an order of magnitude 10^{-1}. However, the ratio of ohmic resistance and polarization resistance varies for all batteries. The time constant can be calculated as follows:

$$\tau = R_p \cdot C \tag{2.20}$$

A time constant with an order of magnitude 10^2 of the RC-element is obtained, meaning that the transient behaviour of the polarization resistance is negligible during the time frame of the fault, 0-5 s. This is also outlined in *figure 2.31.*

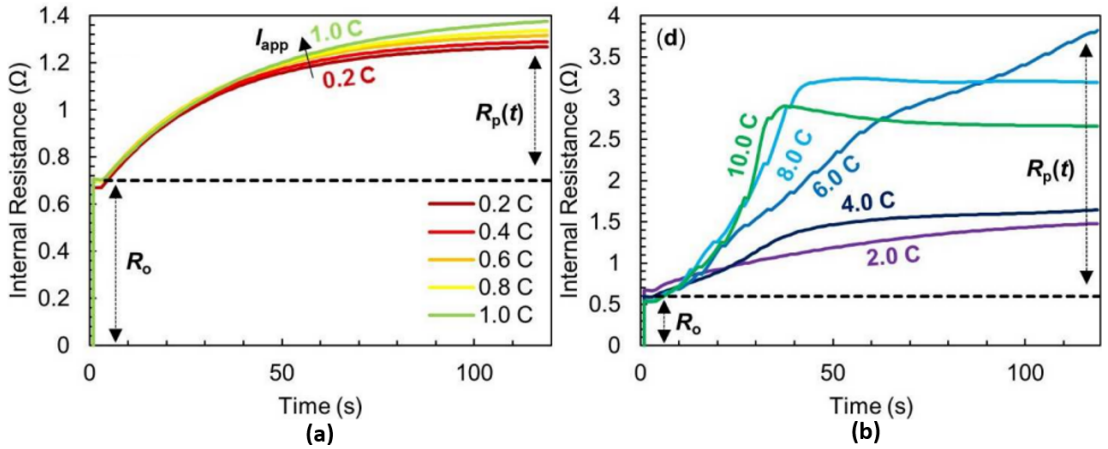

Figure 2.31 *Transient polarization resistance (a) Normal operation (b) High current [59]*

The transient behaviour of the polarization resistance is outlined in this figure. It can be seen that in a time frame of 5 s, the polarization resistance is negligible. Further, into the time profile, the polarization resistance becomes significant.

In the previous subsection, the effect parameters of internal resistance were examined and both ohmic and polarization resistance are considered here. The polarization resistance shows

slow transient behaviour, that is negligible during the time frame of the fault. The proportion of ohmic and polarization resistance for internal resistance affecting parameter discharge current is not specified, but it was given that *figure 2.24* represents the almost initial response, as it is measured by short pulses. In *figure 2.31*, it can be seen that this parameters is transient. However, since the effect is not very significant in a time frame of 5 s, it can be considered as a constant effect. The variations due to SoC and SoH are (almost) exclusively ohmic, so does not change. With the temperature effect, there is an impact both in ohmic and polarization resistance.

If the battery has already been discharging for a significant amount of time and then a fault occurs, polarization resistance needs to be considered. The proportion of polarization resistance in the total internal resistance and capacitance cannot be derived from the datasheets. For that reason, the polarization RC elements are not considered here. Two possibilities can be considered in the BESS model:

- Fault occurs when the BESS has just started discharging, so internal ohmic resistance only needs to be considered
- Fault occurs when transient polarization is completely over, so internal ohmic and polarization resistance both need to be considered.

2.2.4 Temperature

High discharge currents, i.e. fault currents, affect the battery its temperature, as already seen in 2.2.2, but the heat generation of the battery still needs some further explanation. In *figure 2.32*, the temperature response of an operating battery is depicted.

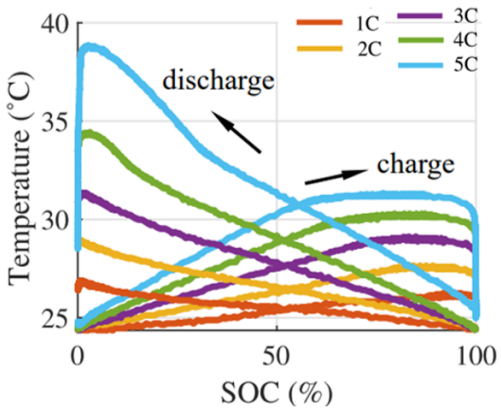

Figure 2.32 *Temperature curve as a function of C-rate [28]*

Charging starts at an SoC = 0% and discharging at an SoC = 100%. For example, when discharging at 5C, the battery's temperature would increase from 26°C to 38°C. It can be noted that the temperature increase is significantly stronger at higher discharge currents. This effect is more limited when the battery is charging. More fault current I_b flowing through the internal resistance of the battery R_{int} results in more heat dissipation q_{joule} according to Joule's law, illustrated with *equation (2.14)*. The increase in temperature ΔT due to the Joule effect can be approximated if the specific heat capacity of the battery $c_{battery}$ is known and assuming it is constant for all SoC and temperatures, the mass of the battery m is known and assuming that the heating of the battery is uniform.

$$\Delta T = \frac{q_{joule}}{c_{battery} \cdot m} \tag{2.21}$$

For Li-ion batteries, the $c_{battery}$ is generally close to 1000 $\frac{J}{kg \cdot K}$ [25].

This is only a small fraction of the heat developed in the battery. The total generated heat in a battery, investigated in [40], can be represented by the formula below:

$$q_{tot} = q_{rev} + q_{irr} \tag{2.22}$$

With q_{tot} being the total heat generated by the battery, q_{rev} the reversible generated heat and q_{irr} the irreversible generated heat. The reversible heat defines the change in entropy during operation. This effect is more dominant at low currents. The irreversible heat is the generated heat due to electrochemical reactions inside the battery. The dissipated Joule heat is only a part of the total generated irreversible heat. It is important to realize that the electrical resistance is not the same as the thermal resistance of the battery. Consequently, the heat development of the battery cannot be determined just using the information obtained from the BESS manufacturer's datasheets.

Batteries have a temperature limit, so this heating effect needs to be counteracted to avoid premature failure of the current due to excessive temperatures (*figure 2.33*).

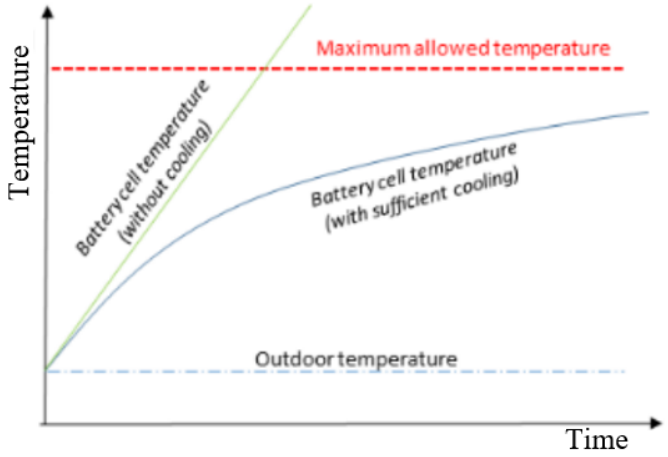

Figure 2.33 *Battery temperature increase curve [11]*

Cooling can be used to slow down the temperature increase of the battery, as can be seen in *figure 2.33*. In the datasheets of BESS, the type of battery cooling can be given (e.g. forced air cooling), but nothing about the details. The cooling of Li-ion battery packs is investigated in [80].
From this research, the following steady-state equation can be formed for cooling:

$$\dot{Q} = \dot{m} \cdot C_p \cdot (T_{outflow} - T_{inflow}) = h \cdot A \cdot (T_{cell} - T_{coolant}) \tag{2.23}$$

$\dot{Q}$	Absorbed heat by the coolant [W]	h	Heat transfer coefficient $[\frac{W}{m^2 \cdot K}]$
$\dot{m}$	Coolant mass flow rate $[\frac{kg}{s}]$	A	Surface of heat transfer $[m^2]$
C_p	Specific heat of the coolant $[\frac{J}{kg \cdot K}]$	T_{cell}	Temperature of the battery cell [K]
$T_{outflow}$	Outflow temperature of the coolant [K]	$T_{coolant}$	Average temperature of the coolant [K]
T_{inflow}	Inflow temperature of the coolant [K]		

This formula is valid if the thermal conductivity of the battery cell k » $h\Delta y$. Δy is here the cell thickness. The cooling capacity depends on how much heat the coolant can absorb. Therefore, the detailed properties of the refrigerant are needed. Since these are not provided by BESS manufacturers, the cooling is not examined here.

Illustrative example

It could be discussed that some heat generation could be added in the model, using *equation (2.14)* and *equation (2.21)*. A time frame of 0-5 s is considered here since the external protection after the inverter should trip after 5 s. During this period, battery heating will usually be negligible, even in fault events.

To illustrate, an example is given using arbitrary but realistic values. Suppose a 48V battery module with 94Ah capacity from Tesvolt with a weight of 34 kg [68]. A maximum short-circuit current of 1200A is provided and a maximum OCV of 58.1V. Therefore, the internal resistance won't be higher than 48mΩ. This battery module can supply 4C for 20 s. Suppose this battery module feeds 4C for 5 s, the amount of Joule heat can be determined:

$$Q_{joule} = I^2 \cdot R_{int} \cdot t = 376^2 \cdot 0.048 \cdot 5 = 33.9kJ$$

Knowing that this is an NMC battery module, with a specific energy of $\approx 1000\frac{J}{kg \cdot K}$, it can be determined how much energy is needed to heat up the battery module a 1 K can be calculated:

$$Q_{joule,1K} = c_{battery} \cdot m = 1000 \cdot 34 = 34kJ$$

In this 5 s overcurrent, the battery heats up 1 K, determined using Joule's law. In reality, heat generation is considered to be less because the battery is cooled and heat also gets lost to the ambient environment. However, this may give an idea of the temperature progression.

2.2.5 Discharge capacity

Discharge capacity can be closely related to the internal resistance of the battery. If the battery has a higher internal resistance, the cell terminal voltage drops more relative to the OCV and the cut-off voltage, or zero voltage if the BMS does not cut the battery off, is reached faster. Although the internal resistance provides useful information about the discharge capacity, it does not provide a linear correlation with it. The OCV is also involved, but other chemical behaviour inside the battery can further influence the discharge capacity. Hence, this parameter is discussed.

State of charge

The discharge capacity has a direct relation with the SoC since this indicates the remaining amount of energy or capacity in the cell.

$$SoC = \frac{Q_{remaining}}{Q_{full}} \cdot 100\% \tag{2.24}$$

$Q_{remaining}$ is the remaining discharge capacity in the battery and Q_{full} is the maximum capacity of the battery. The discharge capacity is used on the x-axis instead of the SoC, but they have basically the same meaning. The discharge capacity is the amount of capacity the battery has already fed during the discharge cycle when the cell voltage is reached.

Discharge current

The discharge rate has already been introduced in previous sections. This defines the rate at which the battery discharges. In fault situations, this discharge rate will be high and for this reason, it is relevant to see how this affects the battery. The discharge capacity can be calculated with the following formula:

$$Q_b = I_{dis} \cdot t_{dis} \tag{2.25}$$

Where Q_b is the discharge capacity for a particular C-rate and I_{dis} is the discharge current. The discharge time t_{dis} is the time until the battery reaches its cut-off voltage during discharge.

The relationship between discharge current and discharge capacity is expressed by Peukert's coefficient PC and can be calculated using Peukert's Law [38]:

$$I^{PC} \cdot t = constant \tag{2.26}$$

With

$$PC = \frac{log\ t_{dis,2} - log\ t_{dis,1}}{log\ I_{dis,1} - log\ I_{dis,2}} \tag{2.27}$$

So to calculate Peukert's coefficient, you need two discharge capacities for two particular C-rates. All factors of *equation (2.27)* can then be determined using *formula (2.25)* and *(2.26)*. However, this equation applies only to constant discharge currents and has no temperature dependence.

Temperature

It is desirable to keep the battery temperature within the desired temperature frame. Lower temperatures reduce electron mobility and lead to sluggish chemistry. High temperatures can cause more friction, and permanent damage and reduce the battery's performance and cycle life 2.2.2. This results in a decrease in discharge capacity as well.

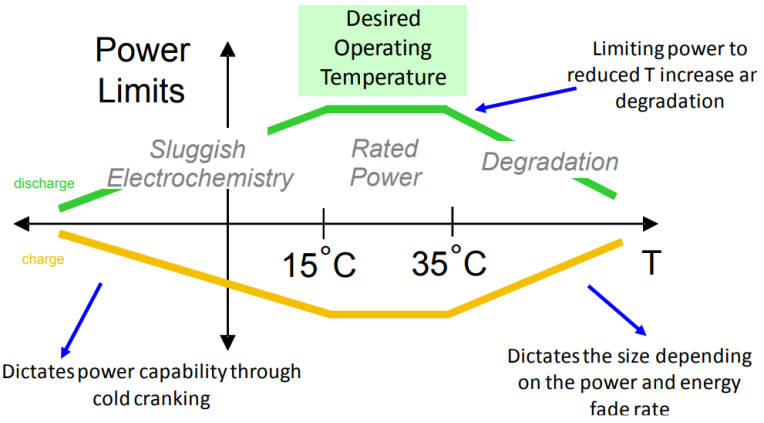

Figure 2.34 *Effect of temperature on charge and discharge power [58]*

In *figure 2.34*, the power capacity P_Q limits are presented. The power capacity is related to the discharge capacity ($P_Q = U_b \cdot Q_b$). The desired battery temperature is usually around 15 to 35°C. If the battery temperature is lower, the discharge capacity decreases due to slow kinetics. If the battery temperature is higher, a lower discharge capacity is obtained due to degradation.

Both temperature and discharge current have an effect on discharge capacity and they also affect each other. This is depicted in *figure 2.35*. This figure illustrates that the discharge capacity is initially higher at higher temperatures, but as higher discharge currents are used, the discharge capacity decreases sharply. With the internal resistance, it is already observed that internal resistance increases at higher discharge currents. If the temperature is higher on top of that, a lot of energy is lost to friction. At lower temperatures, the discharge capacity is generally lower due to sluggish chemistry. At a temperature of -18°C, the battery cannot supply currents higher than 5C. Therefore, many BESS are already shut down at temperatures below -10°C, as this sluggish chemistry can cause damage due to the high internal resistance. As can be seen, the ideal temperature is 25°C. The chemical reactions are sufficiently fast at this temperature and less degradation is obtained due to high discharge currents compared to the higher temperatures.

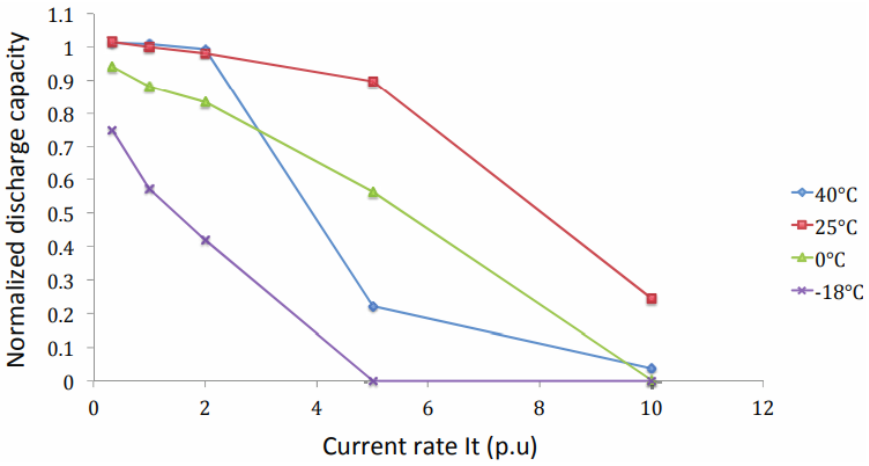

Figure 2.35 *Discharge capacity vs discharge current and temperature [35]*

Cycle age

Ageing of the battery causes the residual discharge capacity of the battery to decrease. The decrease in residual capacity under normal conditions is usually given by the manufacturer, such as in [5].

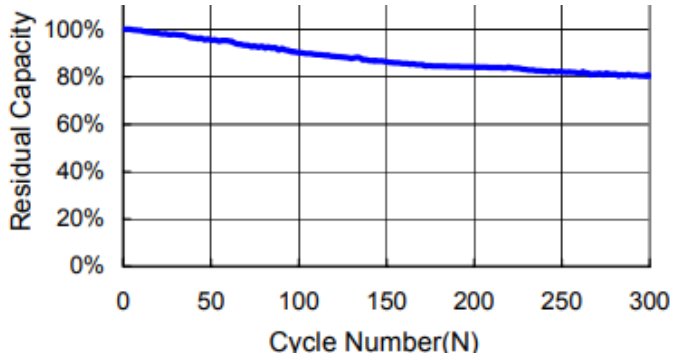

Figure 2.36 *Discharge capacity as a function of cycle age [5]*

A negative linear relationship is visible between discharge capacity and cycle age in *figure 2.36*. Given that the OCV-SoC curve is little to no affected by cycle age (2.2.1), the increase of internal resistance is the one that causes the decrease in discharge capacity.

2.2.6 Battery management system protection

The fault characteristics of the battery are given in previous subsections, but that does not mean that the fault current will actually have that value. Every rechargeable battery has a battery management system (BMS) that monitors the battery and its parameters:

- Voltage
- Current
- Temperature
- Etc.

By monitoring these, limits can be imposed so that the batteries can function optimally without damaging them. Some parameters are discussed below.

Voltage

The manufacturer provides some values for the voltage:

- Nominal voltage
- Minimum operating voltage
- Maximum operating voltage

The nominal voltage is the average voltage that a battery outputs when its charged. The minimum and maximum operating voltage is the range in which the battery can operate. It prevents the battery from overcharging and overdischarging. At these values, the battery is considered fully charged and fully discharged. The BMS ensures that the battery is operating within these limits. When discharging at high current rates, the OCV-SoC curve drops and possibly the undervoltage protection intervenes before the overcurrent protection does in case of excessive currents.

Current

In the datasheet, there are also current related parameters given:

- Recommended charge/discharge current
- Maximum charge/discharge current
- Peak charge/discharge current

The recommended charge/discharge current or recommended C-rate is the current that should be used to extend the battery life. The maximum charge/discharge current is the current at which the battery can continuously operate. The peak discharge current is the current that the battery can provide for just a few seconds without damaging the battery.

Manufacturers do not always provide the peak current for Li-ion batteries. The discharge current is generally limited at 2C [7], but can vary depending on the manufacturer of the BESS. This limit is imposed by the BMS and is often adjustable. There are several methods for limiting the current:

- **Fuse:** If $(I^2t)_{max}$ is exceeded when feeding the overcurrent, the fuse in the DC circuit of the battery cuts the current. This method will mainly be used in home grid storage, where there are rarely vital loads.
- **Limiter:** The BMS limits the fault current at its overcurrent value, e.g. 2C, after detecting the fault. If the fault is not eliminated after n seconds, the BMS reduces the current to its rated magnitude, or a little less to compensate for the generated heat. The value for n is typically around 0-5 s. In this case, the undervoltage protection will typically cut off the battery if the current becomes too high.
- **Limiter + fuse:** The BMS limits the current at its overcurrent value, e.g. 2C, after detecting the fault. If the fault is still there after n seconds, the BMS overcurrent protection cuts the current.

If the short-circuit current is too high, e.g. 10C, the BMS will immediately cut off the battery. This can originate from internal faults as well as external faults with very small fault impedance. If the BESS inverter is strongly oversized relative to the battery, this situation may occur.

Batteries used in BESS systems work closely with the inverter, so the overcurrent limits/protections of the battery and inverter can be adjusted to each other.

Temperature

The heat caused by excessive currents is a factor that can damage the battery. Therefore, the BMS can limit the current to a lower magnitude or cut off faster when the operating temperature is higher. In the event of a fault situation, the temperature of the battery can rise due to the high currents that flow through the internal resistance, see *formula (2.14)*, which can cause damage. A temperature-sensitive fuse can be incorporated into the battery circuit. The cut-off time of these fuses is lower when the ambient temperature is higher to avoid excessive heating. An example of a time-current characteristic of a temperature-sensitive fuse is illustrated in *figure 2.37*.

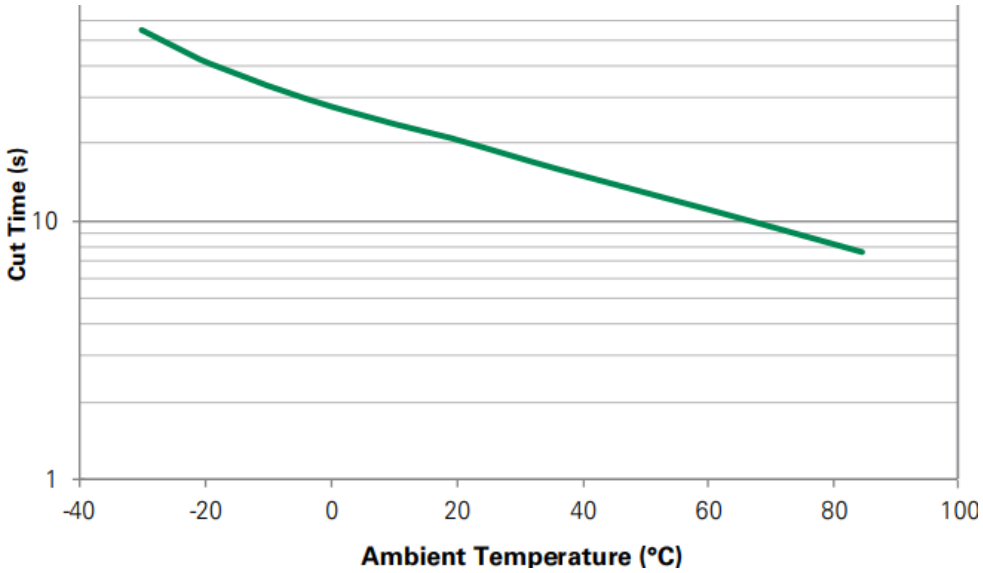

Figure 2.37 *Example of a temperature sensitive fuse: time-temperature curve [54]*

This overcurrent/overtemperature protection device is the last option because if this fuse burns, the battery completely fails and the battery is no longer operational. It can be seen that the current is cut faster when the ambient temperature is higher. It can be assumed that the time-temperature curve for the BMS overcurrent limiting is similar to this one, so also temperature dependent. The BMS does need to ensure that the, e.g., 2C overcurrent is interrupted before this three-terminal fuse burns so that the battery remains operational.

The manufacturers always give an operating temperature range in which the battery may operate. If the temperature of the battery is outside this range, the BMS makes the batery stop feeding. The BMS constantly monitors the battery temperature and cools or heats it as needed.

2.2.7 Overview

In this section, the fault current characteristics of a battery have been discussed. The fault current can be determined using *equation (2.6)*, but both OCV and R_{int} get affected by the SoC, temperature, discharge current and cycle age/SoH. The current does not immediately rise to its highest peak value but is first counteracted somewhat by the inductance of the battery. This ”delay” lasts only 15 ms. As a result of the feeding current, the battery heats up (Joule heat). However, Joule heat is only a fraction of the heat developed and the battery is additionally cooled.

The discharge capacity of the battery depends on the SoC, discharge current, temperature and cycle age. However, considering the time frame of 0-5 s, the period that the fault current can be supplied will depend mainly on the control and protection mechanisms of the battery, rather than the discharge capacity itself. The BMS overcurrent protection can limit or cut the current. The

period that this current can be fed is temperature-dependent. The battery should be able to feed a significant fault current for a sufficiently long time so that an external fuse interrupts the fault before the BMS cuts off the battery. That way, the battery can continue to feed other loads when the fault is cleared. However, the profile of a battery's fault current will always look similar. The principle is illustrated in *figure 2.38*.

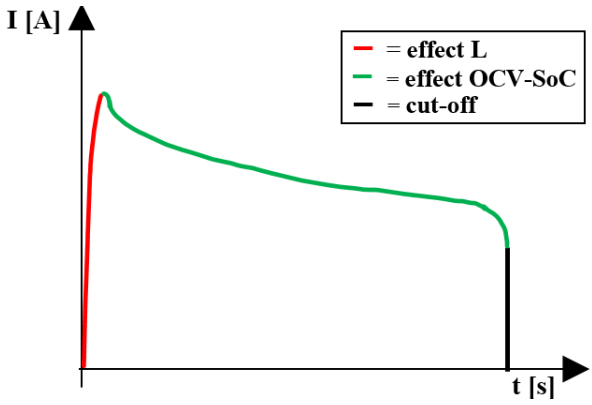

Figure 2.38 *Fault current profile supplied by a battery*

In the first ≈ 15 ms, the battery current rises to the peak value with some delay as a result of the inductance L. Immediately after reaching the peak value, the current decreases due to the decrease in OCV as a result of the decrease in SoC. The discharge current continues to decrease as the battery is discharged until the cut-off voltage is reached. Due to discharge current, temperature and cycle age, the current can vary in magnitude. Polarization behaviour can also cause the current to decrease. The internal resistance of the battery increases due to the RC elements. However, this information cannot be extracted from the manufacturer's datasheets. It should be kept in mind that depending on the order of magnitude of the polarization resistance compared to the ohmic resistance and considered time frame, polarization phenomena can have a significant impact on the fault current.

In an ideal short-circuit, i.e. no fault resistance, both OCV and internal resistance have a significant impact. However, in a BESS there is the impedance of the inverter and other components, so the battery observes more than just its internal resistance. Therefore, the OCV will be the most significant parameter and this parameter is affected mainly by the SoC and discharge current.

2.3 Fault current characteristics of inverters

A BESS is an inverter-based energy source. The inverter converts the DC voltage to AC voltage. Batteries can also operate in rectifier mode when the battery is charging, but this is out of scope. The inverter control will in many cases be the determining factor, but is not the emphasis here. However, the inverter cannot be excluded as it is part of the BESS. The limits of the inverter should be discussed, as they should not be exceeded. So only what the BESS inverter's manufacturer provides is considered here in regard to fault events. With this information, the exact behaviour of the inverter, e.g. switching control and distortion, cannot be determined. The discussed parameter serve an averaged model.

2.3.1 Inverter topologies

The detailed control of the inverter is not discussed in this thesis, but since the inverter is part of the BESS model, the principle of its control circuit should be introduced. The principle of converter control is illustrated in a simplified scheme in *figure 2.39*.

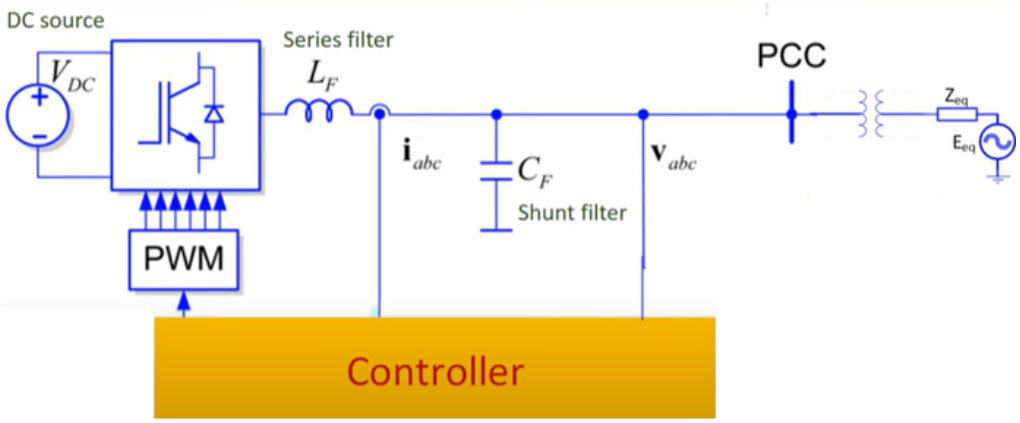

Figure 2.39 *Principle power converter control [33]*

Using pulse width modulation (PWM), the DC voltage is converted to an AC voltage. A sine wave is obtained at the output, but it still contains a lot of distortion, i.e. the desired shape has not yet been obtained. For that reason, filters are added on the output (AC) side of the inverter. These filters reduce the harmonics, to obtain the desired AC sine wave. The PCC is the point where the main grid and the microgrid are connected. Here, the DC source represents a battery. The controller measures the current i_{abc} and voltage v_{abc} of the phases in order to control the active power, reactive power, voltage, etc. of the inverter.

PI controllers are included in its control system. These controllers have upper and lower limits, depending e.g. on what the IGBTs can handle. The measurements can take place, e.g. current measurement before or after the inductor, which in turn determines how the control system is developed and works. The control system depends on the type of converter used. In article [33], a distinction is made between 3 types of converters:

- Grid-following converters
- Grid-forming converters
- Grid-supporting converters

The grid-following converters need another voltage source to operate. Grid-following converters themselves cannot operate in island mode, i.e., an AC microgrid needs a grid-forming inverter that sets the voltage amplitude and frequency to operate independently of the grid. The grid-forming converters can work independently without another voltage source, e.g. without the main utility grid. The AC voltage generated by the grid-forming converter is the reference for the rest of the connected power converters. For example, a grid-forming converter can be used for a UPS system.

The grid-supporting converters are in between the grid-forming and grid-following converters. They can both operate in grid-connected and island mode. A grid-supporting converter can be created from the grid-following control system and created from a grid-forming control system. Depending on the control system, the converter may or may not form its own grid, as already explained above. Also, the primary source of the converter is important, as it is difficult to form a grid with, e.g., PV systems. The fluctuations with batteries are much smaller. Hence, it is also easier to form a grid with this primary source. In 1.3, it is already mentioned that the worst-case scenario is when the BESS feeds the fault current in island mode, so the focus here is on grid-forming inverters.

2.3.2 Time frames of a fault

For IBDER, there are two different periods that provide fault current characterization [64]:

- **Period before the inverter detects the fault:** The period before fault detection by the IBDER is usually only 1-2 periods (20-40 ms). This is the generalized time period for IBDER, i.e. wind turbines, PV systems and BESS, but might be shorter for BESS as the battery output can be controlled faster. During this period, two factors are important: the residual terminal voltage of the inverter and the pre-fault operating condition. Power is proportional to the product of voltage and current. To keep the output power constant at this lower residual voltage, the output current increases normally to 1.1-2.0 p.u., after (possibly) a short spike in the current.
- **Period after the inverter detects the fault:** Once the inverter has detected the fault, the inverter control determines the characteristics of the fault current. The fault current is maintained at a particular magnitude, depending on the voltage drop at the terminals and the characteristics of the inverter.

2.3.3 Output current limiting

If the inverter is not strongly oversized, i.e. relative to the nominal needed capacity, IBDER cannot provide the same high currents as synchronous generators. Although passive components such as inductors, capacitors and transformers can withstand the short-circuit currents if they are properly designed, the switching components, e.g. IGBTs, cannot withstand high short-circuit currents. If an fault occurs, the voltage will drop while the inverter's reference powers remain the same. As a result, the current rises dramatically and the power electronic components may be damaged. Therefore, current limiting is needed. As a result, when an IBDER is operating in island mode, the fault current can be much smaller than when the main grid is feeding the fault current. The maximum current that can flow through an inverter corresponds to the current through the inductor L_f, which is measured by the inverter control (*figure 2.39*).

Overcurrent

If a fault occurs and the overcurrent limits are exceeded, the inverter does not always react the same. However, time-current curves can be constructed but manufacturers rarely provide these.

Generally, an overcurrent value is provided, but no details about the current limiting itself, so assumptions need to be made. The principles are illustrated using an example. The manufacturer gives an overcurrent limit of 1.5 p.u. and this current can be fed for 10 s.

Option 1: The inverter acts like a fuse and cuts the current when $(I^2t)_{max}$ is exceeded.

$$(I^2t)_{max} = 1,5^2 \cdot 10 = 22.5 \ A^2s \ ^* \tag{2.28}$$

(** Current in [p.u.], so 'A^{2}s' is incorrect, but assume that $I_{rated} = 1A$ to illustrate the principle*)

When the current is different from 1.5 p.u., the interruption time can be calculated.

$$t = \frac{(I^2t)_{max}}{I_{inv}^2} \tag{2.29}$$

This means that at a current of, e.g., 3 p.u., the current is interrupted after 2.5 s. If the inverter current $\leq$ 1.0 p.u., the current can be fed for an unlimited amount of time. The time-current curve is illustrated in *figure 2.40*.

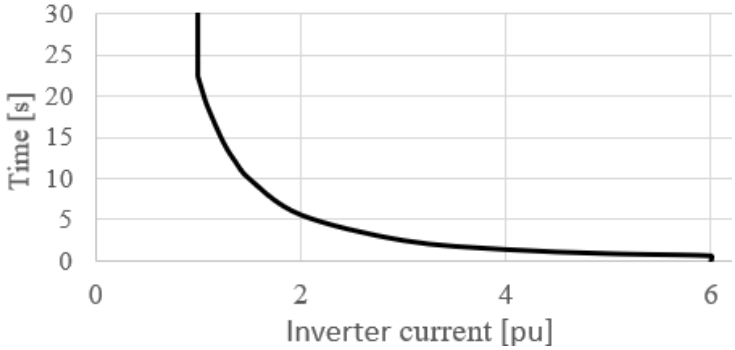

Figure 2.40 *Time-current limit inverter: option 1*

There is also a current level where the inverter cuts off immediately. In the current-time curve above, 6 p.u. is taken as the instantaneous cut-off current. These are realistic, but not general, values to outline the principle. This mode could be used for non-critical loads.

Option 2: Most inverters will limit the current at a particular threshold value. The control circuit limits the current if it goes above the rated current. In this situation, the inverter goes from voltage control to current control/limiting. The overcurrent-time curve can be seen in *figure 2.41*.

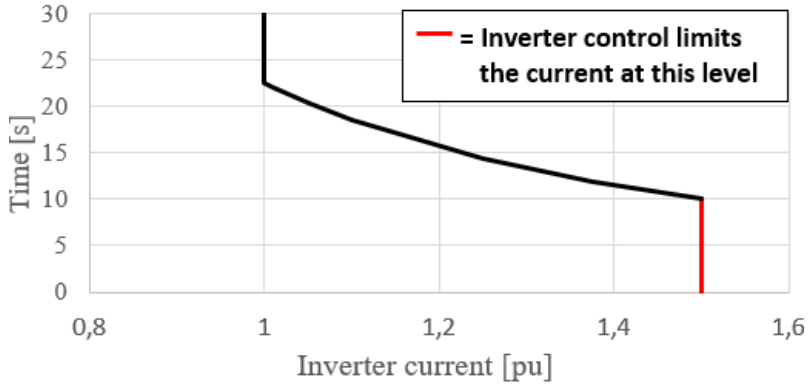

Figure 2.41 *Time-current limit inverter: option 2*

This curve can be interpreted in two ways:

- **Fuse:** The inverter operates as a fuse protection, so if I^2t is exceeded, the inverter cuts off.
  1. $\mathbf{I_{inv} \leq 1.0}$ **p.u.:** The inverter can feed this current continuously.
  2. **1.0 p.u.** $\mathbf{< I_{inv} \leq 1.5}$ **p.u.:** The maximum energy $(I^2t)_{max} = 1.5^2 \cdot 10 = 22.5\ A^2s$ cannot be exceeded. For example $I_{inv} = 1.25A : 1.25^2 \cdot t_{cut-off} > 22.5 \rightarrow\ t_{cut-off} = 14.4\ s$
  3. $\mathbf{I_{inv} > 1.5}$ **p.u.:** Current is limited to 1.5 p.u.. If the fault is not cleared after 10 s, the inverter stops working.
- **Limiting:** The inverter doesn't cut off the current but limits the current to the values which can be derived from the curve in *figure 2.41*.
  1. $\mathbf{I_{inv} \leq 1.0}$ **p.u.:** The inverter can feed this current continuously.
  2. **1.0 p.u.** $\mathbf{< I_{inv} \leq 1.5}$ **p.u.:** If the initial current value is 1.25 p.u., the inverter feeds this current for 14.4 s. After this period, the current is limited to lower currents, e.g. 1.0 p.u.
  3. $\mathbf{I_{inv} > 1.5}$ **p.u.:** Current is limited to 1.5 p.u. This current can be fed for 10 s according to the curve, but the current is going to be reduced to 1.0 p.u. over a period of time. The limiter can also reduce the current to lower magnitudes than 1.0 to counter the heat due to the overcurrent.

Assume that the current > 1.5 p.u. and the inverter limits the current. In case of a symmetrical fault (e.g. three-phase fault) all phase currents will be limited to 1.5 p.u.. The output current i_o as a function of time in this situation is shown in *figure 2.42*.

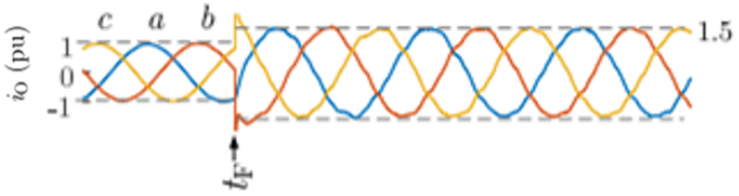

Figure 2.42 *Output current limited in symmetrical three phase fault event [55]*

The fault occurs at time t_f. At t_f, a short peak can be seen indicating that the limiter has not been able to react yet. After this, the current in each phase is limited to 1.5 p.u.. The current is not always limited in each phase in the presence of a fault, e.g. unsymmetrical faults. An example of the current behaviour of an asymmetrical fault is shown in *figure 2.43*.

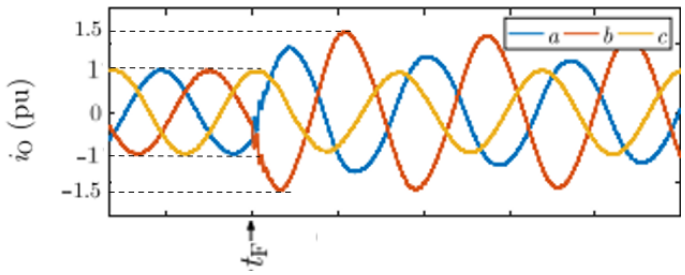

Figure 2.43 *Output current limited in asymmetrical single line to ground fault event[55]*

The current is limited in phase b, but not in phases a and c. This means that the current threshold is not reached in phases a and c, so no limiting is needed. The overcurrent limit response depends on the inverter's control strategy. Since the IGBTs must not carry too much current, the current is assumed to be limited to the peak value, not the RMS value. The sine waves will be flat topped in reality. The curves in *figure 2.42* and *figure 2.43* outline the principle, not the exact dynamic behavior. The limiting is usually done at the DC side, because of the lower switching frequency, resulting in fewer switching losses. In this way the current does not exceed the upper limit, apart from the short spike in the beginning. Current limiting is commonly used in inverters.

Manufacturers rarely disclose whether the current is limited or gets cut off, assumptions must be made based on the application. This thesis investigates BESS that have islanding capability. The design requirements for inverters that have islanding capability, i.e. grid-forming converters, can differ from grid-connected converters. It can be needed that the inverter has the ability to feed 2-3 times the rated load current for up to 10 s to support stand-alone applications [64].

2.3.4 Output voltage

Due to a fault in the grid, the voltage at the PCC can drop significantly. In *figure 2.44*, an example of a fault current circuit is illustrated.

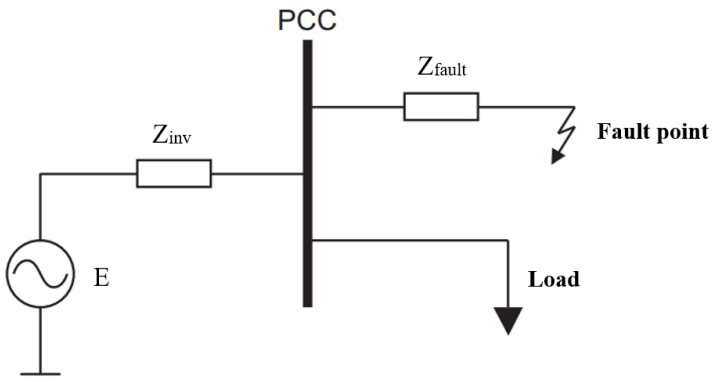

Figure 2.44 *Example fault situation*

The steady-state voltage at the PCC V_{PCC} during the fault can be calculated:

$$V_{PCC} = E \cdot \frac{Z_{fault}}{Z_{fault} + Z_{inv}} \tag{2.30}$$

Where E is the internal voltage of the inverter, Z_{fault} is the fault impedance and Z_{inv} the internal impedance of the inverter. This principle applies for both conventional generators and IBDER, but additional issues for IBDER must be discussed. Inverters do not the same as synchronous generators, where the voltage drop at the PCC can be determined from physical laws. Inverters behave differently because their regulators can react to fault currents, which can affect the voltage at the PCC.

Components

The conversion of DC voltage to AC voltage contains distortion, so filters are used. In the inverter control topology in *figure 2.39*, the use of an LC filter can be seen. To make a realistic grid-forming inverter model, the filter must be considered. For the determination of the values of inductance and capacitance, methods specified in [44] are used. An LCL filter is considered. The configuration of this filter is illustrated in *figure 2.45*.

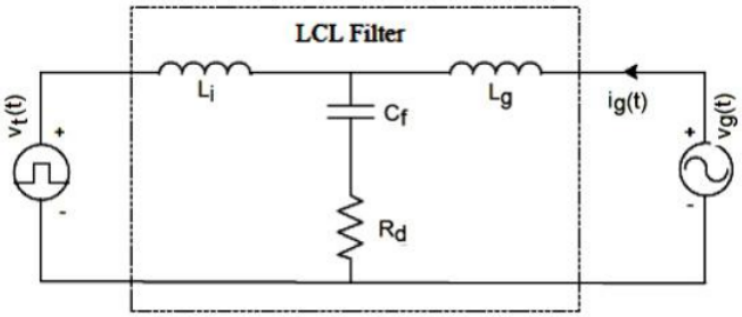

Figure 2.45 *Inverter LCL filter [44]*

$$L_i = \frac{V_{DC} \cdot U_n}{16 \cdot f_s \cdot 0.01 \cdot P_n \cdot \sqrt{2}} \tag{2.31}$$

$$C_f = \frac{0.05 \cdot S_n}{\omega_n \cdot U_n^2} \tag{2.32}$$

$$L_g = 0.6 \cdot L_i \tag{2.33}$$

$$R_d = \frac{1}{3 \cdot C_f} \cdot \sqrt{\frac{L_i \cdot L_g \cdot C_f}{L_i + L_g}} \tag{2.34}$$

- V_{DC} is the DC input voltage of the inverter [V]
- U_n is the nominal AC voltage [V]
- f_s is the switching frequency of the inverter [Hz]
- P_n is the nominal active output power [W]
- P_n is the nominal apparent output power [VA]
- ω_n is the angular grid frequency $= 2\pi \cdot f_n$ [Hz]

Controlled voltage drop during fault

The voltage of the grid-forming inverter can be controlled by droop control during normal operation. The internal voltage of the inverter source itself is controlled. Although control circuits are not considered in the simplified model, this principle should be introduced to get an idea of what happens to the inverter voltage during fault situations.

An example of a circuit where the voltage can be regulated using droop control is presented in *figure 2.46*.

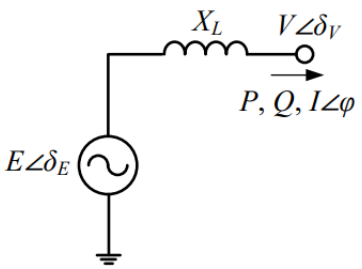

Figure 2.46 *Equivalent circuit inverter internal voltage and coupling reactance [47]*

In this figure, a coupling reactance X_L is also added to connect the inverter to the LVAC grid. This reactance is important for the design of the droop controller. The behaviour in normal operation is discussed in [47] but is beyond the scope of this thesis.

During normal operation, this droop control regulates the voltage, but during fault events, a fault current limiting function can be activated. This function can be activated if $I > I_{max}$.

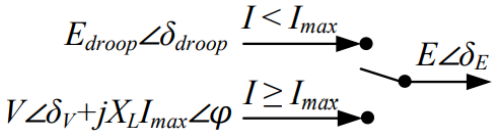

Figure 2.47 *Fault current limiting function [47]*

When switching to fault current limiting mode, the internal voltage of the inverter can be calculated using the sum of the terminal voltage $V\angle\delta_v$, coupling reactance X_L and new current phasor $I_{max}\angle\phi$, as illustrated in *figure 2.47*. Consequently, in fault events, the internal voltage can be much lower than the nominal internal voltage E.

Fault-ride-through

The ideal fault response to a voltage dip of an electrical generator is represented in *figure 2.48*. The current response to an asymmetrical fault, i.e. the DC offset, is illustrated here.

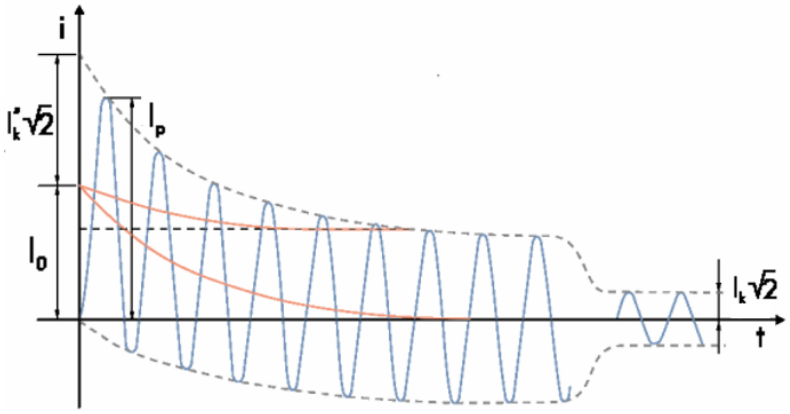

Figure 2.48 *Response to voltage dips of synchronous generators [60]*

This curve applies to conventional generators, such as an synchronous generators. The same curve can be applicable for an IBDER, if the control is not restricting the current, but there is a difference in the magnitude of fault current and progression in terms of time. This means that the X/R ratio of the inverter is lower than for conventional electric generators, resulting in less inertia in the current. However, similar values can be established such as the peak short-circuit surge current I_p, RMS initial symmetrical short-circuit current $I_{k"}$ and RMS uninterrupted short-circuit current I_k. For SMA inverters [60], I_p lasts no longer than 40 μs and varies typically between 2 to 10 times the inverter's maximum current. If there is a battery on the DC side, it should not be able to feed these high currents to cause them. Short surges can be fed by a small capacitance. $I_{k"}$ lasts up to 50 ms and varies between 1 to 2 p.u.. After this 50 ms, I_k, with a usual magnitude of 1.0 p.u., is maintained during the entire period of the voltage drop. These periods may vary depending on the manufacturer of the inverter, so these are not universal values. The magnitudes of these currents depend on the type of inverter. These values can be found in the manufacturer's datasheet [60].

The capability of the inverter to remain in service during voltage dips and inject reactive current to support the grid voltage is called fault ride-through (FRT) or low voltage ride-trough (LVRT). Likewise, when an island is formed, the inverter must continue to supply if the voltage drops at the PCC. Inverters can have three FRT modes: full FRT, partial FRT and a combination of both [60] [17].

- **Full fault-ride through:** The inverter continues to feed regardless of the voltage at the PCC. If mode is selected, the inverter will still stop feeding after a few tens to hundreds of milliseconds, if the fault is not cleared during this time period, since loads cannot operate at low voltages. Because of the inertia of the loads, they can tolerate short dips. This can be used to avoid power loss when a grid fault causes a very short but large voltage drop.
- **Partial fault-ride through:** In this mode, a threshold is established that is lower than 1.0 p.u. When the voltage at the PCC drops below this threshold, the inverter stops feeding the current.
- **Combination:** The FRT can be a V-t curve, as illustrated in *figure 2.51*. This can be seen as a combination of full FRT and partial FRT. This capability is imposed by the grid operators for larger IBDER (> 1MW) to avoid large power losses due to grid faults.

The output phase voltages and current response of a full FRT inverter to a voltage dip due to a fault is given in *figure 2.49*.

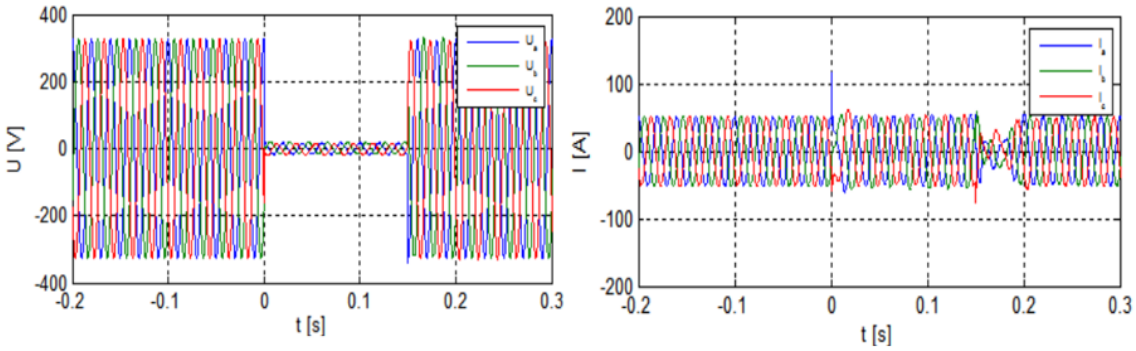

Figure 2.49 *Reponse inverter with full FRT capability to a voltage dip [60]*

Full FRT capability means that the inverter remains connected when a voltage dip occurs. The voltage dip occurs on t=0 s. The inverter continues supplying current during the 150 ms lasting voltage dip. The I_p, $I_{k"}$ and I_k are visible in the output current response.

In partial FRT mode, the inverter stops feeding if the PCC voltage drops below a particular threshold, under the condition that the maximum current limit of the inverter is not exceeded. In figure *figure 2.50*, an example of an inverter that has an FRT threshold of 70% V_n is shown.
The inverter rides through when the voltage during the voltage dip remains above the threshold of 70% of the nominal voltage. In *figure 2.50a*, it can be seen that the inverter rides through when the voltage at the PCC is kept above the 70% threshold. When the voltage at the PCC can't be kept above 70% of the nominal voltage, the inverter stops feeding, as illustrated in *figure 2.50b*.

When integrating BESS, or IBDER in general, the installation must comply with the grid code. In Finland, the grid code is created by Fingrid, the national transmission grid operator [17]. For BESS that have an output power higher than 1 MW and are integrated into the grid, a requirement called fault-ride-through (FRT) or low voltage ride-through (LVRT) is imposed.

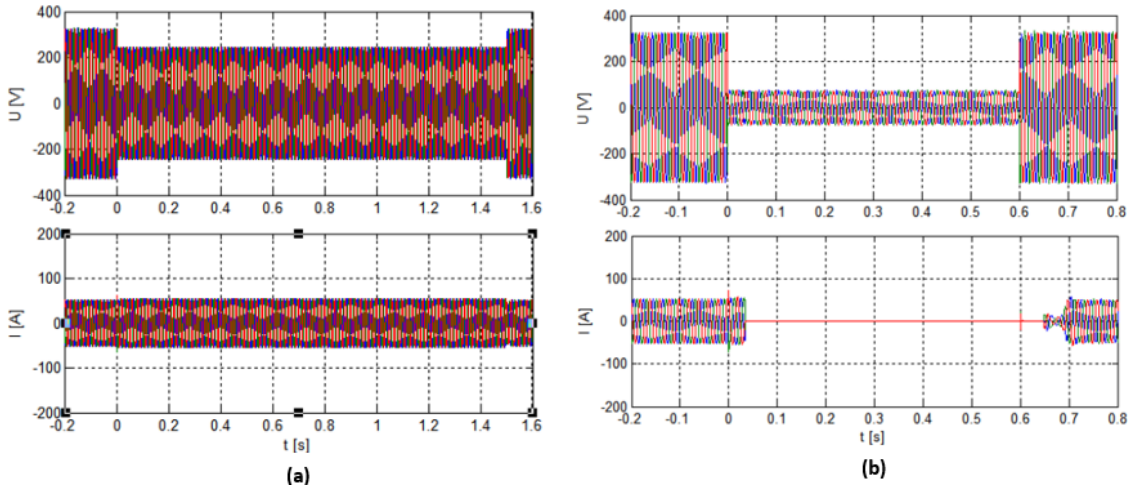

Figure 2.50 *Reponse inverter with partial FRT threshold of 70% V_n (a) Voltage dip to 75% V_n (b) Voltage dip to 30% V_n [60]*

This means that the IBDER must remain connected when the voltage drop from an external fault falls within the fault-ride-through requirement of the grid code. These requirements are similar across most regulators, subject to some minor differences. The FRT requirements; imposed by Fingrid; are illustrated in *figure 2.51*.

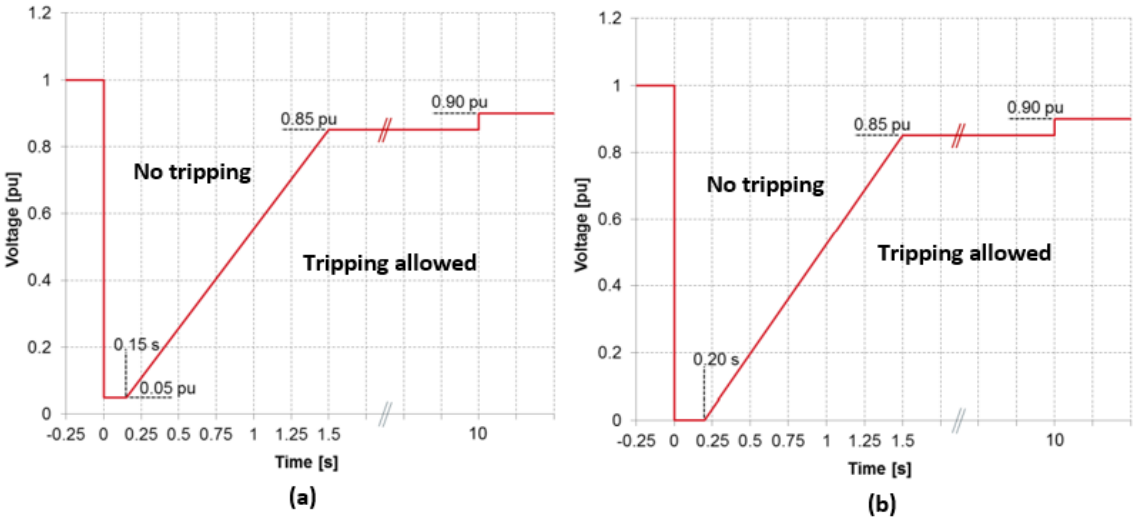

Figure 2.51 *Fault-ride-through requirement by Finnish grid code (a) 1 MW < P_{IBDER} ≤ 30 MW (b) P_{IBDER} > 30 MW [17]*

Fingrid imposes different requirements for IBDER with $P_{IBDER} > 1MW$. The code is different for 1 MW < $P_{IBDER} \leq 30$ MW and $P_{IBDER} > 30$ MW. These requirements are given in respectively *figure 2.51*a and b. No FRT requirements are imposed by Fingrid for IBDER < 1 MW.

2.3.5 Other technical data

Efficiency

Inverters have losses converting DC voltage to AC voltage. This efficiency is the ratio of AC power it can provide for the given input DC power and is given by the manufacturers as a function of the output power [61]. An example of an efficiency curve is illustrated in *figure 2.52*.

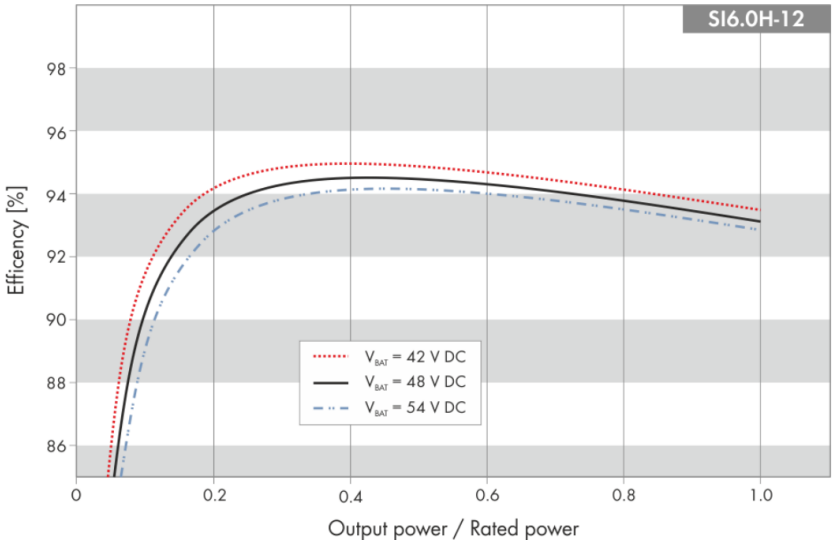

Figure 2.52 *Example efficiency curve inverter [62]*

Inverters generally have an efficiency close to 100%. In *figure 2.52*, it can be seen that the efficiency of this inverter varies slightly as a function of output power. Note that the efficiency is higher for lower input voltages. The impact of the input voltage on the inverter's efficiency depends on the type of inverter, no general correlation can be drawn up. In general, the efficiency is 90-98%.

The highest efficiency is reached at $\approx$ 0.4 p.u. output power. If the output power is even higher, an approximately linear relationship between output power and efficiency can be observed. Comparing the 0.4 p.u. output power and 1.0 p.u. output power, the efficiency is 1% lower. Assuming that this relationship remains linear when feeding overcurrents, the efficiency is $\approx$ 90% when feeding 2.5 p.u. current. These values are not generally the same. For SMA inverters, the relationship between the efficiency and output power for $p_{output} > 0.4$ p.u. is usually linear.

DC input

In a BESS, the battery is connected to the DC side. The battery should be able to feed enough power, but it should also work in the right range. There is a DC voltage range within which the inverter can operate. If the input DC voltage drops below the minimum input voltage, the inverter stops operating. Likewise, there is also a maximum operating voltage.

A maximum DC input discharge current can be provided by the manufacturer. It is possible for the inverter to cut the battery if this current is exceeded. In general, a rated current value is provided. However, if the overcurrent capability of the inverter is 1.5 p.u., it can be assumed that the maximum DC overcurrent is 1.5 p.u. as well because it flows through the same IGBTs. To protect the electrical connection between the DC source, i.e. battery here, and the inverter, a DC battery fuse can be added.

2.3.6 Overview

In this section, the fault current characteristics of an inverter has been discussed. Manufacturers typically give the overcurrent capabilities of the inverter, but not how they behave. Hence assumptions are needed for the behaviour of the overcurrent. In fault events, the voltage of the inverter can drop. This is the result of the voltage drop across the filter reactance, but also the current limiting droop control of the inverter. As a result of the voltage drop, the inverter might stop feeding, depending on the FRT characteristics.

2.4 Existing BESS models

So a BESS does not just consist of a battery itself. The inverter is needed to connect to the AC grid. In this section, some pre-existing models are presented that serve as support for creating the "own" BESS model for RMS fault calculations. The developed model will have a similar structure to the model whose block diagram is given below in *figure 2.53*.

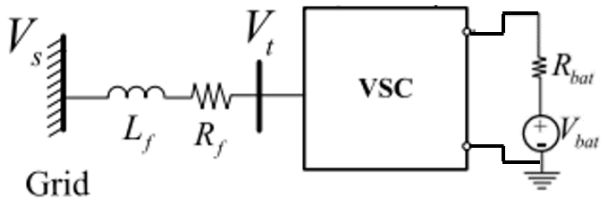

Figure 2.53 *Block diagram of BESS model with battery pack and inverter [36]*

This battery is connected to the voltage source converter (VSC). The voltage V_t at the output terminals of the inverter is filtered, here by the filter inductance L_f and has a resistance R_f. Here, the grid-connected mode is represented. The voltage V_s represents the voltage at the PCC. As depicted in *figure 2.53*, the DC side of the BESS, i.e. the battery side, is electrically isolated from the AC side, so these are not connected with conductors. However, these are linked to each other by control circuits.

2.4.1 Battery models

Because of the complexity of batteries, a lot of equivalent models have already been created. In [30] and [29], some created equivalent battery models are discussed. A lot of models are hard to interpret and define their parameters or not accurate enough. Discussing all existing models takes things too far. For this reason, three different types of battery models are discussed. These three models represent the three of the most commonly used types of battery models: the Rint model, the Thevenin model and the Shepherd model. The conclusions for similar models (e.g. first and second-order Thevenin model) are similar.

Rint battery model

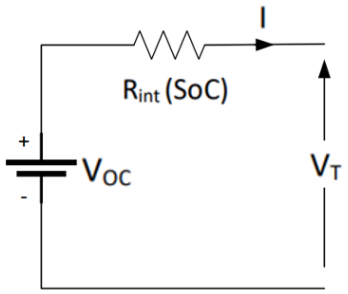

Figure 2.54 *Rint battery model [30]*

The first battery model is the internal resistance or Rint model from article [30], presented in *figure 2.54*. In this model, V_{oc} is taken as a constant value and R_{int} is taken as a function of SoC.
The voltage at the output terminal V_T can be calculated with the formula:

$$V_T = V_{oc} - R_{int}(SoC) \cdot I \tag{2.35}$$

With

$$R_{int}(SoC) = \frac{R_o}{SoC^K} \tag{2.36}$$

In this last formula is R_o the initial internal resistance of the battery when it is fully charged, SoC the state of charge of the battery and K a coefficient that is a function of the discharge rate.

Advantages:
This is one of the simplest battery models. Although the model itself does not consider many parameters, it is easy to further develop this model using information obtained from the manufacturer. As a starting point for the development of a new model, this model might be better than others since it is easy to interpret and extend. For example, this model was expanded in [69]. This model proved to be the best model for high C-rates. The discharge rate can be high in fault events, so this is an interesting fact.

Disadvantages:
A limitation of this model is that it does not take into account the fact that OCV depends on the SoC. Another constraint is that the model does not consider the temperature, discharge current and ageing dependence of the internal resistance. In normal operation, this approximation may be sufficient. In fault situations, OCV and internal resistance are strong determinants, see *equation (2.6)*, so the behaviour of these components must be more detailed.

Thevenin battery model

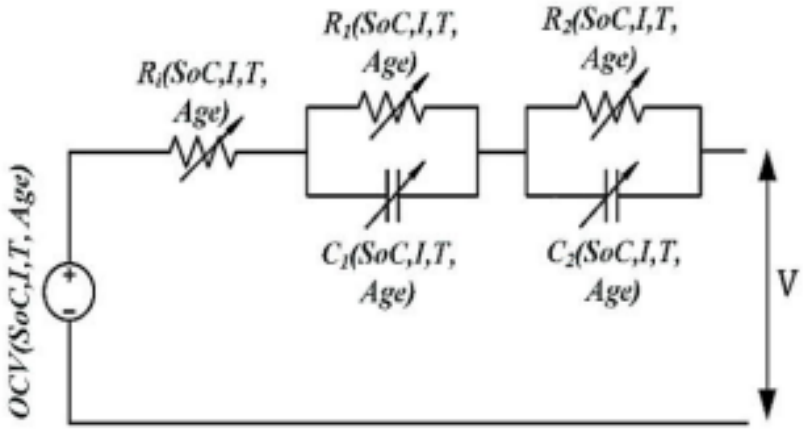

Figure 2.55 *Second order Thevenin equivalent battery model [20]*

In [20], a second-order Thevenin equivalent model is proposed (*figure 2.55*). The principle is similar to a first-order Thevenin model. This model indicates the OCV and R_{int} dependence of SoC, temperature, discharge current and cycle age.
The terminal voltage V can be given by the following formula:

$$V(t) = V_{oc} + R_i \cdot I(t) + R_1 \cdot I(t)(1 - e^{\frac{-t}{\tau 1}}) + R_2 \cdot I(t)(1 - e^{\frac{-t}{\tau 2}}) \tag{2.37}$$

With

$$\tau 1 = R_1 \cdot C_1 \tag{2.38}$$

$$\tau 2 = R_2 \cdot C_2 \tag{2.39}$$

The battery current $I(t)$ is negative in discharging mode. R_i is the ohmic resistance and the RC components in the model define the polarization resistance. Time constants τ_1 en τ_2 represent respectively the short-term and long-term transient behaviour.

The cycle age dependence of all components in the model is plotted in this article (*figure 2.56*). Note that this is an example and cannot be generalized.

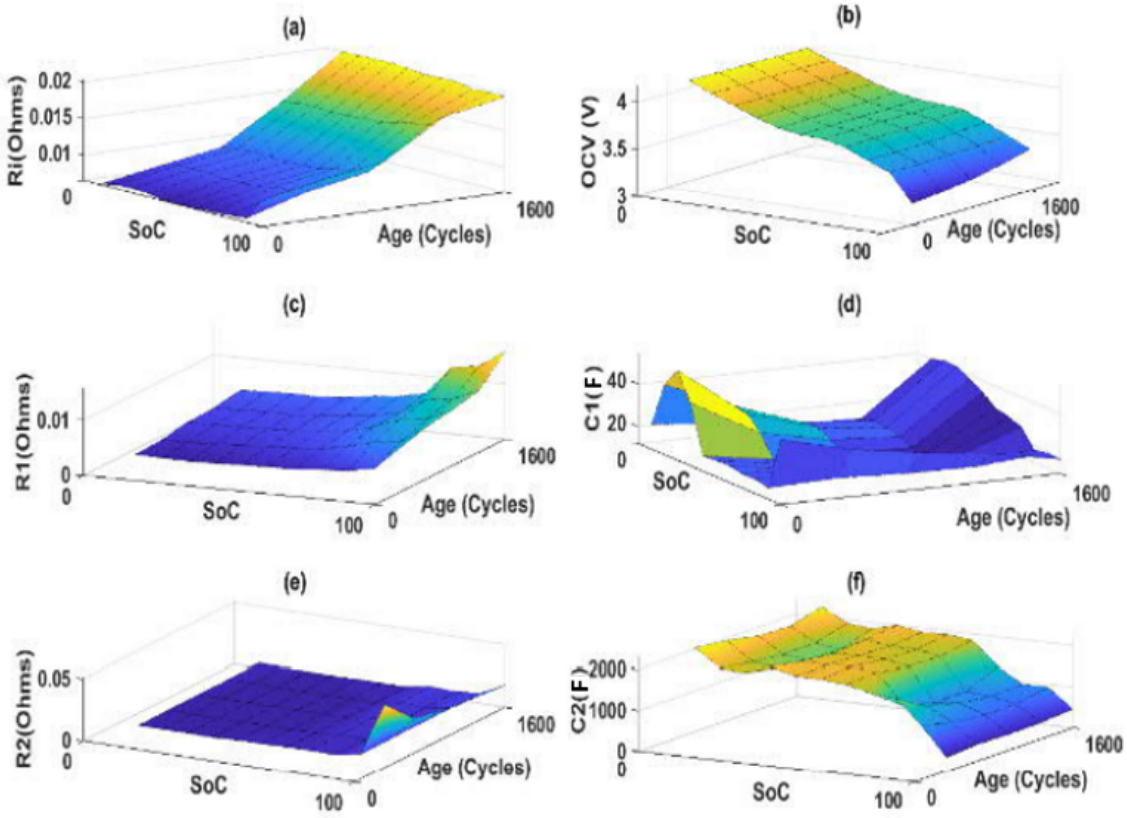

Figure 2.56 *3D plot of cycle age dependence of second-order Thevenin model components [20]*

The same things can be deduced from the article as from 2.2.2. After several cycles, the internal resistance increases. For capacitors, no clear relationship can be found between cycle age and capacitance. Note that the OCV decreases at higher SoC in this figure. This should probably be the DoD instead of the SoC.

Advantanges:

The internal resistance in this model depends on cycle age, operating temperature, SoC and current. These parameters are consistent with the parameters described in 2.2.2. In addition, the overall transient behaviour of the battery can be determined with this model.

Disadvantages:

Despite pointing out the effect of temperature and discharge current, these are not described in the article. The parameters are defined as a function of SoC and cycle age. It is difficult to determine all the resistive and capacitive components in Thevenin models without using complex impedance measurement methods, so the model is not very user-friendly relying on the information generally obtained from the manufacturer.

Non-linear battery model

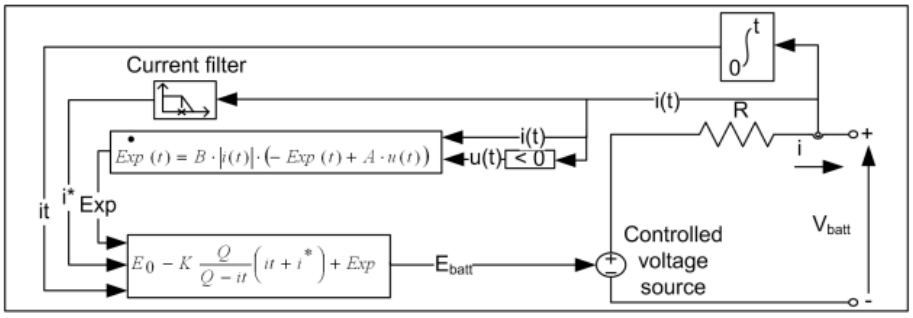

Figure 2.57 *Non-linear discharge battery model [70]*

In [70], a non-linear model for Li-ion batteries is proposed. The model is slightly different for charge and discharge modes, but since this thesis focuses on fault currents in discharge mode, the discharge battery model is presented. This model is based on the Shepherd model [1]. The mathematical equation describes the electrochemical characteristics of the battery in terms of the battery voltage, terminal voltage, internal resistance, discharge current and state of charge.

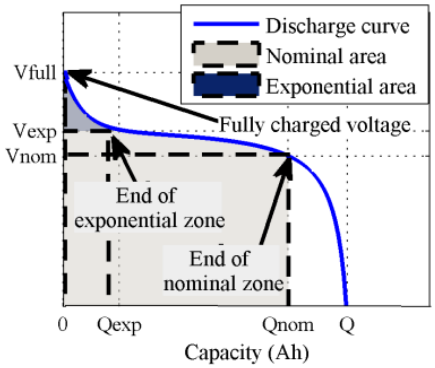

Figure 2.58 *Typical discharge curve NiMH battery [70]*

This discharge curve in *figure 2.58* is similar to other typical Li-ion batteries, e.g. LFP batteries. The curve is divided into an exponential and a nominal zone.
Using the discharge curve, that is usually provided by the manufacturer, the parameters for the following equation can easily be determined:

$$V_{batt} = E_0 - K\frac{Q}{Q - it} \cdot (it + i^*) + A \cdot e^{-B \cdot it} - R \cdot i \tag{2.40}$$

V_{batt}	Output terminal voltage of the battery [V]
E_0	Battery constant voltage [V]
K	Polarization constant $[\frac{V}{Ah}]$
Q	Actual battery charge [Ah]
$it = \int i \cdot dt$	Battery capacity [Ah]
i^*	Filtered current [A]
A	Exponential zone amplitude [V]
B	Exponential zone time constant inverse $[Ah^{-1}]$
R	Internal resistance of the battery [Ω]
i	Battery current [A]

To extract these parameters, some points must be determined on the discharge curve. The voltage at which the battery is fully charged V_{full}, the parameters at the end of the exponential zone V_{exp} and Q_{exp}, the parameters at the end of the nominal zone V_{nom} and Q_{nom} and the maximum discharge capacity Q (see *figure 2.58*). The internal resistance R is considered constant and is given by the manufacturer. In steady-state, the filtered current i^* is equal to the battery current i. When the battery is fully charged (V_{full}), there is no discharge current so i and i^* are 0. The battery constant voltage E_0 is set equal to V_{exp}. From *equation (2.40)*, A can be determined:

$$V_{full} = V_{exp} + A \tag{2.41}$$

This parameter A is the voltage drop of the exponential zone. At the end of the exponential zone, the time constant B can be approximated as follows:

$$B = \frac{3}{Q_{exp}} \tag{2.42}$$

Factor 3 is used here because after 3 time constants, the energy of the exponential term ≈ 0 (5%). Considering the end of the nominal zone, the factor K can be calculated using *equation (2.40)*:

$$K = \frac{(V_{full} - V_{nom} - R \cdot i + A \cdot e^{-B \cdot Q_{nom}}) \cdot (Q - Q_{nom})}{Q \cdot (Q_{nom} + i)} \tag{2.43}$$

The battery constant voltage can then be calculated as follows:

$$E_0 = V_{full} + K + R \cdot i - A \tag{2.44}$$

With i here being the rated current, which is often 1C (e.g. 100A for 100Ah battery).
For the development of this battery model, some assumptions were made:

- The internal resistance R is constant during the process
- The battery's capacity does not change by different discharge currents (no Peukert)
- The battery model is unaffected by the operating temperature
- No self-discharge of the battery
- The battery has no memory effect. This is the effect that the battery seems to lose capacity due to repeatedly recharging after partially discharging. However, Li-ion batteries are considered to have no memory effect [72].

Besides, this model has also some limitations:

- The minimum battery voltage V_{batt} is 0 V and the maximum battery voltage $2 \cdot E_0$.
- The battery has a minimum capacity of 0Ah and cannot be overcharged (less relevant for discharge mode)

In article [29], the Shepherd model is compared with the other similar non-linear models: Manegon model and the Coppetti model. The Coppetti model is considered to be the most accurate model in this article. However, it is noted that this model is much more complex and the parameters are more difficult to determine. In terms of combining user-friendliness and accuracy, the Shepherd model is the most applicable.

Advantanges:
This is already a well-developed model that can make accurate approximations for cell voltage. With this model, it is possible to accurately estimate the terminal voltage of the battery as a function of current and SoC.

Disadvantages:
For higher discharge currents, the model is unable to make correct approximations of the terminal voltage. This was investigated in [69] and it was found that for a discharge current of 6.67C, the discharge curve could not be properly approximated using the Shepherd model. Given the objective is to develop a model for fault currents, i.e. high currents, this is a drawback.

Evaluation battery model

For the evaluation of battery models, a table is created with three parameters:

- **Complexity:** If the battery model is very complex, it sacrifices user-friendliness. It should be assumed that the user is not necessarily someone with a lot of background knowledge about batteries. Complex models are more difficult to improve or extend, so this is also undesirable for the purpose of this thesis.
- **Accuracy:** The models should predict the behaviour of the battery as well as possible. Particularly accuracy at higher discharge currents, i.e. fault currents, is important
- **Data:** The battery model is developed to predict the fault currents as best as possible using easily obtained data. If the values of the components in the model must be determined using experiments, usability is compromised.

In the table, (+) and (-) are used to rate the models: (+)(+) = very good, (+) = good, (-) = bad and (-)(-) = very bad.

Model	Complexity	Accuracy	Data
Rint model	(+)(+): Easy model to interpret and extend to a better model, as it only consists two components	(-)(-): In general not very accurate, no transient behaviour included when modeling only resistance	(+): All data is available from the manufacturer
Thevenin model	(+): Basic components and extendable to higher order Thevenin models, but high order models can become very complex	(+): The voltage's transient behaviour is included. Accurate in normal operation but less accurate for high discharge currents, as current itself affects the values of the components	(-)(-): Values of components need to be determined from experiments
Shepherd model	(-): The battery's behaviour is modeled with control loops, which makes it harder to extend	(-): Accurate in normal operation, but there are limitations in this model. Not accurate for high currents	(+): All data is available from the manufacturer. The constants can be determined based on the discharge curve

Table 2.1 *Evaluation existing battery models*

The Thevenin model is very accurate in normal operation, but requires experiments to determine the RC components. Besides, it is not very accurate for high currents if the affecting parameters of the components are not properly considered. Therefore, this model is not chosen. The Shepherd model is not accurate for high currents and is comparatively complex. Therefore, the choice is made to improve the simple Rint model. It is easily interpretable and expandable into a better battery model for fault current calculations.

2.4.2 Inverter model

In discharge mode, the AC side of the BESS is everything outgoing from the inverter. As mentioned in 2.3.1, there are different types of inverters. Consequently, their equivalent models differ. The simplified representation of inverters is discussed in [33]. Since the focus is on grid-forming inverters, models of grid-forming inverters are discussed in this section.

Grid-forming inverter

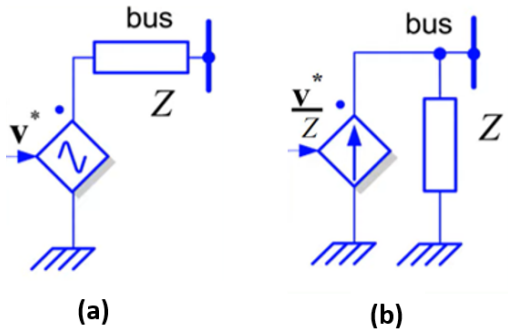

Figure 2.59 *Simplified representation of grid-forming inverter (a) Voltage source (b) Current source [33]*

In *figure 2.59*, the simplified model of a grid-forming inverter is outlined. This model also applies to grid-supporting forming inverters. This type of inverter is usually modeled as a voltage source with a series impedance *figure 2.59a*. This is because grid-forming inverters control voltage (and frequency), not power. This voltage source is represented as a complex current because it controls the active and reactive power output of the inverter. The impedance in series with the voltage source is small, so the inverter can often be approximated as an ideal voltage source. This is only considering the capability and limits of the inverter. If other factors are also considered, this impedance is variable and cannot be neglected.

The grid-forming inverters can also be represented as a current source by converting the Thevenin model of *figure 2.59a* to the Norton model in *figure 2.59b*. The Thevenin and Norton impedance are the same. The Norton current source can be calculated using Ohm's law:

$$i^* = \frac{v^*}{Z} \tag{2.45}$$

However, the approach of current-source modeling for grid-forming inverter is often inadequate.

Averaged inverter model

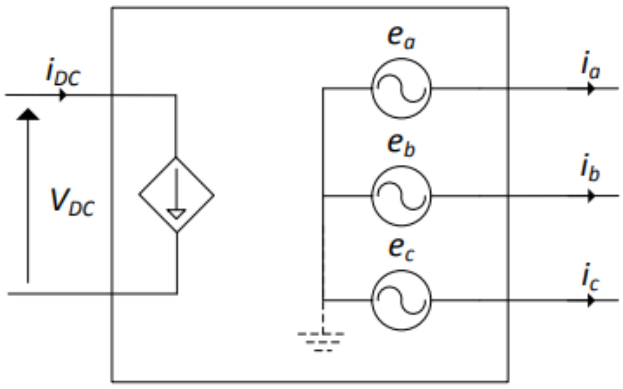

Figure 2.60 *Averaged inverter model [13]*

This averaged model is proposed for three-phase inverters in [13]. The DC and AC sides are electrically isolated from each other. This model doesn't consider harmonic distortion or other effects by PWM, since the switching action is not modeled. If the inverter is assumed to be lossless, the DC input power P_{DC} is equal to the output power P_{AC}. The power balance is given by the following formula:

$$V_{DC} \cdot i_{DC} = \sum_{j=a,b,c} e_j \cdot i_j \tag{2.46}$$

With V_{DC} and i_{DC} being the voltage and current on the DC level and e_j and i_j the voltage and current of the three phases a, b and c on the AC level. Since the AC voltage sources in grid-forming inverters operate as ideal voltage sources for which an amplitude of the voltage is imposed, no information about the PWM is needed.

Note that this is a simplified model. The discussed parameters in 2.3 serve this averaged model. To describe the exact operation, more details about the voltage conversion and the control system are needed.

3 Modeling BESS parameters

Based on the information in the literature survey, an own BESS model is developed, including the affecting parameters of the BESS. Both the battery and the inverter are assumed to be possible restrictive components. This model does not describe the full transient behaviour of the battery, only in a time frame of the first 5 to 10 s after the start of discharge.

3.1 Curve fitting

The affecting parameters must be estimated. This can be done by deriving equations using curve fitting. This method was chosen because, for example, the OCV-SoC curves of different types of Li-ion batteries have approximately the same shape, but the magnitudes can vary. All curve-fitting figures can be found in *Appendix A*. The Matlab Curve Fitting tool is used for this purpose. To assess if the original curve and fitted curve match sufficiently, two statistical terms are used that quantify how well the regression model fits the data: R^2 and $RMSE$. Linear fitting is used. The original curves are these obtained from experimental data/studies, which has been discussed in 2.2. Note that all curves discussed here were considered from theoretical findings or measurements and there is a margin of error here. However, it is stated that this is sufficient enough to approach the affecting parameters.

3.1.1 R-squared

As an evaluation of the curve fitting, the R^2 is determined. This is a metric that is the proportion of variation between the original curve and the fitted curve. It can be calculated as follows [24]:

$$R^2 = 1 - \frac{SSR}{SST} = 1 - \frac{\sum(y_i - \hat{y}_i)^2}{\sum(y_i - \overline{y})^2} \tag{3.1}$$

Where y_i is the y-value of the original curve, $\hat{y}_i$ is the y-value of the fitted curve and $\overline{y}$ is the mean of y. The value of this R^2 varies between 0 and 1. The higher the R^2, the better the fitted curve [14].

3.1.2 Root-mean-square error

Another evaluation method of curve fitting is the RMSE. This value tells the distance between the actual value and predicted value using the regression model [24]. It can be calculated as follows:

$$RMSE = \sqrt{\frac{\sum(\hat{y}_i - y_i)^2}{N}} \tag{3.2}$$

Where y_i is the y-value of the original curve, $\hat{y}_i$ is the y-value of the fitted curve and N is the number of samples.

R^2 and $RMSE$ are both evaluative parameters but tell different things. For this reason, it is interesting to determine both values. However, these are no guarantee of success. In addition to these evaluative parameters, the profile of the curve fits should be visually compared with the profiles illustrated 2.2.

3.2 Battery model

The fault current affecting parameters that are discussed in 2.2 will be incorporated into this model. To develop the model, the starting point is the Rint model, discussed in 2.4.1 and presented in *figure 2.54*. This is a basic model, but easy to modify and expand to a better model. This section defines the fault current affecting parameters. Protection devices must also be considered, so they are also defined.

3.2.1 Battery pack

The model being developed serves for BESS. This means that the battery must be able to provide an adequate amount of power and the voltage at the output terminal must be high enough to stay within the operating range of the inverter. In 2.2.2, it has already been outlined that series and parallel placing of batteries increases the battery voltage and current, so the power increases as well. Knowing this, the equivalent model of the battery pack is presented in *figure 3.1*

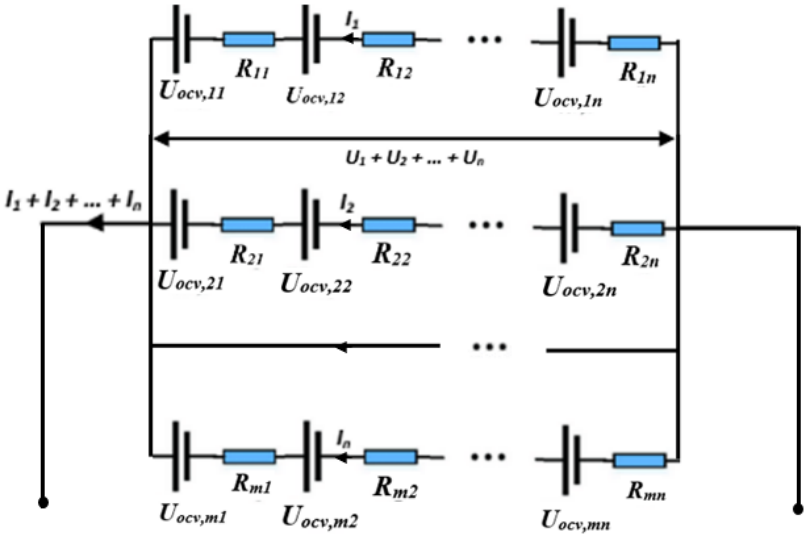

Figure 3.1 *Equivalent model battery pack with series and parallel connected batteries*

The equivalent resistance R_{eq} of this battery pack can be calculated using *equation (2.1)* and *(2.2)*. Combined, the resulting formula is obtained:

$$R_{int} = (\frac{1}{R_{11} + ... + R_{1n}} + \frac{1}{R_{21} + ... + R_{2n}} + ... + \frac{1}{R_{m1} + ... + R_{mn}})^{-1} \tag{3.3}$$

The equivalent current I_{eq} and voltage U_{eq} and can also be determined:

$$I_{DC} = \sum_{i=1}^{m} I_i \tag{3.4}$$

$$V_{oc} = \sum_{j=1}^{n} U_{ocv,1j} = \sum_{j=1}^{n} U_{ocv,2j} = ... = \sum_{j=1}^{n} U_{ocv,mj} \tag{3.5}$$

From these calculations, the equivalent scheme of the battery pack can be reduced to:
The battery pack is presented as a single battery with internal resistance R_{int} and OCV V_{oc}. With this equivalent model, the output voltage V_{DC} in discharge mode can be calculated.

$$V_{DC} = V_{oc} - R_{int} \cdot I_{DC} \tag{3.6}$$

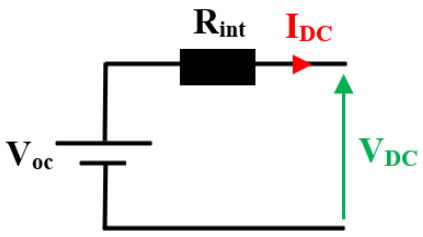

***Figure** 3.2 Equivalent model battery pack*

Note that it is assumed that every battery cell in the battery pack behaves the same. This means that they have the same internal resistance, OCV and capacity. In other words, it is assumed that the cells are balanced at all times. Besides, the connections between batteries and contactors in the battery pack are neglected here, so this method may provide inaccurate results. This method of internal resistance determination is not recommended but should be mentioned to understand the principle of the battery pack.

In many cases, the battery pack of the BESS will already be given as one battery in the datasheet. In that case, the equivalent model of the battery pack must be derived from the data of the BESS. The structure of the equivalent model remains the same as the one given in *figure 3.2*. The remainder of this chapter will always refer to "the battery" with the assumption that, as described above, the battery pack can be considered a single battery.

3.2.2 Open-circuit voltage

The OCV-SoC curves can be determined based on the typical OCV-SoC curves in *figure 2.14* or with measurements. The most accurate results will be obtained if the OCV-SoC curve is measured for the specific BESS. Using predefined values, it should be possible to make a good approach. As said in 1.1, two different types of Li-ion batteries are generally used for grid storage:

- LFP batteries for home batteries
- NMC batteries for grid storage

Since **NMC batteries** are mainly used for grid storage, the main focus is on these types of batteries. However, all Li-ion batteries exhibit similar behaviour. The correlations can be generalized because the influencing parameters are the same. The OCV-SoC curves apply to a single battery cell as well as to an entire BESS [43]. If several batteries are in series, simply multiply the voltage by the number of batteries (*equation (2.13)*).

Usually, the BESS is given as one unit and the OCV-SoC curves are not provided by the manufacturer. If the battery type is provided and the number of batteries are given, the curves can be derived with the already-mentioned items. Another method is to measure the OCV, as introduced in 2.2.1.

Initial OCV-DoD curve

Because discharge mode is considered, DoD is chosen instead of SoC. This DoD can be calculated with *equation (2.9)*. The initial curve is valid for a new Li-ion battery at rest and an ambient temperature of 25°C. In the further course of the section, the temperature is expressed in [K] instead of [°C], where 0°C = 273.15K. The OCV-DoD curves can be determined in two methods:

- Tabular data
- Approach with equation

As an example, the tabular data of an NMC battery cell is given in *table 3.1.*

DoD [-]	V_{oc} **[V]**	**DoD [-]**	V_{oc} **[V]**
0	4.20	0.55	3.79
0.05	4.12	0.60	3.77
0.10	4.07	0.65	3.75
0.15	4.02	0.70	3.73
0.20	3.98	0.75	3.70
0.25	3.94	0.80	3.66
0.30	3.91	0.85	3.60
0.35	3.89	0.90	3.52
0.40	3.85	0.95	3.42
0.45	3.82	1.00	3.05
0.50	3.80		

Table 3.1 *Tabular data OCV-DoD NMC battery cell under normal operating conditions [9]*

The data points is the table are deduced from *figure 2.14.* Note that the data in the table was obtained using measurements. In addition, an OCV value is read for each 5% change in DoD. Thus, there is a certain margin of error on these values. However, they can serve as a reference for realistic values. Extrapolation is not needed here, since the battery can only operate within this voltage frame. The OCV-DoD can be approached using curve fitting. From the polynomial fitting (*figure 1*), a quintic equation is obtained:

$$V_{oc}(DoD) = a_1 \cdot DoD^5 + a_2 \cdot DoD^4 + a_3 \cdot DoD^3 + a_4 \cdot DoD^2 + a_5 \cdot DoD + a_6 \tag{3.7}$$

- DoD is expressed as a fraction of a unit
- $V_{oc}(DoD)$ is the OCV dependent on the DoD in [V]
- $a_1, ..., a_6$ are the battery type dependent constants

As an example, the equation of an NMC battery cell is determined in *figure 1.* The resulting equation is obtained:

$$\begin{aligned} V_{oc}(DoD) = &-15.34 \cdot DoD^5 + 32.20 \cdot DoD^4 \\ &- 24.63 \cdot DoD^3 + 8.741 \cdot DoD^2 - 2.086 \cdot DoD + 4.20 \end{aligned} \tag{3.8}$$

An R^2 of 0.9934 and RMSE of 0.0233 are obtained. When the battery is almost fully discharged, i.e. high DoD, the OCV decreases strongly compared to the lower DoD. In *figure 2.14*, no remarkable fluctuations are noticeable. Hence, this approach is also considered sufficient enough for high DoD.

Although there can be small variations, the OCV-DoD curve of an NMC battery will generally be similar for the entire discharge cycle. However, the maximum voltage and minimum voltage limits, i.e. voltages at which the battery is considered fully charged and discharged. DoD = 0 and DoD = 1 are not the actual values at which the battery is fully charged and discharged. These are the values where the BMS considers the battery to be fully charged and discharged to ensure that they are not damaged. If the battery is overdischarged, a DoD = 1.05 can virtually be obtained, but the BMS does not allow this. For this reason, the equations may need to be adjusted. It is assumed that the voltage of a single NMC battery cell remains within the range of 3.05 V and 4.2 V. Two different instances may apply:

- **Minimum operating voltage per NMC cell > 3.05 V**: This means that the battery is assumed to be fully discharged at a, considering the curve obtained from *table 3.1* or *equation (3.8)*, lower DoD. The DoD at a particular OCV must be redetermined.

  1. Check what the DoD is in the original OCV-DoD curve at the specified minimum operating voltage, this DoD is the $(1 - \Delta DoD)$

  $$DoD_{new} = DoD_{old} + \Delta DoD \cdot \frac{DoD_{old}}{1 - \Delta DoD} \tag{3.9}$$

     - ΔDoD is the 1 - DoD of the original curve at V_{min}, expressed as a fraction of a unit
     - DoD_{new} and DoD_{old} are the DoD of the new curve and the original curve, respectively, expressed as a fraction of a unit
  2. Determine the new constants of *equation (3.7)* using data points with the new DoD

- **Maximum operating voltage per NMC cell < 4.2 V**: This means that the battery is assumed to be fully charged at a, relative to the curve prepared from *table 3.1* or *equation (3.8)*, higher DoD. The DoD at a particular OCV must be redetermined.

  1. Check what the DoD is in the original OCV-DoD curve at the specified maximum operating voltage, this DoD is ΔDoD

  $$DoD_{new} = DoD_{old} - \Delta DoD \cdot (1 - \frac{DoD_{old} - \Delta DoD}{1 - \Delta DoD}) \tag{3.10}$$

     - ΔDoD is the DoD of the original curve at V_{max}, expressed as a fraction of a unit
     - DoD_{new} and DoD_{old} are the DoD of the new curve and the original curve, respectively, expressed as a fraction of a unit
  2. Determine the new constants of *equation (3.7)* using data points with the new DoD

Possibly, if the battery operates within a smaller OCV frame, the curve fit can be simplified. The high order of the equation is the result of large variations when the battery is nearly fully charged or discharged. If the BMS ensures that these states are not reached, the curve can be approached with a cubic equation or even linear.

The OCV-DoD curve depends on cycle age, operating temperature and discharge current. The resistance of a fault current circuit is small, making it important to accurately predict the OCV-DoD curve. These affecting parameters must therefore be included in the battery model.

Effect of temperature

In *figure 2.17* the effect of temperature on the entire OCV-DoD curve is shown. From this figure, it can be considered that the effects are significant from a DoD of 0.7. From this figure, it can be considered that the effects are significant from a DoD of 0.7. Hence, only DoD $\geq$ 0.7 are considered for these curves. The OCV change relative to the curve in normal operating conditions, namely at 25°C or 298.15 K, can be determined. This per unit voltage change $\Delta V_{oc}(DoD)$ can be calculated.

$$\Delta v_{oc}(DoD, T) = \frac{V_{oc}(DoD, 298.15K) - V_{oc}(DoD, T)}{V_{oc}(DoD, 298.15K) \cdot |298.15K - T|} \tag{3.11}$$

- $\Delta v_{oc}(DoD, T)$ is the OCV drop per K in [p.u.]

- $V_{oc}(DoD, 298.15K)$ and $V_{oc}(DoD, T)$ are the OCV at 298.15 K and temperature T, respectively, in [V]
- T is the temperature in [K]

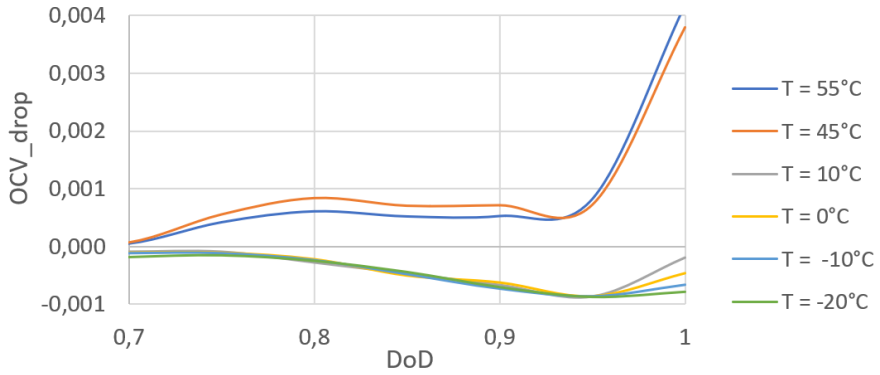

Figure 3.3 *OCV-DoD drop per K for NMC battery cell relative to 298.15 K [76]*

Figure 3.3 shows the per unit decrease in OCV per K for different DoD. There is a distinction visible between when OCV decreases due to higher temperatures vs when OCV increases due to lower temperatures. However, if one separates the phenomena, it can be seen that the voltage drop per K is always in the same order of magnitude.

In *figure 3.4*, the average per unit voltage drop curves for higher and lower temperatures, relative to the 298.15 K OCV-DoD curve, are depicted.

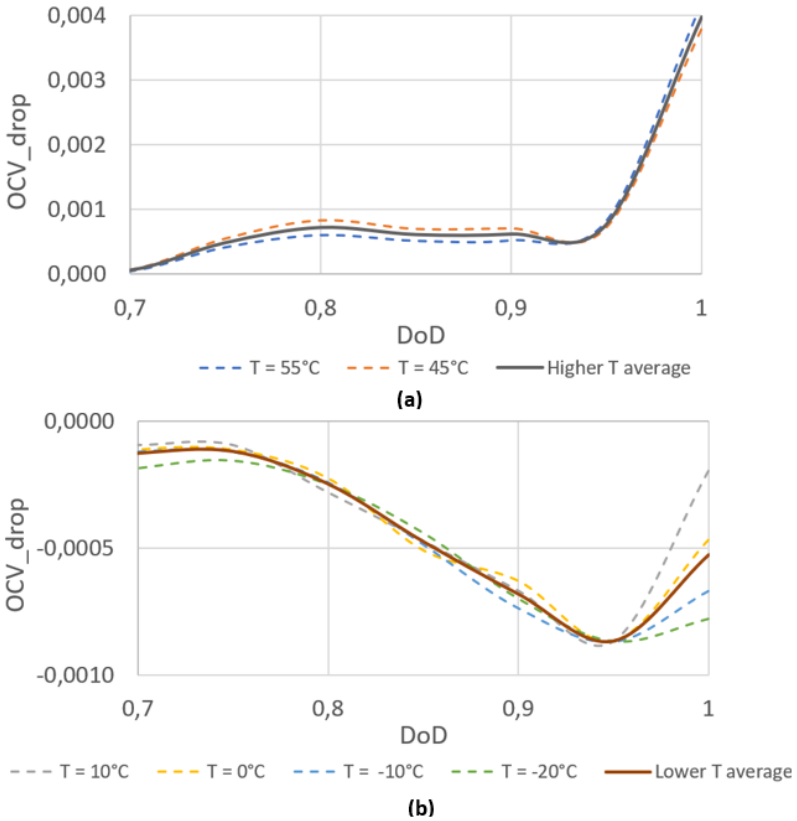

Figure 3.4 *Average OCV-DoD drop per K relative to 298.15 K (a) Higher temperature (b) Lower temperature [76]*

The curves in *figure 2.17* were obtained from experiments. There is a certain margin of error in experimental data. The average curves of OCV variation can be approximated using curve fitting. A data point is considered for every 5% change in DoD.

- For **temperatures > 298.15 K**, Gaussian regression is used. The changes in temperature have a significant impact when the OCV is lower, i.e. DoD is higher. This can be deduced from both *figure 2.16* and *figure 2.17*.
- For **temperatures < 298.15 K**, Gaussian regression is used as well, because of the same reasons mentioned earlier for temperatures > 298.15 K. The curve at 243.15 K is not considered in *figure 3.4b* because of its difference from the other curves and since the minimum operating temperature of Li-ion batteries is typically 253.15 K or more. The magnitude of the OCV change at DoD between 0.95 and 1 is not considered for curve fit. The changes in OCV reduce with increasing DoD, but this may be due to the measurement error in *figure 2.17*. This measurement error is less significant at higher temperatures, as the change in OCV is greater at high DoD, as can be seen in

From the curve fit, the following equations can be obtained from Gaussian and polynomial regression (*figure 2*):

$$\Delta V_{oc}(DoD,T) = \begin{cases} V_{oc}(DoD,298.15K)\cdot|298.15K-T|(d_1\cdot e^{-(\frac{DoD-d_2}{d_3})^2}) & \text{if } T>298.15K \\ V_{oc}(DoD,298.15K)\cdot|298.15K-T|(c_1\cdot e^{-(\frac{DoD-c_2}{c_3})^2}) & \text{if } T<298.15K \end{cases} \tag{3.12}$$

$\Delta V_{oc}(DoD,T)$ is the OCV change as a function of temperature, relative to the OCV at 298.15 K. The OCV change is positive when the temperature > 298.15 K and negative when T < 298.15 K. To determine the constants c_1, c_2, c_3, d_1, d_2 and d_3, curve fitting is used. These constants can vary for different types of batteries but will have the same order of magnitude. Depending on the desired accuracy of the model, one can choose to use the values derived from *figure 3.4*. The constants from formula (3.21) are determined for NMC batteries, using the curve fit in *figure 2*.

$$\Delta V_{oc}(DoD,T) = \begin{cases} -(V_{oc}(DoD,298.15K)\cdot|298.15K-T|(0.004502\cdot e^{-(\frac{DoD-1.026}{0.06706})^2})) & \text{if } T>298.15K \\ V_{oc}(DoD,298.15K)\cdot|298.15K-T|(1.08\cdot10^{-3}\cdot e^{-(\frac{DoD-1.013}{0.1602})^2}) & \text{if } T<298.15K \end{cases} \tag{3.13}$$

For higher temperatures than 298.15 K, the R^2 of the curve fit is 0.8482 and RMSE is 0.000534. For lower temperatures than 298.15 K, the R^2 of the curve fit is 0.9523 and RMSE is 0.000095.

Effect of discharge current

The shifting of the OCV curve in discharge mode is presented in *figure 2.19*. Here it was already stated that the OCV-DoD shift downwards linear with 1.5% per 1C. From this, the following equation for the OCV decrease is obtained:

$$\Delta V_{oc,I_c} = -(V_{oc}(DoD,0)\cdot 0.015\cdot I_c) \tag{3.14}$$

- $\Delta V_{oc}(DoD,I_c)$ is the total OCV variation as a function of discharge rate, relative to the curve in rest [V]
- I_c is the discharge rate

Effect of cycle age

As *figure 2.21*, the effect of cycle age is significant when the DoD is higher than 0.8. As an approach for the OCV-DoD curves, data points are determined using *figure 2.21* for each step in DoD of 0.05 since no remarkable fluctuations are noticeable in the curve. The drop in OCV is calculated as follows:

$$\Delta v_{oc}(DoD, SoH) = \frac{V_{oc}(DoD, 1) - V_{oc}(DoD, SoH_{aged})}{V_{oc}(DoD, 1) \cdot SoH_{aged} \cdot 100} \tag{3.15}$$

- SoH is expressed as a fraction of a unit
- SoH_{aged} is the SoH of the aged battery, expressed as a fraction of a unit
- $\Delta v_{oc}(DoD, SoH)$ is the OCV drop per percentage decrease in SoH, expressed in [p.u.]
- $V_{oc}(DoD, 1)$ and $V_{oc}(DoD, SoH_{aged})$ are OCV of the new battery and the aged battery [V]

To calculate the $\Delta V_{oc}(DoD, SoH)$, the SoH is needed. This is normally monitored, but if an approximation of the fault current must be made in a situation where the battery has already done more cycles, a estimation of this SoH must be made. In *figure 2.36*, it can be seen that the drop in residual capacity is approximately linear. From this, a formula for the SoH can be obtained.

$$SoH = 1 - \frac{Q_{new} - Q_{eol}}{Q_{new}} \cdot \frac{\#cycles_{cur}}{\#cycles_{eol}} \tag{3.16}$$

- Q_{new} and Q_{eol} are the capacities of a new battery and of an end-of-life battery [Ah]
- $\#cycles_{cur}$ and $\#cycles_{eol}$ are the current amount of cycles and the number of cycles at end of life

Here it is assumed that the battery always operates under the same operating conditions, e.g. discharge current 1C. This means that the effect of previous faults or overloads is neglected.

To approach the effect of SoH on the OCV, exponential regression is used (*figure 3*).

$$\Delta V_{oc}(DoD, SoH) = \begin{cases} V_{oc}(DoD, 1) \cdot 100 \cdot (1 - SoH) \cdot (b_1 \cdot e^{b_2 \cdot DoD}) & \text{if } DoD > 0.8 \\ 0 & \text{if } DoD \leq 0.8 \end{cases} \tag{3.17}$$

- $\Delta V_{oc}(DoD, SoH)$ is the OCV change as a function of SoH, relative to the OCV at SoH = 1
- b_1 and b_2 are the battery type dependent constants

The constants b_1 and b_2 can be conjectured to be the same for all types of Li-ion batteries, but limited variations are possible. Note it is the voltage drop per % drop in SoH. That is the reason why it is multiplied by 100. For an NMC battery, the constants in *equation (3.17)* can be obtained using *figure 3*.

$$\Delta V_{oc}(DoD, SoH) = -(V_{oc}(DoD, 1) \cdot 100 \cdot (1 - SoH) \cdot (3.834 \cdot 10^{-12} \cdot e^{21.23 \cdot DoD})) \tag{3.18}$$

The R^2 of the curve fit is 0.9898 and RMSE is 0.000275. No remarkable fluctuations are observed compared to *figure 2.21*.

3.2.3 Output voltage

In 2.2, the fault current characteristics of batteries were investigated. The objective is to include all parameters that have a significant effect on the fault current of the battery. An extended Rint model is being developed so the following formula is important no matter what parameters have an effect:

$$V_{DC} = V_{oc} - R_{int} \cdot I_{DC} \tag{3.19}$$

Where V_{oc} and R_{int} are the OCV and internal resistance of the battery. V_{DC} and I_{DC} are the input voltage and current of the inverter and here also the output terminal voltage and current of the battery. These last two parameters must be defined to determine the output power of the battery, and so the input power of the inverter. In order to predict the i_{DC} and V_{DC}, the OCV-SoC curve and the behaviour of R_{int} need to be determined.

3.2.4 Internal resistance

The internal resistance at the beginning of the fault should be known. If the battery has been discharging for some time, the internal resistance can be as a result of the polarization RC elements. This transient behaviour is relatively slow, so has little effect over a 5 s period. If the battery has already been discharging for some time before the fault occurs, the internal resistance can be higher. However, this study attempts to create a BESS model using only the information available from data sheets.

The internal resistance of a single battery has an order of magnitude mΩ. Almost in all cases, the manufacturer of the BESS does not give a value for the internal resistance of the battery module.

From the perspective of protection design, the exact value of the internal resistance at any point in time is less important. However, the worst-case value should be known, as this is when the fault current is smallest. The internal resistance of a battery can be provided by the manufacturer of the batteries in the battery module. The internal resistance of the battery pack in the BESS can be determined if the specific battery type and # number of batteries is given, by using *equation (3.3)*. This value is not very accurate because of multiple reasons:

- The provided value is often '< ...mΩ'. Under what conditions this value was determined is rarely provided. This can be the value after one hour of charging, end-of-life or both.
- The resistances of the contactors and connections between batteries are not included in the total internal resistance when using *equation (3.3)*.

Therefore, the internal resistance can seem higher or lower than it actually is. If there is uncertainty, the worst-case value should be used. As a simplification, it can be assumed that the value given by the battery manufacturer is the value of a new fully charged battery at rest and a temperature of 25°C. These are very rough approximations that may underestimate internal resistance. A measurement of internal resistance under certain conditions is recommended.

As an example, curve fitting is used for NMC batteries, but the behaviour of all Li-ion batteries is similar. The same correlations apply, but the constants can vary.

Initial Rint-DoD curve

Similar to the OCV-DoD curves, a R_{int}-DoD curve can be constructed. The R_{int} in this curve does not have, unlike the OCV-DoD curves, the same magnitudes for all battery cells with the

same chemical composition. From there, per-unit values are used. It is assumed that the 1 p.u. value occurs with a new, fully charged battery at rest and at T = 298.15 K. The p.u. values of the internal resistance r_{int} can be calculated with the equation below:

$$r_{int}(DoD) = \frac{R_{int}(DoD)}{R_{int}(0)} \tag{3.20}$$

The DoD is expressed as a fraction of a unit. The Rint-SoC curve in *figure 2.22* is used to construct the per unit Rint-DoD curve in *Figure 3.5*.

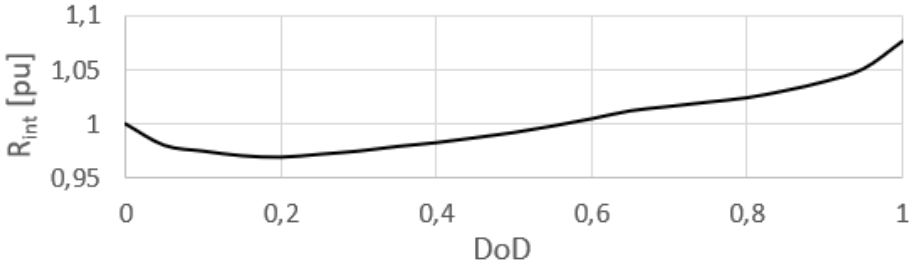

Figure 3.5 *Rint-DoD curve NMC battery in per unit [32]*

The p.u. value of the resistance generally varies between 0.95 p.u. and 1.1 p.u.. These magnitudes can also vary, depending on when the batteries were developed. Also, the optimum, at which Rint is smallest, can be at DoD = 20% but also at, e.g., DoD = 50%. Again, the internal resistances are read for each change of 5% in DoD. Using these 21 data points, derived from *figure 2.22*, a curve fit is created. Polynomial regression is used *Figure 4* and an equation can be formed. A quadratic equation might seem appropriate here because of its parabolic profile, but at low and high DoD the slope is steeper. This is because at low and high DoD, the chemistry of the battery fluctuates the most. Therefore, a quartic equation is chosen:

$$R_{int}(DoD) = R_{int}(0) \cdot (f_1 \cdot DoD^4 + f_2 \cdot DoD^3 + f_3 \cdot DoD^2 + f_4 \cdot DoD + f_5) \tag{3.21}$$

As an example, the data in *Figure 3.5* is approached by using curve fitting. The values of these constants f_1, f_2, f_3, f_4 and f_5 can be derived from *Figure 4*.

$$R_{int}(DoD) = R_{int}(0) \cdot (0.9372 \cdot DoD^4 - 2 \cdot DoD^3 + 1.528 \cdot DoD^2 - 0.3915 \cdot DoD + 1) \tag{3.22}$$

The R^2 of the curve fit is 0.9935 and RMSE is 0.00238. This can be used as a reference for all Li-ion batteries.

***Alternative method:** Above method assumes that little or nothing is given about the battery pack. In some cases, the battery manufacturer gives the V_T vs. SoC curves for different discharge currents. The internal resistance can be calculated using the following formula:

$$R_{int}(DoD) = \frac{(V_{oc}(DoD, I_x) - V_x(DoD, I_x)) - (V_{oc}(DoD, I_y) - V_y(DoD, I_y))}{I_y - I_x} \tag{3.23}$$

- $R_{int}(DoD)$ the actual value of the internal resistance as a function of DoD and discharge current [Ω]
- I_x and I_y are the discharge current [A]

- $V_{oc}(DoD, I_x)$ and $V_{oc}(DoD, I_y)$ are the OCV at a particular DoD, discharging at current I_x and I_y, respectively [V]
- V_x and V_y are the terminal voltages at a particular DoD, discharging at current I_x and I_y, respectively [V].

This can be a useful method if the internal resistance is not given and the measuring equipment is not available to measure the internal resistance. However, it is concluded that the internal resistance depends on the discharge current. The method will therefore give inaccuracies since the internal resistance does depend on the discharge current. However, it can give a good estimate as long as I_x and I_y do not take on high overcurrent values, i.e. » 1C.

Effect of temperature

The effect of temperature on internal resistance can vary widely between batteries with different chemical compositions and periods of manufacturing as well. However, the shape of the R_{int} vs. T curve will always exhibit the same or at least similar behaviour. The curve in *figure 2.23* is considered. The per unit increase of internal resistance relative to the R_{int} at the normal operating temperature of 298.15 K can be calculated:

$$\Delta r_{int}(T) = \frac{R_{int}(T)}{R_{int}(298.15K)} - 1 \tag{3.24}$$

The increase in internal resistance relative to internal resistance at 298.15 K is illustrated in *figure 3.6*.

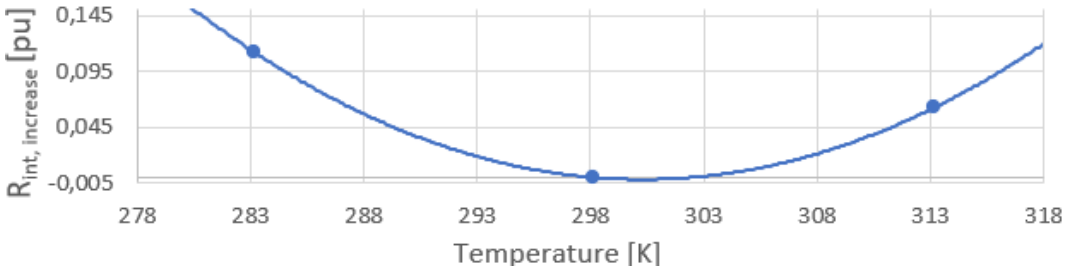

Figure 3.6 *R_{int} variation vs. temperature of Li-ion batteries in per unit [39]*

This is a general approach for all Li-ion batteries. In *figure 2.23*, there were only three data points known. From three data points, a quadratic equation is obtained (*figure 5*):

$$\Delta R_{int}(DoD, T) = R_{int}(DoD, 298.15K) \cdot (g_1 \cdot T^2 + g_2 \cdot T + g_3) \tag{3.25}$$

In this formula, the temperature T is expressed in [K], not in [°C]. The constants g_1, g_2 and g_3 are dependent on the battery's composition, but can also vary for batteries with the same chemical composition. However, the constants can be determined for a Li-ion battery from the data in *figure 3.6* using the curve fit in *figure 5*.

$$\Delta R_{int}(DoD, T) = R_{int}(DoD, 298.15K) \cdot (3.88 \cdot 10^{-4} \cdot T^2 - 0.233 \cdot T + 34.98) \tag{3.26}$$

This equation is valid when the battery operates within its operating temperature frame, imposed by the manufacturer. However, it is undesirable to operate outside these temperatures because the battery will be damaged too much. The BMS will usually shut down the battery when the operating temperature is not in the operating frame. The values of the constants also depend on

the quality of the battery. If old, "underdeveloped" batteries are used, the variations in internal resistance can be larger. For newer, better-developed batteries, these variations can be smaller.

Effect of discharge current

The discharge current dependence on internal resistance is divided into two parts: 'the friction part' and 'the mobility part'. The friction causes the internal resistance to increase at higher discharge currents. The discharge current warms up the battery according to Joule's law. Higher temperature increases electron mobility, resulting in decreasing internal resistance. However, this is the effect of temperature rather than the discharge current itself. The temperature response will be discussed later. The mobility effect is not considered further here. Hence, only increasing friction is considered as the effect of the discharge current. In *figure 2.24*, the internal resistance is determined using short pulses. From there, it is assumed that the heating of the battery can be neglected, so the effect of the discharge current is more friction.

The magnitudes of the internal resistance in *figure 2.24* can be converted to the per unit values. If this value is known, the variation in internal resistance due to increasing discharge current can be determined by subtracting all these values with 1 (= per unit resistance in rest).

$$\Delta r_{int}(I) = \frac{R_{int}(I)}{R_{int}(0)} - 1 \tag{3.27}$$

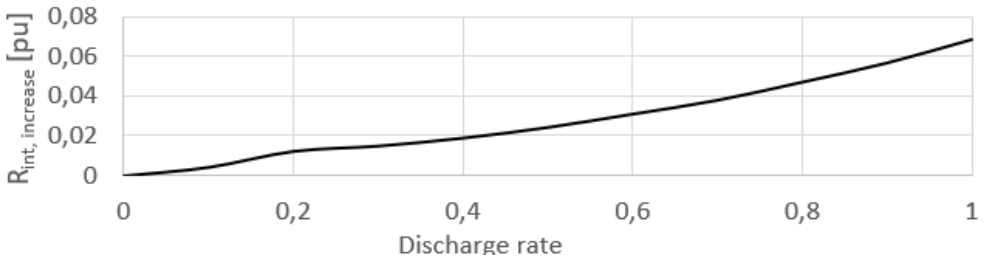

Figure 3.7 *R_{int} variation vs. discharge current of Li-ion batteries in per unit [42]*

The known data in *figure 3.7* is only up to discharge rate 1C. It is assumed that the slope remains unchanged and continues to rise in the same trend, which means extrapolation is used. In *figure 2.31*, the profile for higher currents is evaluated, but not in the right time frame. Since these curves do not provide enough information, the above assumption is necessary.

For curve fitting, data points per 0.1C change in discharge rate is determined up to 1C, as this is the highest current that is known from *figure 2.24*. The curve is assumed to be linear over the whole profile. From this, the following linear equation is obtained (*figure 6*):

$$\Delta R_{int}(DoD, I_c) = R_{int}(DoD, 0) \cdot h_1 \cdot I_c \tag{3.28}$$

Note that I_c is the discharge rate and not the discharge current. The data of *figure 3.7* is used to determine the constant h_1. The curve fit is presented in *figure 6*.

$$\Delta R_{int}(DoD, I_c) = R_{int}(DoD, 0) \cdot 0.0595 \cdot I_c \tag{3.29}$$

The R^2 of the curve fit is 0.9598 and the RMSE is 0.00438.

No temperature dependence of the R_{int} vs. discharge current is considered yet in this formula. When the temperature is higher, the atoms vibrate more and consequently, more friction is expected. Consequently, the slope in *figure 3.7* is expected to become steeper. This has not yet been

investigated using experimental measurements but was deduced from theoretical observations in 2.2.2. This could be investigated using resistance measurements at different loads and temperatures and with short pulses, so battery heating can be neglected. No temperature-dependent profiles or equations have been obtained for the friction effect from existing studies, but assumptions can be made:

$$R_{int}(I_c, T) = R_{int}(I_c, 298.15K) \cdot (\frac{T}{298.15K})^2 \tag{3.30}$$

The quadratic relation is chosen based on Joule's law, $q_{joule} \sim I^2$. Combined with *equation (3.30)*, the total friction effect due to discharge current can be described:

$$\Delta R_{int}(DoD, I_c, T) = R_{int}(DoD) \cdot (0.0595 \cdot I_c) \cdot (\frac{T}{298.15K})^2 \tag{3.31}$$

The internal resistance vs. discharge rate profile is determined for the friction effect.

Effect of cycle age

As the battery ages, the electrical resistance of the materials from which the battery is made increases. In 2.2.2, some equations were already discussed to calculate internal resistance as a function of cycle age/SoH from manufacturers' data. The resistance can be determined with *equation (2.15)*. The rise in internal resistance $\Delta R_{int}(DoD, SoH)$ can be calculated.

$$\Delta R_{int}(DoD, SoH) = R_{int}(DoD, 1) \cdot \frac{1 - SoH}{SoH} \tag{3.32}$$

The SoH can be determined using *equation (3.16)*, so no curve fitting is needed here to implement the effect in the model.

3.2.5 Internal inductance

The delay before reaching the peak current due to the counteracting inductance can be up to 15 ms 2.2.3. This worst-case delay of 15 ms is considered, which corresponds to 5τ. The inductance can be derived using *equation (2.19)*:

$$L_{int} = R_{int} \cdot 0.003 \tag{3.33}$$

It is assumed that internal inductance L_{int} remains constant and internal resistance R_{int} is the resistance of a new, fully charged battery in rest at 25°C/298.15K.

3.2.6 Temperature reponse

There is not enough information about the heat generation and cooling of the battery based on the technical datasheets to model the temperature progression correctly. By using *equation (2.21)* some idea could already be formed what the temperature increase is if only the Joule effect and no cooling are considered. The method using *equation (2.21)* is added to the model to indicate that the battery will heat up while feeding fault current, but it should be kept in mind that the battery may heat up more or less depending on other influencing factors such as cooling. In [25] it is possible to see what the average specific heat of the battery is. For example, the average specific heat of an NMC battery is 1040 $\frac{J}{kg \cdot K}$.

3.2.7 Discharge capacity

The examined time frame here is 0-5 s. After this 5 s, the external fuse in the LV grid should have interrupted the current. Since the battery maximum discharge current of Li-ion batteries is generally 2C, a fully charged battery can feed this current for nearly 10-30 minutes, dependent on the temperature. Even if the battery is only 10% charged, it can still feed the current for a little less than 1-3 minutes (» 5 s). Typically, the battery does not get discharged below 10%, so discharge capacity is not a decisive factor in this time frame. However, the variation in discharge capacity is already incorporated by modeling the dependent factors of the OCV and internal resistance.

3.2.8 Battery protection

To prevent the battery from being damaged, some limits are imposed using protection devices:

- **Voltage range:** Under and overvoltage protections prevent the battery from operating outside its OCV range. If the OCV drops below the minimum voltage during a fault event, the BMS can cut off the battery.
- **Current:** The BMS can either limit the current and keep it constant, act like a fuse or has both a current limiter and overcurrent fuse protection. Based on the application of the BESS, assumptions need to be made.
- **Temperature:** The BMS can limit the current to a lower magnitude or cut off faster when the operating temperature is higher. If the temperature limit of the battery is exceeded, the BMS cuts it off.

3.3 Inverter model

The inverter is represented as a three-phase voltage source. The model proceeds from the averaged inverter model depicted in *figure 2.60*.

3.3.1 Fault response

Initial response to fault events

The response of the inverter in fault events can be provided by the manufacturer in two ways:

- The maximum value of short-circuit current
- The characteristic values for the short-circuit currents in terms of $I_p, I_{k''}$ and I_k

The periods of these currents depend on the inverter's manufacturer, so this cannot be modeled generically. The value of the maximum short-circuit current is more commonly given, so this value is used.

Current limiting

For inverters with overcurrent capability, the time-current curves and method of current limiting are generally not provided by the manufacturer. Based on the application, it is possible to make an assumption of how the inverter will limit the current. For grid-forming inverters, it is possible that the inverter has both modes and is adjustable by the user.

Some inverters can feed 4 to 6 times their rated current for, e.g., 60 ms [62]. This can be assumed to be the absolute maximum short-circuit current. If the current exceeds, e.g., 6 p.u., the inverter shuts down immediately. If the inverter current is less or equal to the maximum short-circuit current, the inverter can reduce the current after, e.g., 60 ms or cut off. Limiting the current is done by reducing the internal voltage of the inverter.

If the maximum AC power is provided that the inverter can feed for a few seconds, the overcurrent can be calculated:

$$I_{oc} = \frac{P_{oc}}{V_{nom}} \tag{3.34}$$

I_{oc} is the maximum overcurrent [A], P_{oc} the output power [W] that can be fed for a few seconds, e.g. during a fault event or overload and V_{nom} the nominal terminal voltage of the inverter [V]. Since the rated output power of the inverter is calculated by most manufacturers as $V_{nom} \cdot I$, it is assumed that it is no different for the AC power at overcurrent. The formula above applies to a one-phase inverter. Three inverters can be used to convert the DC from the battery to the three-phase AC. Then this equation applies to the current in each phase.

The current can be limited by reducing the average voltage of the inverter. Since the inverter control is not modeled, an alternative way to model the reduction in internal inverter voltage is needed. The current is measured in each phase. If the current exceeds the overcurrent limit I_{max}, voltage control must be changed to fault current limiting. Nothing is known about the coupling reactance, so the method of droop control is not used. To lower the internal voltage, a virtual impedance Z_{lim} can be added after the inverter voltage source. based on the current limiting method in [53].

$$Z_{lim} = \frac{V_{pre,fault} - Z_{grid} \cdot I_{max}}{I_{max}} \tag{3.35}$$

- $V_{pre,fault}$ is the output voltage of the inverter in normal operation [V]

- I_{max} is the overcurrent limit [A]
- Z_{grid} is the external inverter impedance at AC side [Ω]

In resistive LV grids, the limiting impedance can be simplified to a limiting resistance. This simplified method suffices only if the load is mainly resistive, so a power factor ≈ 1. The next equation will determine the internal voltage of the inverter in case of excessive currents:

$$V_{post,fault} = V_{pre,fault} - R_{lim} \cdot I_{max} \tag{3.36}$$

- $V_{post,fault}$ is the internal voltage of the inverter after the fault is detected [V]
- R_{lim} is the virtual resistance to limit the current [Ω]

Voltage response

Besides the voltage drop due to current limiting, there will also be some voltage drop across the LCL filter. The values of these filters can be determined using *equation (2.31)*, *equation (2.32)*, *equation (2.33)* and *equation (2.34)*. In addition, transformers are often used in inverters, which also have a particular impedance. If the inverter is coupled to the grid, i.e. the PCC, using a coupling impedance, there is also a voltage drop across this impedance.

Depending on what the FRT limits of the inverter, it continues to feed the fault or cuts off. These FRT limits are determined by the grid operator, inverter manufacturer and/or the user.

3.3.2 Efficiency

The inverter's efficiency differs for all inverters. For SMA inverters, the relationship between efficiency and output power is generally linear when feeding > 0.4 p.u. If the efficiency curve is provided, an approach can be made of the efficiency when feeding overcurrent.

3.3.3 Inverter protection

For the AC side, some of the principles have already been explained, but here is an overview:

- **AC voltage:** For this parameter, the FRT capability is important. Depending on the voltage at the PCC, the inverter will continue to feed or cut off.
- **AC output current** Inverters generally have overcurrent capability and will be able to supply a certain current n seconds. For inverters without overcurrent capability, the maximum current is the rated current.

A battery is connected to the DC side of the inverter. This battery can supply a particular power to the inverter. However, the inverter also has some restrictions for the input voltage and current:

- **DC voltage range:** The DC input voltage of the inverter is equal to the DC output voltage of the battery. If the voltage is not in this permissible range, it doesn't let the power from the battery through, resulting in no output power. This also protects the battery against overcharge and overdischarge.
- **DC input current:** There can be limits for the DC input current as well. If the inverter manufacturer does not provide explicit overcurrent limits for the DC current, it is not considered further in this model. The AC overcurrent protection is then the one that protects the IGBTs against excessive currents.

3.4 BESS model

3.4.1 Structure model

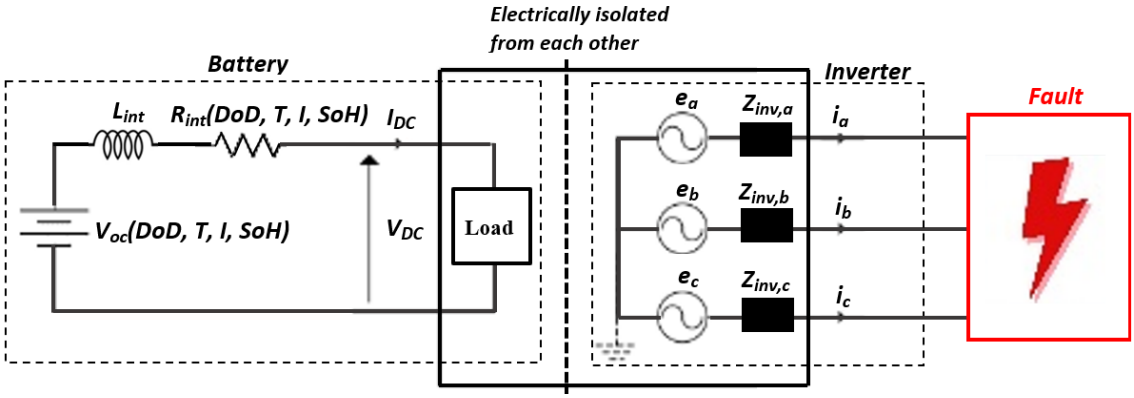

Figure 3.8 *Structure 'own' simplified BESS model*

Now that all impact parameters are known, a comprehensive model can be composed in *figure 3.8*, excluding the fuses and other protection devices. This is an averaged BESS model, meaning distortion and harmonics are not considered. The profile of current on the DC side cannot be estimated with this model. The current is converted from DC to AC, so the battery will not constantly discharge. Only the magnitude is considered here. The OCV and R_{int} of the battery are made dependent on SoC, temperature, current and SoH. The inductance represents the transient behaviour of the battery. The grid-forming inverter is considered to be a non-ideal voltage source. The filter impedance is considered. In addition, there are other losses represented by the efficiency η. The battery and inverter are electrically isolated from each other, but connected with control circuits. The power balance between the battery and inverter can be calculated.

$$\eta \cdot V_{DC} \cdot I_{DC} = \sum_{j=a,b,c} e_j \cdot i_j \tag{3.37}$$

Two different structures are considered to model the AC load at the DC side.

Load as current source

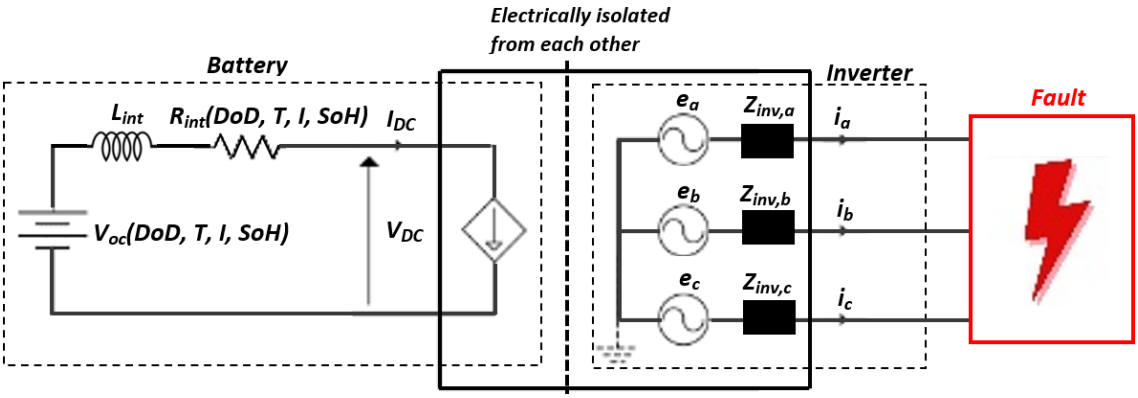

Figure 3.9 *Structure 'own' simplified BESS model: option 1*

In the first case, the load on the AC side is observed as a current source by the battery (*figure*

3.9). The average DC current of the battery is considered to be constant. It can be determined using the initial power demand of the inverter to feed the fault.

$$I_{DC} = (\frac{E_{a,pre-fault}^2}{Z_a} + \frac{E_{b,pre-fault}^2}{Z_b} + \frac{E_{c,pre-fault}^2}{Z_c}) \cdot \frac{1}{\eta \cdot V_{DC,pre-fault}} \tag{3.38}$$

- $E_{j,pre-fault}$ is the internal voltage of the inverter in each phase at the AC side before the fault occurs [V]
- Z_j is the total impedance in each phase at the AC side [Ω]
- $V_{DC,pre-fault}$ is the DC voltage of the battery before the fault occurs [V]
- η is the efficiency of the inverter

The current at the DC side remains constant after 15 ms transient behaviour. It is assumed that the transient current always rises in the same way and the time constant $\tau = 0.003$ from *equation (3.33)* is not variable. The current source can be controlled by multiplying the needed current i_{DC} by $(1 - e^{\frac{-t}{\tau}})$. In this way, the inductance should not be added to the circuit, but its transient behaviour is included. The voltage on the DC side will be the parameter that exhibits further transient behaviour. Since the inverter usually changes from voltage control to current control/limiting during a fault event, it is assumed that the variations in DC voltage affect the internal voltage of the inverter. As of the occurrence of a fault, the transformer's turn ratio remains unchanged, unless a tap changer transformer is used. Consequently as the DC voltage decreases, the AC voltage decreases. The ratio of DC voltage and AC voltage is controlled using a transformer and modulation control. Within the DC voltage range, one is going to use modulation control to regulate the AC voltage. The modulation factor is assumed ≈ 1 and the turn ratio k is adjustable i.e. a tap changer transformer.

$$k = \frac{\sqrt{2} \cdot E_{inv,pre-fault}}{V_{DC,pre-fault}} \tag{3.39}$$

In reality, there will be no tap changer present in the inverter, so this is only a way of modeling the ratio of DC/AC voltage. In this formula, it is assumed that the voltage control does not respond to the quick voltage changes due to a fault.

Advantanges:

Only the turn ratio and requested current on the AC side need to be calculated. If the battery determines the behaviour on the AC side, this should be a good approach.

Disadvantanges:

The current on the DC side remains constant after the transient behaviour due to the inductance. This will not be the case in reality. The transient behaviour is assumed to be independent of the AC side, but this will have an influence.

Load as resistance

The battery won't see the impedance on the AC side as anything other than resistance, so can be modeled as a load resistor (*figure 3.10*). The load resistance can be calculated as follows:

$$P_{load} = (\frac{E_{a,pre-fault}^2}{Z_a} + \frac{E_{b,pre-fault}^2}{Z_b} + \frac{E_{c,pre-fault}^2}{Z_c}) \tag{3.40}$$

$$R_{load} = \frac{\eta \cdot V_{DC,pre-fault}^2}{P_{load}} \tag{3.41}$$

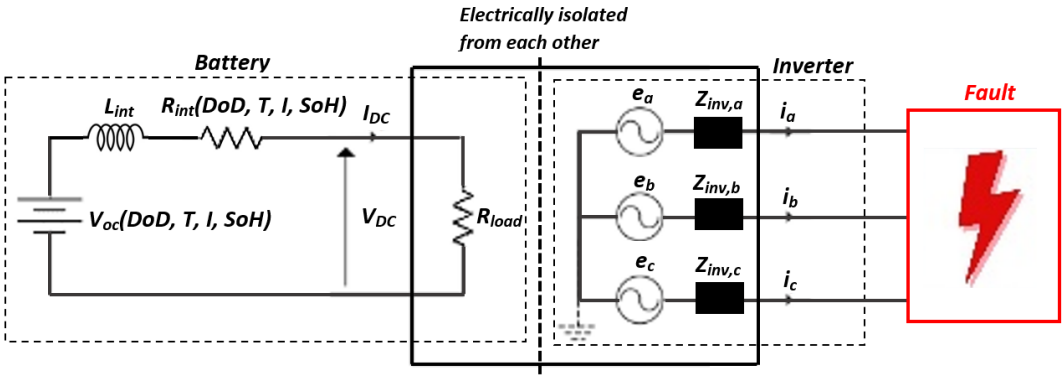

Figure 3.10 *Structure 'own' simplified BESS model: option 2*

In this way, the DC current is not completely constant as the OCV and internal resistance change slightly during operation. However, for the current dependency of the OCV and R_{int}, the varying discharge current cannot be used. The current is obtained by the varying OCV and R_{int}, so using this varying current creates a loop where all the parameters depend on each other. Hence, it is assumed that the initial DC current determines the effect. The initial current can be calculated as follows.

$$I_{DC} = \frac{V_{oc,pre-fault}}{R_{int,pre-fault} + R_{load}} \tag{3.42}$$

- $V_{oc,pre-fault}$ is the OCV at rest at a particular DoD. The SoH and ambient temperature can also be taken into account [V]
- $R_{int,pre-fault}$ is the internal resistance of the battery at rest. The SoH and ambient temperature can also be taken into account [Ω].

Here, the inductance must be physically modeled. The amount of inductance is determined using *equation (3.33)*, where R_{int} is the initial, unaffected internal resistance of the battery. The rest of the model is the same as *option 1.*

Advantanges:
In this model, the behaviour of the battery current corresponds to the behaviour on the AC side. The dynamic behaviour of the current is considered. This gives a more correct view than *option 1.*

Disadvantanges:
More calculations are needed. The effect current is considered to be the initial value, at t = 0 s. If the current decreases sharply over time, its effect is overestimated.

3.4.2 Matlab model

The battery circuit principle in Matlab Simulink is illustrated in *figure 3.11.*
The voltage source and internal resistance are made variable. These have initial values but vary depending on DoD, temperature, discharge current and SoH. The basic structures of the two earlier-mentioned options are presented. The current source in *figure 3.11a* is made controllable so that the transient behaviour of the internal inductance can be incorporated into it. The load resistor *figure 3.11b* remains constant, so it is assumed that the fault impedance at AC side does not change during the fault.

The battery and inverter are electrically isolated from each other in this model. The inverter circuit principle is outlined in Matlab Simulink and is illustrated in *figure 3.12.*

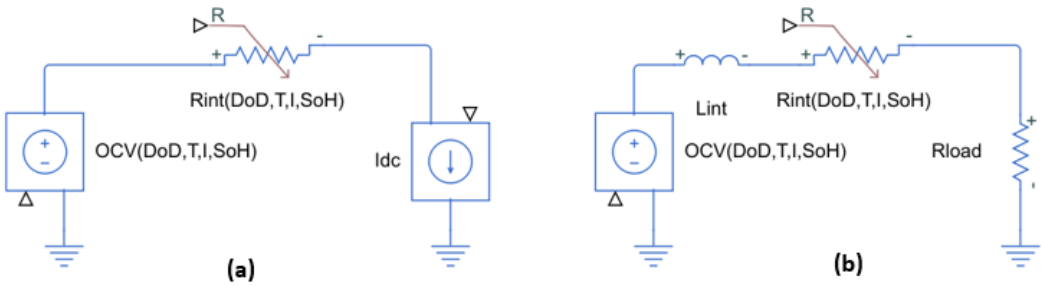

***Figure** 3.11 Basic structure battery model Matlab Simulink (a) Current source (b) Load resistor*

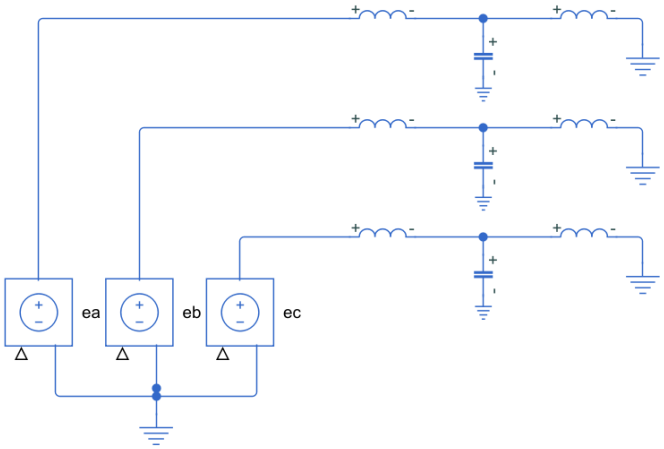

***Figure** 3.12 Basic structure inverter model Matlab Simulink*

Voltage sources are controlled so the voltage can be reduced to limit current. In case the battery cannot supply enough current to the inverter, it is assumed that the internal voltage of the inverter drops. The inverter feeds AC, so to obtain three-phase AC, the signal must be sent to create a sine wave.

$$\begin{cases} e_a = \sqrt{2} \cdot E_a \cdot sin(\omega t) \\ e_b = \sqrt{2} \cdot E_b \cdot sin(\omega t - \frac{2\pi}{3}) \\ e_c = \sqrt{2} \cdot E_c \cdot sin(\omega t - \frac{4\pi}{3}) \end{cases} \tag{3.43}$$

The LCL filters are also included in this model.

3.4.3 Overview input parameters

The more information given, the more accurate the approach will be. The parameters listed here are only those necessary to make a rough approximation of the fault current.

Battery

- Type of battery
- Discharge capacity new battery [Ah], if this value is not provided in [Ah], but in [Wh]:

$$I\ [Ah] = \frac{P\ [Wh]}{V_{nom}\ [V]} \tag{3.44}$$

- Minimum and maximum open-circuit voltage [V]
- Rated current [A]

- Internal resistance of a new, fully charged battery in rest at T = 298.15 K [Ω]
- Initial depth of discharge [-]
- Operating temperature [K]
- Minimum and maximum operating temperature [K]
- Battery mass [kg]
- Current cycle age [-]
- End of life cycle age and discharge capacity in [-] and [Ah], respectively
- Overcurrent limit(s) and time in [A] and [s], respectively

Inverter

- DC input voltage range and nominal voltage [V]
- Nominal AC voltage and FRT threshold(s) [V]
- Rated current [A]
- Efficiency [-]
- Operating temperature [K]
- Overcurrent limit(s) and time in [A] and [s], respectively

4 Evaluation of the model

4.1 BESS setup

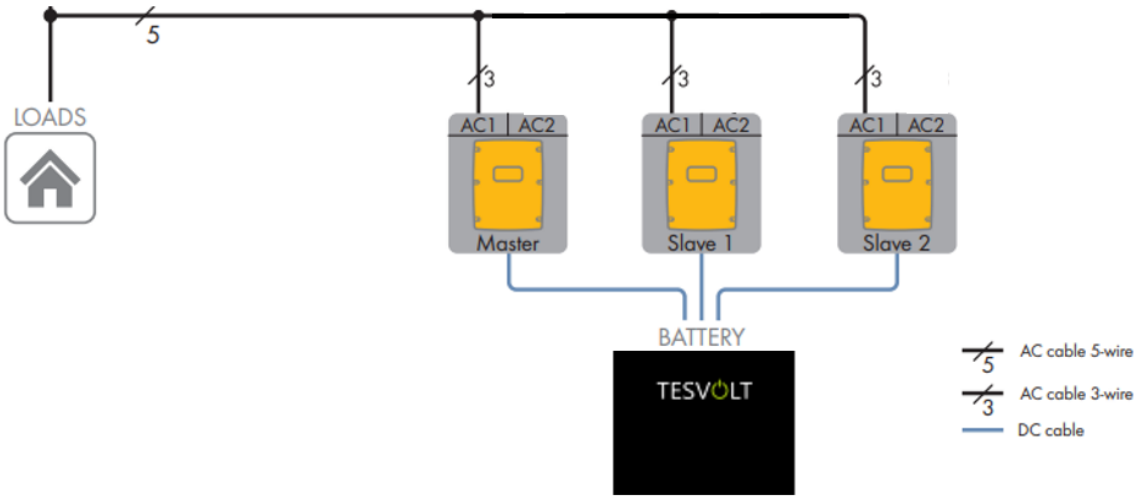

Figure 4.1 *Battery lab set-up: stand-alone mode*

The simulations use data from a set-up that is being developed in the lab. For the battery, three Tesvolt 48 V battery modules are set up in parallel [68]. The conversion from DC to three-phase AC is done using three SMA Sunny Island 6.0H inverters [62].

4.1.1 Battery modules

The 48 V Tesvolt battery modules consist of 14 94 Ah Samsung SDI NMC prismatic cells in series. The specifications of these NMC cells are provided [16]. The internal resistance of these cells is 0.75 mΩ. It is assumed that this internal resistance of a new fully charged battery is at rest and 25°C. In addition, it is assumed that the internal polarization resistance has a negligible effect during the first 5 s of discharge. The internal resistance of a battery module can be determined by:

$$R_{int,module} = 14 \cdot 0.75 \cdot 10^{-3} = 0.0105\ \Omega$$

This does not take into account the cable connections and contactors. There are three battery modules in parallel, so using *equation (2.2)*, the equivalent resistance and discharge capacity can be determined.

$$\begin{cases} R_{int} = (\frac{1}{0.0105} \cdot 3)^{-1} = 0.0035\ \Omega \\ Q_b = 3 \cdot 94Ah = 282\ Ah \end{cases}$$

The minimum and maximum operating OCV are 47.6 V and 58.1 V, respectively. These are the voltages where the battery is considered to be fully charged and discharged. If it is stated that the batteries are perfectly balanced, each can operate between 3.4 V and 4.15 V. This means that *equation (3.8)* needs to be adjusted. The new OCV-DoD curve can be determined using *equation (3.9)* and *equation (3.10)*. In the original curve in *figure 1*, DoD = 0.03 at 4.15 V and DoD = 0.95 at 3.4 V. Using calculation programs Excel or Matlab, the new tabular values can be obtained and the curve fit can be made:

DoD [-]	V_{oc} **[V]**	**DoD [-]**	V_{oc} **[V]**
0	4.15	0.509	3.80
0.021	4.12	0.564	3.79
0.075	4.07	0.618	3.77
0.129	4.02	0.672	3.75
0.184	3.98	0.727	3.73
0.238	3.94	0.781	3.70
0.292	3.91	0.835	3.66
0.346	3.89	0.889	3.60
0.401	3.85	0.944	3.52
0.455	3.82	1	3.40

Table 4.1 *Tabular data OCV-DoD Samsung SDI NMC cell under normal operating conditions*

In this range, the sharp increase due to electrolyte breakdown or the sharp decrease in OCV due to the lack of remaining electrolyte becomes almost imperceptible. Consequently, the quintic equation can be simplified to a cubic equation. From the curve fit in *figure 7*, a new equation can be obtained for the DoD dependency of the OCV.

$$V_{oc}(DoD) = -1.534 \cdot DoD^3 + 2.161 \cdot DoD^2 - 1.348 \cdot DoD + 4.15 \tag{4.1}$$

An R^2 of 0.9949 and RMSE of 0.0152 are obtained, There are 14 NMC cells in series, so the curve fit equation must be multiplied by 14. Following equation results:

$$V_{oc}(DoD) = -21.47 \cdot DoD^3 + 30.26 \cdot DoD^2 - 18.87 \cdot DoD + 58.1 \tag{4.2}$$

Since the other parameters also have an influence as a function of the DoD, namely temperature and SoH, they must also be adjusted. For the affecting parameters, the order of the equations does not change. The curve fits are illustrated in *figure 8* and *figure 9*. Next equations apply:

$$\Delta V_{oc}(DoD, T) = \begin{cases} -(V_{oc}(DoD, 298.15K) \cdot |298.15K - T|(9.19 \cdot 10^{-4} \cdot e^{-(\frac{DoD-1.057}{0.1909})^2})) & \text{if } T > 298.15K \\ (V_{oc}(DoD, 298.15K) \cdot |298.15K - T|(1.094 \cdot 10^{-3} \cdot e^{-(\frac{DoD-1.071}{0.1778})^2}) & \text{if } T < 298.15K \end{cases} \tag{4.3}$$

$$\Delta V_{oc}(DoD, SoH) = -(V_{oc}(DoD, 1) \cdot 100 \cdot (1 - SoH) \cdot (7.1 \cdot 10^{-12} \cdot e^{19.31 \cdot DoD})) \tag{4.4}$$

For the current dependence of the OCV, *equation (3.14)* remains applicable. The R_{int}-DoD curve must also be adjusted according to the new ranges. Since the unstable states of the battery are avoided by keeping the OCV within smaller ranges, the equation can be simplified to a quadratic instead of quartic relation.

$$R_{int}(DoD) = R_{int}(0) \cdot (0.1274 \cdot DoD^2 - 0.075 \cdot DoD + 1) \tag{4.5}$$

For the temperature, current and SoH dependency of the internal resistance, *equation (3.26)*, *equation (3.31)* and *equation (3.32)* remain applicable.

Input parameters

- **Type of battery**: NMC
- **Discharge capacity new battery**: $94Ah \cdot 3 = 282\ Ah$
- **Minimum and maximum OCV:** 47.6 V and 58.1 V

- **Rated current:** $94A \cdot 3 = 282\ A$
- **Internal resistance:** $\frac{0.0105}{3} = 0.0035\ \Omega$
- **End of life cycle age:** 6000 cycles (at 1C and T = 298.15 K)
- **End of life discharge capacity:** $0.7 \cdot 376Ah = 197.4\ Ah$
- **Minimum and maximum operating temperature:** 263.15 K and 323.15 K
- **Battery mass:** $34 \cdot 3 = 102\ kg$ (assuming it can be seen as one pack)

The overcurrent capabilities are not provided in the manufacturer's datasheets. However, there is a general document from Tesvolt indicating that the battery modules can feed 20 s at 4C discharge current without harming the batteries [67]. Besides, there are no restrictions on energy content. Therefore, it can be assumed that the BMS does not limit the current. The BMS has an overcurrent protection that should cut off the battery earlier than the 20 s at 4C. From this, it is stated that the battery can supply 1128 A during the 5 s time frame.

4.1.2 Inverter

Three inverters of type SMA Sunny Island 6.0H are used, which enables the conversion from DC to three-phase AC. These operate on the master-slave principle: one inverter operates as master and the two other operate as slaves. The specifications per inverter, i.e. per phase, are provided by the manufacturer.

Input parameters per inverter

- **Nominal DC input voltage:** 48 V DC
- **DC input voltage range:** 41 V to 63 V DC
- **Nominal AC output voltage:** 230 V AC
- **Fault-ride-through threshold:** Adjustable: full FRT or partial FRT. Some standard values are provided for partial FRT:
  - 0.300 p.u. for 30 ms
  - 0.450 p.u. for 300 ms
  - 0.800 p.u. for 3 s
- **Rated current:** 20 A
- **Overcurrent limits:** Adjustable: limiter or cut off
  - 120 A RMS for 60 ms
  - 47.8 A RMS for 3 s
  - 29.6 A RMS for 5 min
- **Efficiency:** The overcurrent that can be fed for a significant amount of time in the considered time frame of 0-5 s is $\approx$ 2.5 p.u. The efficiency curve of the inverter is illsutrated in *figure 2.52*. From this, an efficiency of 90% when feeding overcurrent is obtained.

4.2 Simulations

4.2.1 Preliminary calculations

For the simulations, the model in *figure 3.10* is used. This is the most accurate model and therefore requires the highest number of calculation steps. For illustrative purposes, the calculations are executed and explained in this thesis, although they can easily be done in Matlab.The load resistance depends on the impedance in each phase at the AC side.

The internal resistance of the battery is known, so the battery inductance can be determined using the time constant, as explained in 2.2.3.

$$L_{int} = 0.003 \cdot R_{int} = 0.003 \cdot 0.0035 = 10.5\ \mu H$$

The values of the filter inductors L_i and L_g, capacitor C_f and the resistor R_d can be approached using *equation (2.31)*, *equation (2.32)*, *equation (2.33)* and *equation (2.34)*. The configuration of the LCL filter is illustrated in *figure 2.45*. For V_{DC}, the nominal DC input voltage of 48 V is chosen. The nominal voltage of the inverter V_n is 230 V. The switching frequency f_s of modern inverters is usually $\approx$ 10000 Hz. The nominal apparent and active power are 4.6 kVA and 4.6 kW. The grid frequency f_n is 50 Hz.

$$L_i = \frac{48 \cdot 230}{16 \cdot 10000 \cdot 0.01 \cdot 4600 \cdot \sqrt{2}} = 1.06\ mH$$

$$C_f = \frac{0.05 \cdot 4600}{2\pi \cdot 50 \cdot 230^2} = 13.8\ \mu F$$

$$L_g = 0.6 \cdot 10.6 \cdot 10^{-3} = 0.636\ mH$$

$$R_d = \frac{1}{3 \cdot 13.8 \cdot 10^{-6}} \cdot \sqrt{\frac{10.6 \cdot 10^{-3} \cdot 0.636 \cdot 10^{-3} \cdot 13.8 \cdot 10^{-6}}{0.636 \cdot 10^{-3} + 10.6 \cdot 10^{-3}}} = 24.7\ \Omega$$

There is an LCL filter in each phase. There is a step-up transformer as well, which has impedance. The power of the inverter is 4.6kVA, meaning that the power of the single-phase transformer will not be much higher. For these small transformers, the X/R ratio $\approx$ 1 [57]. Assume a short-circuit voltage u_{cc} of 4% and a nominal apparent power S_{nom} of 5 kVA.

$$Z_{tr} = \frac{V_s^2 \cdot u_{cc}}{S_{nom}} = \frac{230^2 \cdot 0.04}{5000} = 0.423\ \Omega \tag{4.6}$$

$$Z_{tr} = \sqrt{R_{tr}^2 + X_{tr}^2}\ \ => R_{tr} = X_{tr} = 0.3\ \Omega \tag{4.7}$$

As the X/R ratio is 1, the series resistance and reactance of the transformer are equal. The inductance L of the transformer is $\approx$ 1 mH (X = ωL). Note that this is only an approach.

After the fault occurs, the turn ratio remains constant because voltage control cannot respond to the quick voltage drop due to the fault. The nominal voltage of the inverter is 230V, but it is measured after the filters. The main focus is on resistive LV grids. The total voltage drop across the filters and transformer will be $\approx$ 6V when feeding nominal power. In this way, the turn ratio can be determined:

$$k = \frac{\sqrt{2} \cdot 236}{V_{DC-pre-fault}}$$

4.2.2 Structure

A single-phase fault is simulated here, but the principle of fault current behaviour is the same for other types of faults if and if only the magnitude of the RMS current is considered. In these simulations, no coupling impedance between BESS and PCC is considered. In the simulations, the cable impedance between the PCC and load can be neglected. However, faults with fault resistance are considered. This fault resistance originates from the fault. As this resistance is in series with the resistance of, e.g., the cable, this resistance can represent the cable resistance as well. The affecting parameters of the battery are varied.

- DoD = 0% , 40% and 80%
- T = 278.15 K, 298.15 K and 318.15 K
- #cycles = 0, 2500 and 5000

Different pre-fault situations are simulated.

- Fault in feeder nominal loaded BESS. Fault occurs at the level of the PCC
- Fault in feeder between two loads. Fault does not occur at the PCC

The fault will occur after 20 ms. Fault currents over 120 A are not considered, as the SMA inverter is assumed to stop feeding immediately when the current exceeds this magnitude, i.e. inverter reacts as a fuse to these currents. However, it is also possible that, when the fault current determined only by physical laws > 120 A, the inverter limits the current at 120A and feeds this current for 60 ms. Also note that RMS currents are considered, despite the inverter will in practice limit the peak of the current. The Matlab Simulink model is illustrated in *figure 4.2*.

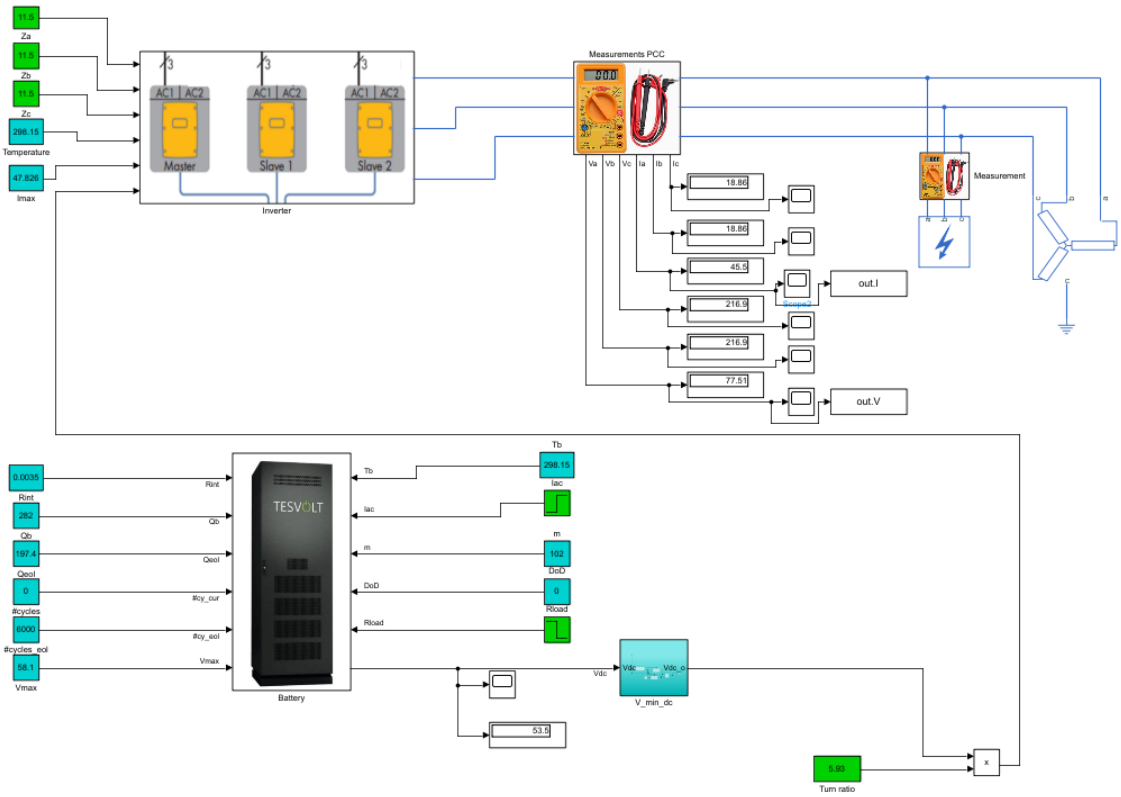

Figure 4.2 *BESS model Matlab Simulink*

The fault current is measured right after the PCC and branch of the fault.

4.2.3 Results

Fault in feeder nominal load

A single-phase fault current is simulated, so the magnitudes of the current in phase a are discussed. The currents in the other phases continue to feed the load. To illustrate, the calculations of the first simulation are outlined here. Because the fault current profiles are studied and the FRT capabilities of this inverter are adjustable, full FRT is considered.

1) $R_f = 2\ \Omega$, DoD = 0, T = 298.15 K and #cycles = 0

A single-phase fault occurs in phase a. In the first simulation, a fault resistance of 2 Ω is considered. This results in a total phase impedance $Z_a = 2.28\ \Omega$. The impedances Z_b and Z_c are 11.8 Ω. The modeled DC load can be calculated using *equation (3.40)* and *equation (3.41)*.

$$P_{load} = (\frac{E^2_{a,pre-fault}}{Z_a} + \frac{E^2_{b,pre-fault}}{Z_b} + \frac{E^2_{c,pre-fault}}{Z_c}) = (\frac{236^2}{2.28} + \frac{236^2}{11.8} \cdot 2) = 33.8\ kW$$

A new, fully charged battery at 298.15 K supplying 20 ms the nominal load on the AC side has a V_{DC} of 56.3V.

$$R_{load} = \frac{\eta \cdot V^2_{DC,pre-fault}}{P_{load}} = \frac{0.9 \cdot 56.3^2}{33.8 \cdot 10^3} = 0.084\ \Omega$$

From *equation (3.42)*, the initial DC current can be determined after the fault occurs.

$$I_{DC} = \frac{V_{oc,pre-fault}}{R_{int,pre-fault} + R_{load}} = \frac{57.6}{0.0036 + 0.088} = 657.5\ A$$

The turn ratio of the transformer k can be determined using *equation (3.39)*.

$$k = \frac{\sqrt{2} \cdot E_{inv,pre-fault}}{V_{DC,pre-fault}} = \frac{236 \cdot \sqrt{2}}{56.3} = 5.93$$

The current and voltage response at the PCC are presented in *figure 4.3*.

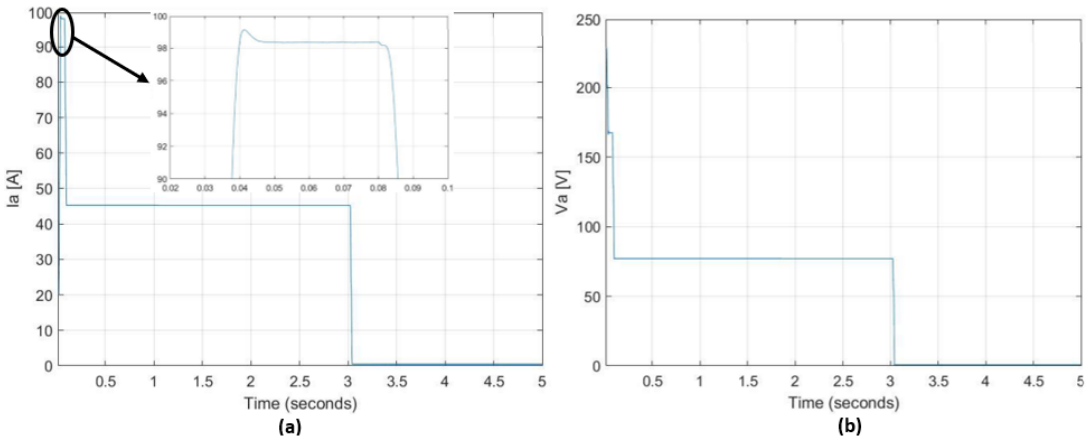

Figure 4.3 *Single-phase fault response of single BESS in island mode with $R_f = 2\ \Omega$ (a) RMS current (b) RMS voltage at PCC*

In *figure 4.3a*, one can see a spike in the RMS current at the beginning of the fault. This current spike is very small and short. This is due to the low X/R ratio, since the fault resistance dominates over the reactance of the inverter. The initial peak has a magnitude of 99.1 A and drops back to 98.3 A. After 60 ms, the current is reduced by the current limiter to 45.5 A. The current is limited

by reducing the average AC voltage. As a consequence, the voltage at the PCC drops to 80V, i.e. 0.350 p.u. If partial FRT was applied, the inverter would already stop feeding after 300 ms, since $V_{a,PCC} \approx 80\ V = 0.350$ p.u. < 0.450 p.u.(*figure 4.3b*).

The RMS current in the situation outlined here with DoD, T, I and SoH dependent battery is compared to a constant 56.3V DC input in *figure 4.4*.

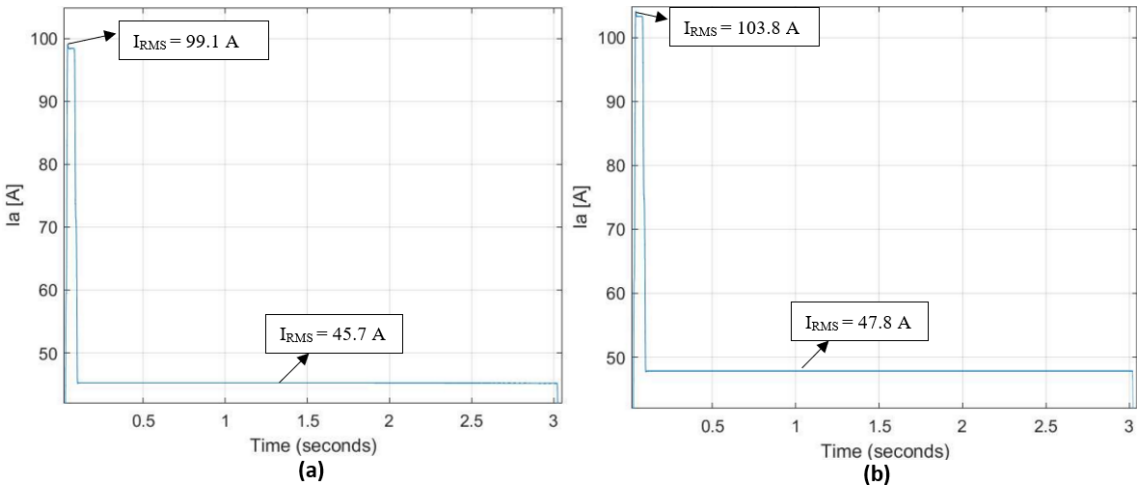

Figure 4.4 *Single-phase a-g fault current response island mode with $R_f = 2\,\Omega$ (a) Dynamic battery voltage (b) Constant battery voltage 56.3 V*

The DC voltage drops due to the varying OCV and R_{int} in the battery. The battery discharges, so the OCV will decrease. In addition, more current is demanded so both OCV and R_{int} will decrease. Consequently, the V_{DC} drops. Since the turn ratio and modulation factor of the voltage are assumed to remain constant during the fault, the voltage on the AC side decreases and as a consequence the fault current. The initial peak in RMS fault current is 4.7 A lower compared to the constant DC voltage. With a constant V_{DC}, the RMS fault current is limited after 60 ms to its given 47.8 A limit. With the dynamic DC voltage, the RMS current is only 45.5 A. After 3 s, the inverter stops feeding due to the overcurrent limits of the inverter.

The RMS current drops after the initial peak. A closer look is needed at first 50-100 ms after the fault occurs. This is illustrated in *figure 4.5*.

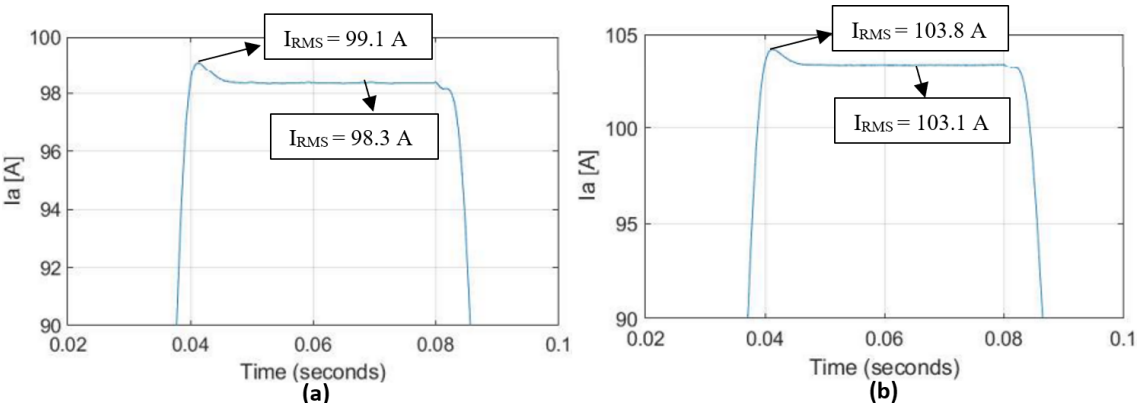

Figure 4.5 *Initial single-phase a-g fault current response island mode with $R_f = 2\,\Omega$ (a) Dynamic battery voltage (b) Constant battery voltage 56.3 V*

After the peak, the RMS current drops by 0.7 a 0.8 A. This has little to nothing to do with the battery behavior, so is equal for dynamic and constant DC voltage.

The current limiting has no influence on the current response after it has limited the current. In *figure 4.6* illustrated what happens to the current after it is limited.

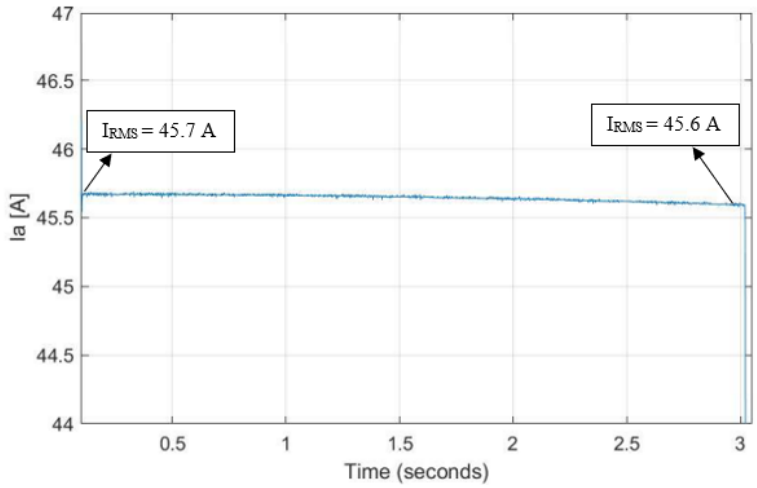

Figure 4.6 *Single-phase a-g fault response BESS with R_f = 2 Ω: limited fault current*

In this case, the difference in current right after limiting at and right before the BESS stops feeding is not very significant, but there is a very small decrease in current visible in *figure 4.6* after 3 s of feeding the overcurrent. At a constant DC voltage, it remains constant 47.8 A and cuts off after 3 s feeding overcurrent as well.

The fault current is also measured here in the branch of the fault. This location is indicated on *Figure 4.2* 'Measurement'. The results can be seen in *table 4.2*.

-	**Dynamic V_{DC}**	**Constant V_{DC}**
$I_{RMS,initial}$	85.0 A	88.8 A
$I_{RMS,after-peak}$	84.2 A	88.1 A
$I_{RMS,after-lim}$	38.8 A	40.8 A
$I_{RMS,3\ s}$	38.7 A	40.8 A

Table 4.2 *Fault event when feeding nominal load with R_f = 2 Ω: current at fault branch*

These values are from the same simulation, but differ from the magnitudes in the earlier shown figures. The current in the fault branch differs from the current right after the PCC. The load and fault have both a resistance. As a result, some current still flows to the load as well during the fault event. In the case of a fault at the PCC with no resistance, all current flows to the fault.

This fault, with particular fault resistance = 2 Ω, is simulated under different battery conditions. For this fault event, tables are created showing the magnitude of the RMS current of the peak, after the peak, after current limiting and right before the inverter cuts off.

2) DoD = variable with R_f = 2 Ω, T = 298.15 K and #cycles = 0

-	**DoD = 0**	**DoD = 0.4**	**DoD = 0.8**
$I_{RMS,initial}$	99.1 A	98.6 A	97.6 A
$I_{RMS,after-peak}$	98.3 A	97.8 A	97.0 A
$I_{RMS,after-lim}$	45.5 A	45.2 A	44.8 A
$I_{RMS,3\ s}$	45.4 A	45.1 A	44.7 A

Table 4.3 *Fault event when feeding nominal load with R_f = 2 Ω for different DoD*

In *table 4.3*, it can be seen that the DoD of the battery has an effect on the fault current. For higher DoD, the fault current is slightly lower. The internal resistance is a more significant factor because the resistance is higher at high DoD. When a fault occurs at DC side, the impedance at AC side drops. As a result, the modeled load resistance decreases, which means that the current at DC side increases. Higher internal resistance and lower load resistance means that the effect of internal resistance is more significant than for lower DoD. This means that the DC voltage decreases more, which causes the internal voltage of the inverter to decrease. Consequently, the current on the AC side is lower.

The results in *table 4.3* imply that, at a DoD of 80%, the battery was charged only 20% and the fault occurs almost immediately after the BESS starts to feed. Since DoD = 0.8 is the worst-case scenario, this DoD is used further to account for the next effects.

3) T = variable with $\mathbf{R_f}$ = 2 Ω, DoD = 0.8 and #cycles = 0

-	**T = 278.15 K**	**T = 298.15 K**	**T = 318.15 K**
$I_{RMS,initial}$	97.9 A	97.5 A	96.8 A
$I_{RMS,after-peak}$	97.2 A	96.8 A	96.1 A
$I_{RMS,after-lim}$	45.0 A	44.8 A	44.5 A
$I_{RMS,3\ s}$	44.9 A	44.7 A	44.4 A

Table 4.4 *Fault event when feeding nominal load with R_f = 2 Ω for different battery temperatures*

In *table 4.4*, one can see that the fault current is higher at lower temperatures. However, this does not mean that feeding at lower temperatures is wanted. There are more losses at lower temperatures, which means the battery has to feed more power. The current is higher because the OCV is higher at lower temperatures. Since the battery has only 20% of its capacity left at the time of the fault, the temperature has a significant impact on the OCV (*Figure 2.17*).

4) #cycles = variable with $\mathbf{R_f}$ = 2 Ω, DoD = 0.8 and T = 298.15 K

In this model, it is assumed that the battery has suffered no additional damage in the cycles prior to the fault, and has consistently delivered its rated current of 1C. The DoD = 0.8 and T = 298.15 K. The results are presented in *table 4.5*.

-	**#cycles = 0**	**#cycles = 2500**	**#cycles = 5000**
$I_{RMS,initial}$	97.6 A	97.2 A	96.6 A
$I_{RMS,after-peak}$	97.0 A	96.5 A	96.0 A
$I_{RMS,after-lim}$	44.8 A	44.6 A	44.3 A
$I_{RMS,3\ s}$	44.7 A	44.5 A	44.2 A

Table 4.5 *Fault event when feeding nominal load with R_f = 2 Ω for different battery temperatures*

If the battery has already done more cycles, i.e. SoH is lower, the OCV decreases and the internal resistance of the battery increases. This causes more losses on the one hand, but also less fault current.

If the scenario with a DoD = 0.8 and #cycles = 5000 is compared with the scenario with constant V_{DC}, a 7.5% decrease in fault current is observed.

Fault in between two loads

The next simulated fault is a single-phase fault in between two loads. The load power per individual load is one-third of the nominal load of the BESS. This is illustrated in *Figure 4.7*.

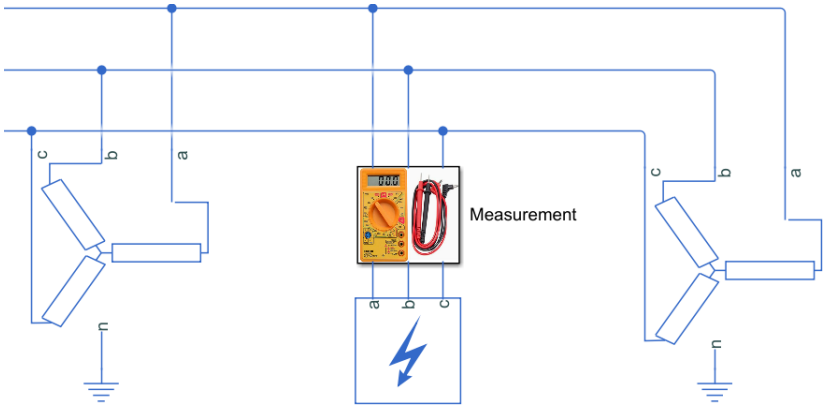

Figure 4.7 *Single-phase fault in between two loads*

1) $R_f = 2\ \Omega$, DoD = 0, T = 298.15 K and #cycles = 0

Since this fault has the same fault resistance, the fault current is expected to be approximately the same as in the previous situation.

First, the simulations of the dynamic battery parameters are compared again with the constant DC voltage.

-	Dynamic V_{DC}	Constant V_{DC}
$I_{RMS,initial}$	96.0 A	100.5 A
$I_{RMS,after-peak}$	95.3 A	99.8 A
$I_{RMS,after-lim}$	45.5 A	47.8 A
$I_{RMS,3\ s}$	45.4 A	47.8 A

Table 4.6 *Fault in between loads with $R_f = 2\ \Omega$: current at PCC*

The initial fault current, on which the inverter's control has not yet reacted, will be slightly lower because the BESS was not nominally loaded. The inverter drew less current pre-fault, i.e., the impedance is higher than the rated load impedance, the equivalent resistance seen by the inverter during the fault is slightly smaller and draws more current. The fault current gets limited to the same magnitude as the first scenario. This is logical since it does not matter for the current limiter what current was flowing in the first 60 ms, it always has to limit the current to the same value. The voltage at the PCC after limiting is 82 V, which is higher than in the first scenario. Since the current limiter has to reduce the current less, the needed decrease in voltage is less. However, with partial FRT, the inverter would still cut off after 300 ms since 82 V is 0.356 p.u. $<$ 0.450 p.u.

The fault current in branch of the fault is measured as well, see *Figure 4.7*. The results are represented in *table 4.7*.

-	Dynamic V_{DC}	Constant V_{DC}
$I_{RMS,initial}$	86.0 A	90.2 A
$I_{RMS,after-peak}$	85.3 A	89.5 A
$I_{RMS,after-lim}$	40.8 A	42.9 A
$I_{RMS,3\ s}$	40.7 A	42.9 A

Table 4.7 *Fault in between loads with $R_f = 2\ \Omega$: current at fault location*

The magnitude of the fault current is here higher than in scenario 1. In the previous situation, the inverter was rated load and here it was only $\frac{2}{3}$ of its nominal load. This means that the load draws less current and so there is more current in the branch of the fault.

Comparison with grid-connected BESS

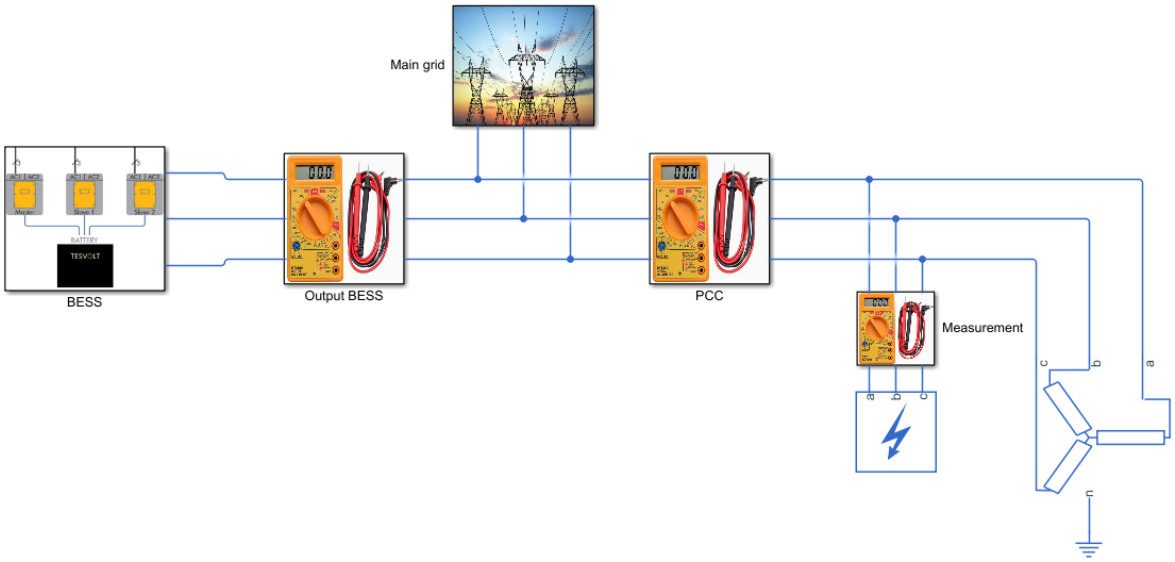

Figure 4.8 *Matlab Simulink model with grid-connected BESS*

For comparison with on-grid, the first scenario is taken. The load is 4.6 kW and $R_f = 2\ \Omega$. In the first simulation, the battery has a DoD = 0, T = 298.15 K and #cycles = 0. The grid voltage is 230 V. The main grid has a short-circuit capacity of 0.5 MW and the X/R ratio is 15. These are not general, but realistic values. The main grid feeds in parallel with the BESS. No further control strategies or modifications have been added. The results of this grid-feeding mode are illustrated in *figure 4.9*.

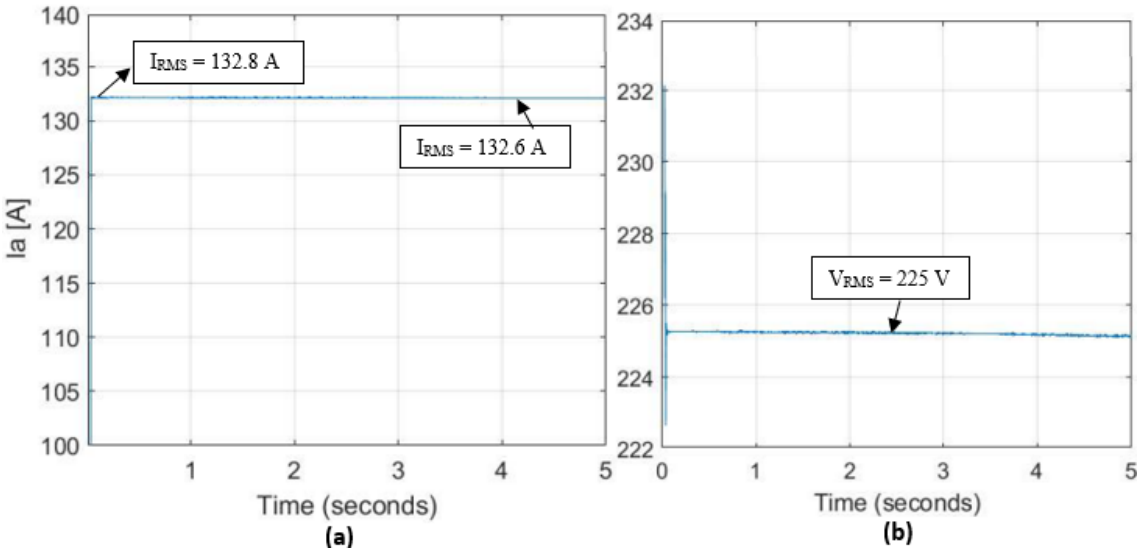

Figure 4.9 *Single-phase fault response grid-connected BESS with $R_f = 2\ \Omega$ (a) RMS current (b) RMS voltage at PCC*

It can be observed that the current and voltage at the PCC are higher compared to the islanded BESS. No high peaks in RMS current are observed, despite the high X/R ratio of the grid. This is because the impedance of the parent main grid is negligible compared to the resistive impedance of the fault. There is also no current limiting or cut off. The more robust main grid can tolerate

higher fault currents than the sensitive components of the inverter. The voltage at the PCC is close to the nominal voltage, since the equivalent grid impedance, i.e. main grid and inverter, is low compared to the fault resistance of 2Ω. With an ideal short circuit on the PCC, i.e. no fault resistance, the voltage at the PCC is 0 V.

The output current of the BESS is also evaluated during the fault. The current profile is illustrated in *Figure 4.10*.

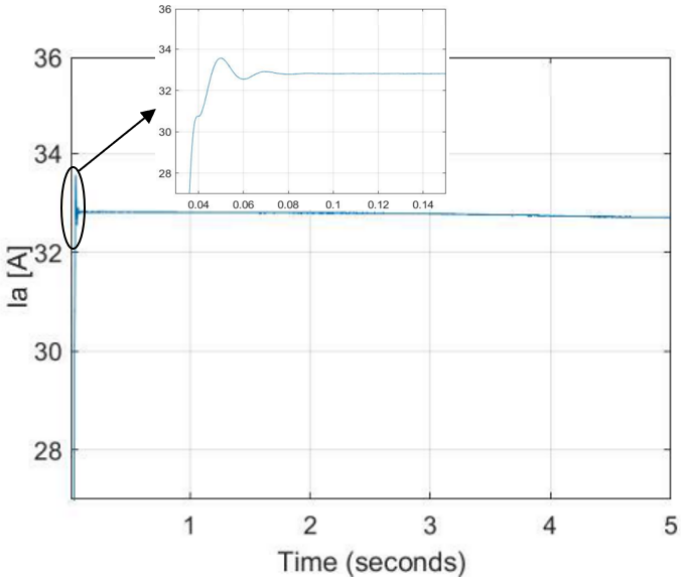

Figure 4.10 *Output current BESS in grid-connected mode during fault with R_f = 2 Ω*

The peak in RMS current, which can be observed in *Figure 4.10* at t ≈ 0.05 s, is more significant compared to the steady state-current than in island mode. This is because the equivalent resistance that the BESS inverter sees is smaller and consequently the X/R ratio is higher. However, the current is much lower. The main grid feeds almost all the fault current, putting much less load on the inverter. After the peak of 33.8 A, the fault current remains ≈ 32.8 A. In grid-connected mode, the BESS can continue feeding the fault for more than 5 s due to the lower current, which the inverter can tolerate better. The output voltage at the terminals of the inverter is the same as the voltage at the PCC.

Since the currents on the AC side are smaller, the battery is also under less load. This results in less current, which means the OCV will downshift less and the internal resistance of the battery is lower. The situation is simulated where DoD = 0.8, T = 318.15 K and #cycles = 0. This was the situation for which the islanded BESS already stopped feeding due to the low OCV. The results for the grid-connected BESS are presented in *table 4.8*.

-	**At terminals inverter**	**At PCC**
$I_{RMS,initial}$	33.0 A	131.8 A
$I_{RMS,5\ s}$	32.0 A	131.6 A

Table 4.8 *Fault event grid-connected BESS with R_f = 2 Ω, DoD = 0.8, T = 318.15 K and #cycles = 0*

A difference < 1% in fault current at PCC between this situation and a fully charged battery at T = 298.15 K is observed.

4.3 Analysis results

For this BESS, the inverter will be the restrictive component in many cases. However, battery parameters affect the fault current.

- The fault current is lower when the battery is more discharged, i.e. DoD is higher. This is due to the lower OCV and higher R_{int} when the battery is more discharged.
- In the simulations, it was observed that the fault current was lower at higher temperatures. However, at lower temperatures, there are more losses due to sluggish chemistry. This low temperature was already there before the fault, so the modulation control of the inverter had already adapted to the lower V_{DC} due to the higher R_{int}. Due to high fault currents, the (extra) voltage drop across the internal resistance will be higher, but at lower temperatures, the OCV is also higher. Especially when the battery is almost fully discharged, this has a significant effect. This effect is then dominant over the voltage drop across the internal resistance of the battery. The fact that fault current is higher at lower temperatures cannot be generalized. For lower DoD, the OCV will change negligibly as a function of temperature, but the voltage drop across the higher internal resistance remains. Hence, it is possible that the fault current is lower at lower temperatures. However, here the focus is on the worst-case scenarios and that is when the battery is almost fully discharged. Note that this applies to temperatures within the battery's operating frame.
- The fault current is lower when the battery already did more cycles, resulting in more damage, i.e. SoH is lower. This is due to the lower OCV and higher internal resistance when the battery is more damaged.

Decreases in fault current of 5-10% are observed relative to constant V_{DC} for this BESS. The difference in current after current limiting is possibly overestimated here. The method of current limiting used is dissipation in a resistor. In practice, this will be done with control circuits. If this is done by lowering the battery voltage, the current on the DC side will also be smaller and consequently the effects of the discharge current will be weaker, i.e. less downshift in the OCV-DoD curve and less internal resistance.

In the simulations, discharge currents of 4C (= 1128 A), which can be fed by the battery modules for 20 s, were never reached. If the inverter is strongly oversized, the battery can be cut off due to excessive currents.

The internal resistance is determined with a rough approximation based on the cells used internally, but possibly there are more internal resistance connections and other components in and between the battery modules. For more exact behaviour, resistance measurements are needed. The internal resistance is here very small compared to the load resistance that represents the AC-side. If the internal resistance is higher, the fault resistance is lower and the inverter is oversized, the internal resistance can have a significant impact.

Some situations that are yet to emerge in the performed simulations, but are possible:

- The battery heats up due to the fault current and reaches its maximum temperature before the AC fuse cuts off the fault current. The BMS cuts off the battery prematurely.
- Due to a previous fault, the battery's electrolyte has broken down to the extent that the battery's internal resistance has strongly increased. Consequently, the DC voltage is too low and the inverter does not let the power through.
- The inverter is significantly oversized and can feed a lot more fault current.

- The overcurrent fuse of the battery cuts the excessive DC current.
- The OCV drops at that high rate due to the high current on the DC side causing the BMS undervoltage protection to cut off the battery.
- The voltage drop across the internal resistance of the battery is so high due to the high DC current that the V_{DC} is no longer in the input range of the inverter. Consecutively, the inverter does not let the current through.

The simulations require a number of assumptions to be made. Possibly, the control system of the inverter works differently so that, e.g., higher currents than 120 A are still limited to 120 A and get cut off after 60 ms or get further limited to 47.8 A. Inverters will behave very similarly, but manufacturers each have their design methods and differences in design are very likely.

Comparisons were made with grid-connected mode and it can be observed that the voltage at the PCC and fault current are higher. Since the main grid feeds most of the fault current, the BESS is under less load and the impactful parameters of the battery have less effect.

5 Discussion

A BESS model was developed based on existing research and the manufacturer's datasheets, with the battery part as the main focus. Curve fitting was used to incorporate the affecting parameters into a model. NMC batteries are mainly considered here, as this is the most common chemistry in today's BESS. Different chemical structures do not react in the same way. For example, the difference in potential is different between NMC and LFP batteries. However, the curves always have the same/a similar shape. The correlations can be generalised for all Li-ion batteries, but the constants vary. It is assumed that the OCV curves of batteries with the same chemical composition are always the same, apart from the voltage at which they can operate. Small variations are possible, but as a simplification, it suffices. The internal resistance of the battery is determined using the manufacturers' datasheets. This method can have inaccuracies. The internal resistance depends on how long the batteries have already been discharging. Polarization phenomena can have an effect and these effects cannot be derived without more complex measurements such as EIS or PRBS. Besides, multiple batteries are connected in a BESS, so connections and contactors cause additional resistance. As a reference value, the method used in this thesis suffices, but resistance measurements are recommended. The BMS and its protection systems will ensure that the battery is not damaged while feeding fault currents and cut off in time. It must be taken into account that some assumptions/simplifications were made. For example, battery cooling is not considered.

The initial equations were developed based on the scenario where the batteries may fall into less stable states resulting in, e.g., electrolyte breakdown due to low and high OCV. Depending on the range in which the batteries can operate, the curves need to be adjusted. Simplified equations, i.e. lower order equations, are possible if the BESS manufacturer tightens the operating voltage range. The simulations used a set-up with Tesvolt battery modules. The curve fits are adjusted to these battery modules.

In the datasheet of the inverter manufacturer SMA, overcurrent limits are given, but the inverter can both cut off and limit the current. Hence, the most probable situation is chosen. No explicit FRT guidelines are provided by the grid operator for IBDER < 1 MW. This is also important for the islanded BESS, as this is a determining factor whether the BESS continues to feed during a fault or not.

In the simulations, it was found that the fault current fed by the islanded BESS is lower with the dynamic V_{DC}, compared to constant V_{DC}. A reduction in fault current of 5-10% is possible, under the condition that the inverter's voltage control switches off/cannot regulate the voltage during the fault. Therefore, this should be considered for sizing the fuses. A possibility to size the fuses is to consider the situation where the battery has the lowest SoC, highest operating temperature and is at end-of-life. For grid operators, who are not aware of how many cycles the battery has already done or what the state of charge is at the moment of the fault, the worst-case scenario should be considered.

For the BESS considered here, the islanded BESS can feed less fault current than in grid-connected mode. This is not necessarily the case. As mentioned earlier, the manufacturer can set the internal voltage of the BESS slightly higher than 1.00 p.u. if feeding in island mode, so the fed fault current may be higher. This means that grid-connected should still be considered.

6 Conclusions

This thesis addressed the parameters that affect the fault current of the battery for BESS fault calculation purposes. The objective was to develop a model using information available from the BESS manufacturer and pre-existing studies. The output of this model is the fault current on the AC side. The BESS operating in island mode is the scenario where the fault current is often the smallest, so is considered here. The considered time frame is 0-5 s, as the overcurrent protection at the AC side should react within this period.

The OCV and internal resistance of the battery are the parameters that determine the battery's behaviour during a fault. The inverter is also included in this model to obtain a fault current model for an entire BESS. The main research question was:

'Which parameters affect the fault current of a feeding BESS in LV grids?'

It was obtained that the OCV and R_{int} of the battery are affected by the state of charge, temperature, discharge current and cycle age. If the battery is more discharged, the available fault current is lower. The same applies to the cycle age. For the operating temperature it is important to work in the correct temperature frame because at lower temperatures there are more losses and at higher temperatures, there is less fault current available and the battery might cut off prematurely. At higher discharge currents, the OCV will be lower and the R_{int} higher. This results in a decrease in V_{DC}, meaning that the voltage at the AC side reduces as well. Furthermore, batteries and inverters are sensitive components, so the protection systems have a strong influence on how much and how long a particular fault current can be supplied. The inverter can limit the fault current if it becomes too high. This is done by reducing the internal voltage, which lowers the voltage at the PCC and therefore the fault current as well.

Another question was: *'Can a general fault current model be developed for all Li-ion BESS?'*. This is possible if the constants are adjusted in the equations obtained with curve fitting. The correlations will always show the same behaviour/similar behavior, but, e.g., the OCV differ between Li-ion batteries. In addition, batteries are always improving, so the effect of impactful parameters can become less significant.

The final question was: *'Is it possible to make a BESS fault current model only using information from the manufacturer's datasheet?'*. The grid operators want one particular model for BESS. To work towards this particular, simplified model, it is necessary to evaluate all the affecting parameters. It can be concluded here that the battery parameters can cause the fault current to be lower on the AC side, so a correction factor will be needed in the model indicating this. BESS manufacturers do not provide the internal resistance of the battery, but it does affect the available fault current. The internal resistance under certain conditions or the worst-case internal resistance should be known. BESS have different operating modes, so some simplifications and assumptions must be made. For example, it should be taken into account that the current can be reduced by the current limiter in the inverter. The fault-ride-through capabilities is an important factor as well. General specifications for IBDER $<$ 1 MW are recommended to obtain one particular BESS model for fault calculations in LV grids. It can be concluded that not all necessary parameters can be found in manufacturers' datasheets.

A possible application was to size fuses in the LV grid. The worst-case scenario, based on the battery, is the situation where the battery is almost fully discharged, operating at a high temperature, and is at end-of-life cycle age. Higher discharge currents can also reduce the fault current. This depends on the equivalent resistance at the AC side and the AC/DC voltage ratio.

The higher the voltage at AC side is compared to the DC side, the lower the equivalent resistance in a certain fault event, the higher the average current at DC side. Higher discharge current reduces the OCV and increases the internal resistance, resulting in less current. Besides, the protection of the battery and inverter must also be taken into account. The fuses in the LVAC grid must intervene earlier to avoid cutting off too much of the LV grid.

6.1 Future work

This thesis is the first part of the development of a general BESS fault current model. Internal resistance measurements for the battery are recommended. The results can be compared with the internal resistance obtained in this thesis, which is determined based on the information from manufacturers' datasheets. It can be evaluated whether the datasheet method is sufficient or if measurements are necessary. The affecting parameters were obtained from various studies. Another challenge may be to use more complex methods such as PRBS or EIS to further evaluate all these impactful parameters for different types of batteries in one research.

To obtain one particular BESS model, simulations and measurements are recommended for different BESS. From this, a conclusion can possibly be obtained that the fault current in island mode is, e.g., 5-10% smaller when the battery is nearly discharged and at the end of its life. Temperature measurements during fault situations are also recommended to evaluate if the battery is sufficiently cooled during the fault.

References

[1] C. M. Shepherd (1965). *Design of Primary and Secondary Cells: II . An Equation Describing Battery Discharge.* URL: https://iopscience.iop.org/article/10.1149/1.2423659/pdf. (visited: 9.10.2022).

[2] Cooper Bussmann (2005). *Selective Coordination Fuses.* URL: https://www.eaton.com/content/dam/eaton/products/electrical-circuit-protection/fuses/solution-center/bus-ele-tech-lib-fuses-selective-coordination.pdf. (visited: 16.10.2022).

[3] Maria Brucoli (2008). *Fault behaviour and fault detection in islanded inverter-only microgrids.* URL: https://core.ac.uk/download/1590830.pdf. (visited: 16.09.2022).

[4] SFS (2008). *SFS-EN 60269-1 Pienjännitevarokkeet. Osa 1: Yleiset vaatimukset.* URL: https://online.sfs.fi/. (visited: 11.10.2022).

[5] EEMB (2010). *Lithium-ion Battery DATA SHEET: LIR18650 2600mAh.* URL: https://www.ineltro.ch/media/downloads/SAAItem/45/45958/36e3e7f3-2049-4adb-a2a7-79c654d92915.pdf. (visited: 20.10.2022).

[6] Electrical Engineering Portal (2013). *An overview of short-circuit current.* URL: https://electrical-engineering-portal.com/an-overview-of-short-circuit-current-part-2. (visited: 5.11.2022).

[7] Peng Zhang (2013). *48V Battery management unit.* URL: https://trepo.tuni.fi/bitstream/handle/123456789/21964/Zhang.pdf?sequence=3&isAllowed=y. (visited: 23.11.2022).

[8] Jacob Klimstra (2014). *Power supply challenges.* URL: https://cdn.wartsila.com/docs/default-source/smartpowergeneration/content-center/power-supply-challenges_english.pdf. (visited: 5.09.2022).

[9] Nadim Maluf (2014). *LCO, LFP, NMC… cryptic live of the cathode.* URL: https://www.qnovo.com/blogs/lco-lfp-nmc-cryptic-lives-of-the-cathode. (visited: 20.10.2022).

[10] Yong Li; Lifang Wang; Chenglin Liao; Lingfei Wu; Junfeng Li; Yanjie Guo (2014). *Effects of temperature on dynamic characteristics of li-ion batteries in electric vehicle applications.* URL: https://ieeexplore.ieee.org/document/6940648. (visited: 2.11.2022).

[11] Alexander Erik Magnusson (2016). *Modelling of battery cooling for Formula Student application.* URL: http://www.diva-portal.org/smash/get/diva2:970700/FULLTEXT01.pdf. (visited: 23.11.2022).

[12] Electrical Concepts (2016). *Concept of Subtransient; Transient and Steady State.* URL: https://electricalbaba.com/concept-of-subtransient-transient-steady-state/. (visited: 5.11.2022).

[13] Pietro Raboni (2016). *Modelling, Control and Integration of Distributed Generators for Enhanced Ancillary Services.* URL: https://www.researchgate.net/publication/333651312_Modelling_Control_and_Integration_of_Distributed_Generators_for_Enhanced_Ancillary_Services. (visited: 16.10.2022).

[14] Data Science Central (2017). *How To Interpret R-squared and Goodness-of-Fit in Regression Analysis.* URL: https://www.datasciencecentral.com/regression-analysis-how-do-i-interpret-r-squared-and-assess-the/. (visited: 8.11.2022).

[15] Jussi Sihvo (2017). *Internal impedance measurement techniques and charger-dynamics for lithium-ion batteries.* URL: https://trepo.tuni.fi/bitstream/handle/123456789/25350/Sihvo.pdf?sequence=4. (visited: 10.10.2022).

[16] EV lithium (2018). *Samsung SDI94 Li Ion 3.7V 94AH NMC Lithium Prismatic Battery.* URL: https://www.evlithium.com/hot-lithium-battery/845.html. (visited: 10.09.2022).

[17] Fingrid (2018). *Grid Code Specifications for Power Generating Facilities VJV2018.* URL: https://www.fingrid.fi/globalassets/dokumentit/en/customers/grid-connection/grid-code-specifications-for-power-generating-facilities-vjv2018-.pdf. (visited: 21.09.2022).

[18] John B. Goodenough (2018). *How we made the Li-ion rechargeable battery.* URL: https://www.nature.com/articles/s41928-018-0048-6. (visited: 1.11.2022).

[19] Bob Zollo (2019). *Temperature Impact on OCV of Lithium-Ion Cells.* URL: https://www.electronicdesign.com/technologies/test-measurement/article/21808722/temperature-impact-on-ocv-of-lithiumion-cells. (visited: 27.10.2022).

[20] Parthasarathy Chethan; Hafezi Hossein; Laaksonen Hannu (2020). *Lithium-ion BESS integration for smart grid applications : ECM modelling approach.* URL: https://ieeexplore.ieee.org/document/9087741. (visited: 4.10.2022).

[21] Battery university (2021). *BU-808b: What Causes Li-ion to Die?* URL: https://batteryuniversity.com/article/bu-808b-what-causes-li-ion-to-die. (visited: 29.11.2022).

[22] Battery University (2021). *BU-103: Global Battery Markets.* URL: https://batteryuniversity.com/article/bu-103-global-battery-markets. (visited: 28.08.2022).

[23] Cedric Benoit (2021). *Disassembly of electric vehicle battery packs.* URL: https://repository-teneo-libis-be.kuleuven.e-bronnen.be/delivery/DeliveryManagerServlet?dps_pid=IE15948182&. (visited: 1.11.2022).

[24] Statology (2021). *RMSE vs. R-Squared: Which Metric Should You Use?* URL: https://www.statology.org/rmse-vs-r-squared/. (visited: 8.11.2022).

[25] Battery design (2022). *Specific Heat Capacity of Lithium Ion Cells.* URL: https://www.batterydesign.net/specific-heat-capacity-of-lithium-ion-cells/. (visited: 1.12.2022).

[26] Flash Battery (2022). *Which chemistry is most suitable for electrification of your vehicle?* URL: https://www.flashbattery.tech/en/types-of-lithium-batteries-which-chemistry-use/. (visited: 28.10.2022).

[27] Jeff Shepard (2022). *What battery chemistries are used in grid-scale energy storage?* URL: https://www.batterypowertips.com/what-battery-chemistries-are-used-in-grid-scale-energy-storage-faq/. (visited: 20.10.2022).

[28] Zeyang Geng (2022). *Characterization methods and modelling for Li-ion batteries.* URL: https://research.chalmers.se/publication/530015/file/530015_Fulltext.pdf. (visited: 20.09.2022).

[29] Aicha Degla; Madjid Chikh; Chouder Aissa and Bouchafaa Farid (2019). *Comparison study and parameter identification of three battery models for an off-grid photovoltaic system.* URL: https://www.researchgate.net/publication/330634265_Comparison_study_and_parameter_identification_of_three_battery_models_for_an_off-grid_photovoltaic_system. (visited: 20.10.2022).

[30] Gaizka Saldaña; José Ignacio San Martín; Inmaculada Zamora; Francisco Javier Asensio and Oier Oñederra (2019). *Analysis of the Current Electric Battery Models for Electric Vehicle Simulation*. URL: https://www.researchgate.net/publication/334564888_Analysis_of_the_Current_Electric_Battery_Models_for_Electric_Vehicle_Simulation. (visited: 17.09.2022).

[31] Liu Yun; Duy Linh; Li Shui; Xiongbin Peng; Akhil Garg; My Loan Phung LE; Saeed Asghari and Jayne Sandoval (2018). *Metallurgical and mechanical methods for recycling of lithium-ion battery pack for electric vehicles*. URL: https://www.sciencedirect.com/science/article/pii/S0921344918301599. (visited: 2.11.2022).

[32] Dian Wang; Yun Bao and Jianjun Shi (2017). *Online Lithium-Ion Battery Internal Resistance Measurement Application in State-of-Charge Estimation Using the Extended Kalman Filter*. URL: https://www.mdpi.com/1996-1073/10/9/1284. (visited: 17.10.2022).

[33] Joan Rocabert; Alvaro Luna; Frede Blaabjerg and Pedro Rodrıguez (2012). *Control of Power Converters in AC Microgrids*. URL: https://ieeexplore.ieee.org/stamp/stamp.jsp?tp=&arnumber=6200347. (visited: 13.09.2022).

[34] Michael A Roscher; Oliver Bohlen and Jens Vetter (2011). *OCV Hysteresis in Li-Ion Batteries including Two-Phase Transition Materials*. URL: https://www.researchgate.net/publication/228818328_OCV_Hysteresis_in_Li-Ion_Batteries_including_Two-Phase_Transition_Materials. (visited: 11.11.2022).

[35] Noshin Omar; Peter Van den Bossche; Thierry Coosemans and Joeri Van Mierlo (2013). *Peukert Revisited—Critical Appraisal and Need for Modification for Lithium-Ion Batteries*. URL: https://www.mdpi.com/1996-1073/6/11/5625. (visited: 18.10.2022).

[36] Fabian Calero; Claudio A. Cañizares and Kankar Bhattacharya (2020). *Dynamic Modeling of Battery Energy Storage and Applications in Transmission Systems*. URL: https://ieeexplore.ieee.org/stamp/stamp.jsp?tp=&arnumber=9166575. (visited: 6.10.2022).

[37] S. Chowdhury; S. P. Chowdhury and P. Crossley (2009). *Microgrids and Active Distribution Networks*. URL: http://www.farzadrazavi.com/files/Courses/microgrid/902/bookiee.pdf. (visited: 12.09.2022).

[38] Dennis Doerffel and Suleiman Abu Sharkh (2006). *A critical review of using the Peukert equation for determining the remaining capacity of lead-acid and lithium-ion batteries*. URL: https://www.sciencedirect.com/science/article/pii/S0378775305007093. (visited: 2.10.2022).

[39] Yang Chen Yan; Ma Peng Duan and Hong Chen (2018). *Estimation of State of Charge for Lithium-ion Battery Considering Effect of Aging and Temperature*. URL: https://ieeexplore.ieee.org/stamp/stamp.jsp?tp=&arnumber=8483968. (visited: 7.09.2022).

[40] Kelvin Frank and Reza Qasemi (2020). *Thermal Management of Lithium-Ion Battery Pack*. URL: https://www.diva-portal.org/smash/get/diva2:1520751/FULLTEXT01.pdf. (visited: 17.10.2022).

[41] Thomas Bowen; Ilya Chernyakhovskiy; Kaifeng Xu; Sika Gadzanku and Kamyria Coney (2021). *Usaid grid-scale energy storage technologies primer*. URL: https://www.nrel.gov/docs/fy21osti/76097.pdf. (visited: 20.10.2022).

[42] Daehyun Kim; Keunhwi Koo; Jae Jin Jeong; Taedong Goh and Sang Woo Kim (2013). *Second-Order Discrete-Time Sliding Mode Observer for State of Charge Determination Based on a Dynamic Resistance Li-Ion Battery Model*. URL: https://www.researchgate.net/publication/276036436_Second-Order_Discrete-Time_Sliding_Mode_Observer_for_State_of_Charge_Determination_Based_on_a_Dynamic_Resistance_Li-Ion_Battery_Model. (visited: 8.09.2022).

[43] Leony Ortiz; Rogelio Orizondo; Alexander Aguila Téllez; Jorge W. González; Jorge W. González and Idi Isaac (2019). *Hybrid AC/DC microgrid test system simulation: grid-connected mode*. URL: https://www.researchgate.net/publication/337823736_Hybrid_ACDC_microgrid_test_system_simulation_grid-connected_mode. (visited: 20.10.2022).

[44] A.E.W.H. Kahlane; L. Hassaine and M. Kherchi (2014). *LCL filter design for photovoltaic grid connected systems*. URL: https://www.cder.dz/download/sienr2014_31.pdf. (visited: 12.12.2022).

[45] Hioki. *What is open-circuit voltage (OCV) testing of lithium-ion batteries?* URL: https://www.hioki.com/in-en/industries-solutions/manufacturing/liion-ocv-test.html. (visited: 12.11.2022).

[46] Christiana Honsberg and Stuart Bowden (2019). *Batteries: Nernst Equation*. URL: https://www.pveducation.org/pvcdrom/battery-basics/nernst-equation. (visited: 1.12.2022).

[47] Wei Du; Yuan Liu; Francis K. Tuffner; Renke Huang and Zhenyu Huang (2021). *Model Specification of Droop-Controlled, Grid-Forming Inverters*. URL: https://www.wecc.org/Administrative/Model%5C%20Specification%5C%20of%5C%20Droop-Controlled,%5C%20Grid-Forming%5C%20Inverters_PNNL.pdf. (visited: 7.12.2022).

[48] IEEE. *1375-1998 - IEEE Guide for the Protection of Stationary Battery Systems*. URL: https://ieeexplore.ieee.org/stamp/stamp.jsp?arnumber=705934. (visited: 10.09.2022).

[49] Chao Li; Bowen Liu; Ningyi Jiang and Yi Ding (2022). *Elucidating the charge-transfer and Li-ion-migration mechanisms in commercial lithium-ion batteries with advanced electron microscopy*. URL: https://www.sciopen.com/article/pdf/10.26599/NRE.2022.9120031.pdf. (visited: 9.12.2022).

[50] Yu Miao; Patrick Hynan; Annette von Jouanne and Alexandre Yokochi (2019). *Current Li-Ion Battery Technologies in Electric Vehicles and Opportunities for Advancements*. URL: https://doi.org/10.3390/en12061074. (visited: 1.09.2022).

[51] Christian Campestrini; Stephan Kosch and Andreas Jossen (2017). *Influence of change in open circuit voltage on the state of charge estimation with an extended Kalman filter*. URL: https://www.sciencedirect.com/science/article/abs/pii/S2352152X17300658. (visited: 22.10.2022).

[52] Andrzej Łebkowski. *Temperature, Overcharge and Short-Circuit Studies of Batteries used in Electric Vehicles (2017)*. URL: https://www.researchgate.net/publication/316171277_Temperature_Overcharge_and_Short-Circuit_Studies_of_Batteries_used_in_Electric_Vehicles. (visited: 10.09.2022).

[53] Behnam Mahamedi; Jian Guo Zhu; Mohsen Eskandari; Li Li and Ali Mehrizi-Sani. *Analysis of Fault Response of Inverter-Interfaced Distributed Generators in Sequence Networks*. URL: https://ieeexplore.ieee.org/document/8544547. (visited: 8.10.2022).

[54] M-fuse. *MF 100VDC Max*. URL: https://ep-fr.mersen.com/sites/mersen_fr/files/DS-m-fuse-MF-100VDC-EN.pdf. (visited: 28.11.2022).

[55] Behnam Mahamedi and John E. Fletcher (2020). *The Equivalent Models of Grid-Forming Inverters in the Sequence Domain for the Steady-State Analysis of Power Systems*. URL: https://ieeexplore.ieee.org/stamp/stamp.jsp?tp=&arnumber=8966488. (visited: 24.09.2022).

[56] Gavin D. Peckham and Ian J. McNaugh (2011). *The Variation of Electrochemical Cell Potentials with Temperature*. URL: https://pubs.acs.org/doi/pdf/10.1021/ed100966r5. (visited: 15.12.2022).

[57] King Fahd University of Petroleum and Minerals (2018). *Impedance Data for Single-Phase Transformers*. URL: https://www.coursehero.com/file/p4cd8fs2/Impedance-Data-for-Single-Phase-Transformers-Suggested-Normal-Range-Impedance/. (visited: 15.12.2022).

[58] Ahmad P.; Shriram S. and Gi-Heon K. (2013). *Addressing the Impact of Temperature Extremes on Large Format Li-Ion Batteries for Vehicle Applications*. URL: https://www.nrel.gov/docs/fy13osti/58145.pdf. (visited: 30.09.2022).

[59] Daniel J. Noelle; Meng Wang; Anh V. Le; Yang Shi and Yu Qiao (2018). *Internal resistance and polarization dynamics of lithium-ion batteries upon internal shorting*. URL: https://www.sciencedirect.com/science/article/pii/S0306261917318093. (visited: 3.11.2022).

[60] SMA. *Short-Circuit Currents Information on short-circuit currents in SMA PV inverters*. URL: https://files.sma.de/downloads/Iscpv-TI-en-21.pdf. (visited: 23.09.2022).

[61] SMA. *Sunny boy US / Sunny tripower US / Sunnu highpower US Efficiency and Derating*. URL: https://files.sma.de/downloads/WKG-Derating-US-TI-en-19.pdf. (visited: 18.10.2022).

[62] SMA. *Sunny island 4.4M / 6.0H / 8.0H*. URL: https://files.sma.de/downloads/SI44M-80H-13-DS-en-30.pdf. (visited: 11.11.2022).

[63] A.G. Stefanopoulou and Y. Kim (2015). *System-level management of rechargeable lithium-ion batteries*. URL: https://www.sciencedirect.com/topics/engineering/coulomb-counting. (visited: 28.10.2022).

[64] Working Group C32 of the System Protection Subcommittee (2020). *Protection Challenges and Practices for Interconnecting Inverter Based Resources to Utility Transmission Systems*. URL: https://www.pacw.org/protection-challenges-and-practices-for-interconnecting-inverter-based-resources-to-utility-transmission-systems. (visited: 20.09.2022).

[65] Kotub Uddin; Alessandro Picarelli; Christopher Lyness; Nigel Taylor and James Marco (2014). *An Acausal Li-Ion Battery Pack Model for Automotive Applications*. URL: https://www.researchgate.net/publication/273226470_An_Acausal_Li-Ion_Battery_Pack_Model_for_Automotive_Applications. (visited: 15.10.2022).

[66] Ana-Irina Stroe; Jinhao Meng; Daniel-Ioan Stroe; Maciej Swierczynski; Remus Teodorescu and Søren Knudsen Kær. *Influence of Battery Parametric Uncertainties on the State-of-Charge Estimation of Lithium Titanate Oxide-Based Batteries*. URL: https://www.researchgate.net/publication/324117029_Influence_of_Battery_Parametric_Uncertainties_on_the_State-of-Charge_Estimation_of_Lithium_Titanate_Oxide-Based_Batteries. (visited: 22.10.2022).

[67] Tesvolt. *Key facts: High performance without compromise*. URL: https://www.perma-batteries.com/product/batteries-tesvolt-ts/. (visited: 9.12.2022).

[68] Tesvolt. *TS 48 V lithium storage system.* URL: https://www.tesvolt.com/en/products/a-series/ts-48-v.html. (visited: 8.12.2022).

[69] Nicola Campagna; Vincenzo Castiglia; Rosario Miceli; Rosa Anna Mastromauro; Ciro Spataro; Marco Trapanese and Fabio Viola (2020). *Battery Models for Battery Powered Applications: A Comparative Study.* URL: https://www.researchgate.net/publication/343515320_Battery_Models_for_Battery_Powered_Applications_A_Comparative_Study. (visited: 15.10.2022).

[70] Olivier Tremblay and Louis-A. Dessaint (2009). *Experimental Validation of a Battery Dynamic Model for EV Applications.* URL: https://www.mdpi.com/2032-6653/3/2/289. (visited: 9.10.2022).

[71] Tukes. *Technical Requirements for Electrical Installations.* URL: https://tukes.fi/en/electricity/electrical-works-and-contracting/technical-requirements-for-electrical-installations. (visited: 29.08.2022).

[72] Tsuyoshi Sasaki; Yoshio Ukyo and Petr Novák. *Memory effect in a lithium-ion battery.* URL: https://pubmed.ncbi.nlm.nih.gov/23584142/. (visited: 4.11.2022).

[73] F. Baronti; N. Femia; R. Saletti; C. Visone and W. Zamboni (2014). *Hysteresis Modeling in Li-Ion Batteries.* URL: https://www.semanticscholar.org/paper/Hysteresis-Modeling-in-Li-Ion-Batteries-Baronti-Femia/409e34db18e9ee0613db40ff7178bac451537d71. (visited: 11.11.2022).

[74] Paridhi Wadhwani and Vrushal Vara (2021). *How to Calculate State of Charge(SOC)? Battery and Energy Technologies.* URL: https://www.bacancytechnology.com/blog/state-of-charge-calculation-for-battery-energy. (visited: 7.11.2022).

[75] Quan-Qing Yu; Rui Xiong; Le-Yi Wang and Cheng Lin (2018). *A Comparative Study on Open Circuit Voltage Models for Lithium-ion Batteries.* URL: https://cjme.springeropen.com/articles/10.1186/s10033-018-0268-8. (visited: 22.10.2022).

[76] Ruifeng Zhang; Bizhong Xia; Baohua Li; Yongzhi Lai; Weiwei Zheng; Huawen Wang; Wei Wang and Mingwang Wang (2018). *Study on the Characteristics of a High Capacity Nickel Manganese Cobalt Oxide (NMC) Lithium-Ion Battery—An Experimental Investigation.* URL: https://www.mdpi.com/1996-1073/11/9/2275. (visited: 9.11.2022).

[77] Carola Schultz; Sven Vedder; Martin Wintera and Sascha Nowaka (2016). *Investigation of the decomposition of organic solvent-based lithium ion battery electrolytes with liquid chromatography-mass spectrometry.* URL: https://www.spectroscopyeurope.com/system/files/pdf/LIB-28_5.pdf. (visited: 1.11.2022).

[78] Yi Xie and Fei Feng (2018). *A novel resistance-based thermal model for lithium-ion batteries.* URL: https://www.researchgate.net/publication/327075034_A_novel_resistance-based_thermal_model_for_lithium-ion_batteries. (visited: 8.09.2022).

[79] Dai Haifeng; Wei Xuezhe and Sun Zechang (2009). *A New SOH Prediction Concept for the Power Lithium-ion Battery Used on HEVs.* URL: https://ieeexplore.ieee.org/stamp/stamp.jsp?arnumber=5289654. (visited: 7.09.2022).

[80] Taeyoung Han; Bahram Khalighi; Erik C. Yen and Shailendra Kaushik (2018). *Li-Ion Battery Pack Thermal Management: Liquid Versus Air Cooling.* URL: https://www.researchgate.net/publication/327959636_Li-ion_Battery_Pack_Thermal_Management_Liquid_vs_Air_Cooling. (visited: 13.10.2022).

[81] Lihua Liu; Jianguo Zhu and Linfeng Zheng (2020). *An Effective Method for Estimating State of Charge of Lithium-Ion Batteries Based on an Electrochemical Model and Nernst Equation*. URL: https://ieeexplore.ieee.org/stamp/stamp.jsp?tp=&arnumber=9266035. (visited: 15.12.2022).

[82] Reinhold Koch; Robert Kuhn; Ilya Zilberman and Andreas Jossen (2014). *Electrochemical Impedance Spectroscopy for Online Battery Monitoring - Power Electronics Control*. URL: https://ieeexplore.ieee.org/stamp/stamp.jsp?tp=&arnumber=6910907. (visited: 6.09.2022).

APPENDIX A. Curve fitting

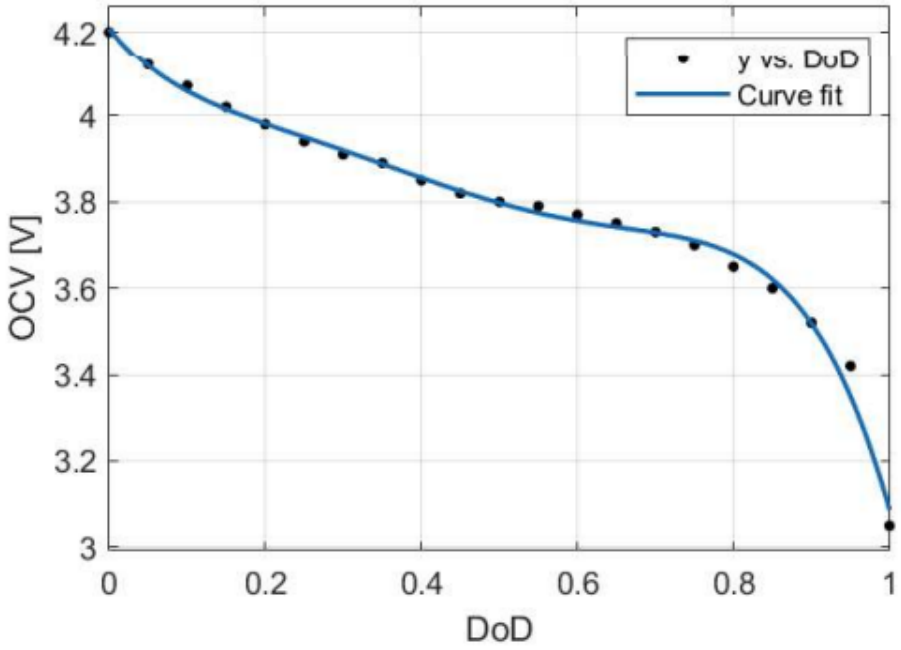

Figure 1 *OCV-DoD curve fitting of an NMC battery cell*

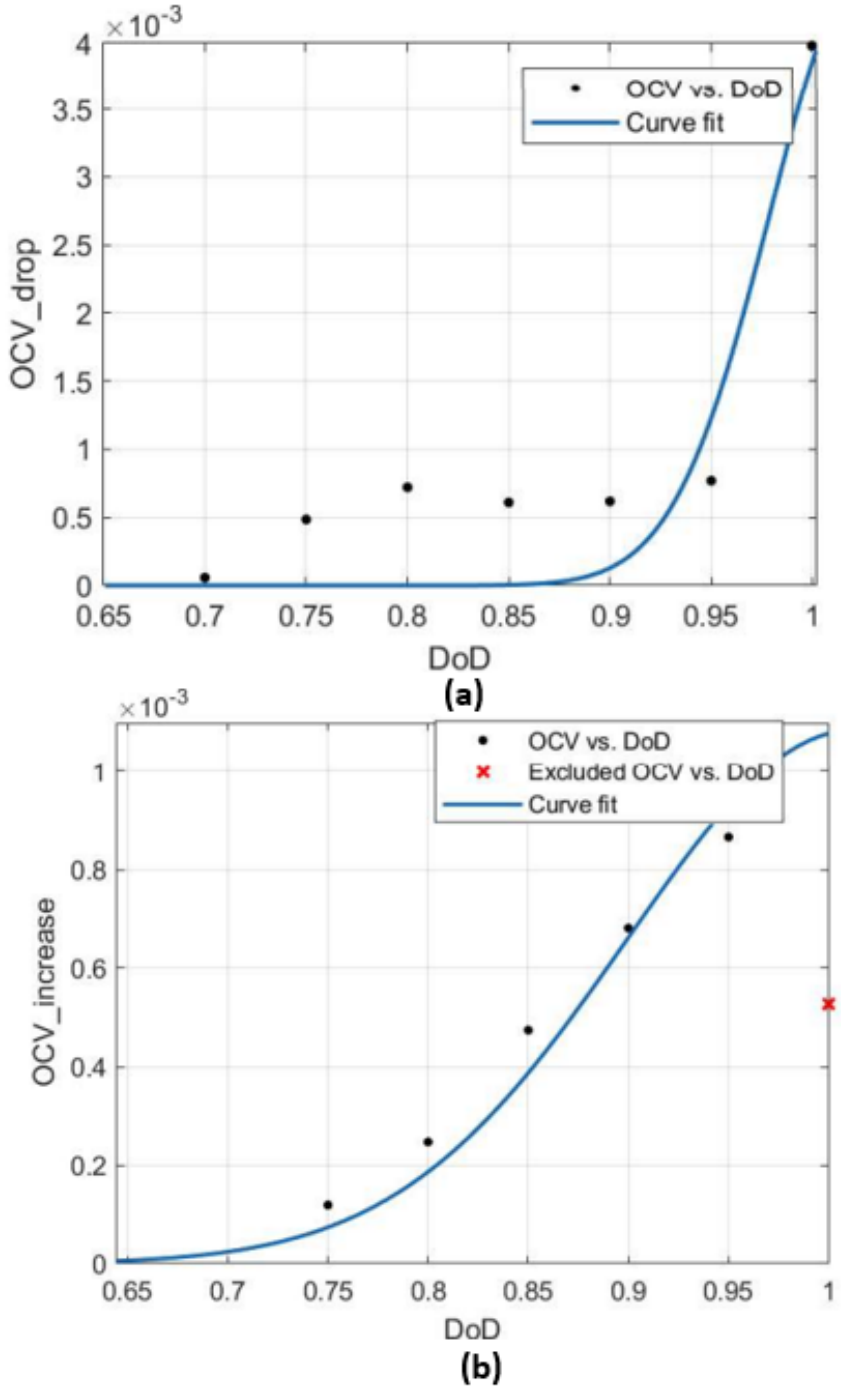

Figure 2 *Curve fitting average OCV-DoD variation relative to 298.15 K (a) Higher temperature (b) Lower temperature*

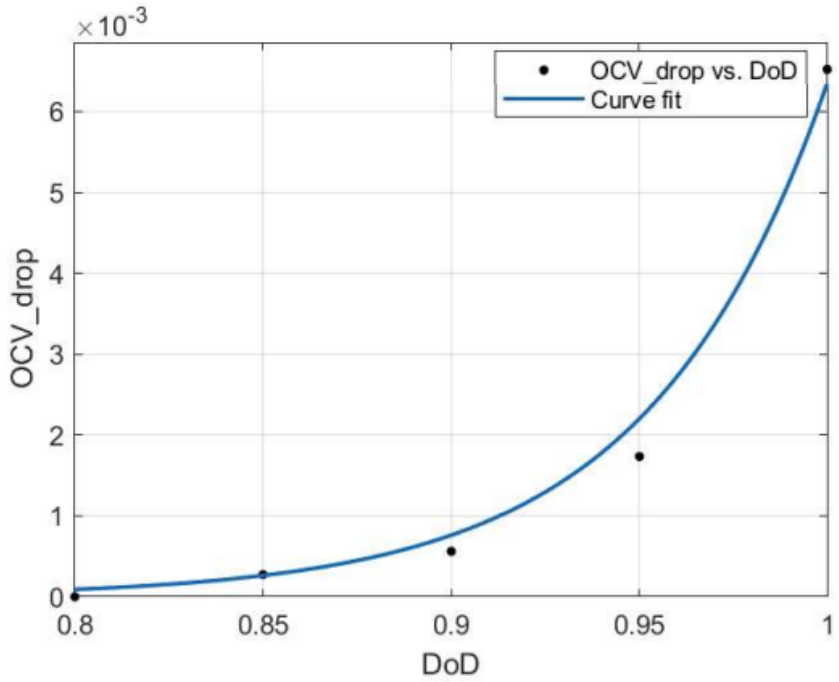

Figure 3 *OCV-DoD curve fitting of an NMC battery cell for different SoH*

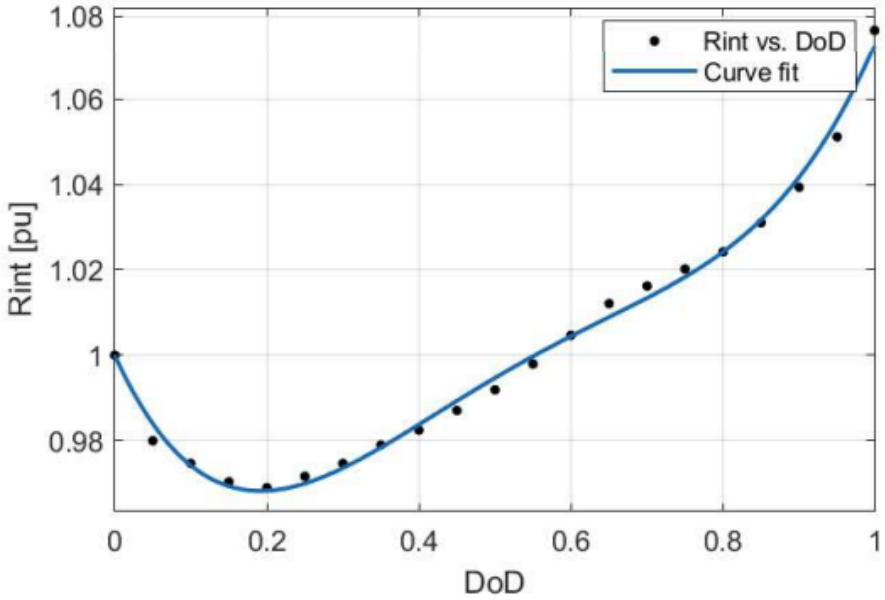

Figure 4 *Curve fitting Rint-DoD curve of a Li-ion battery*

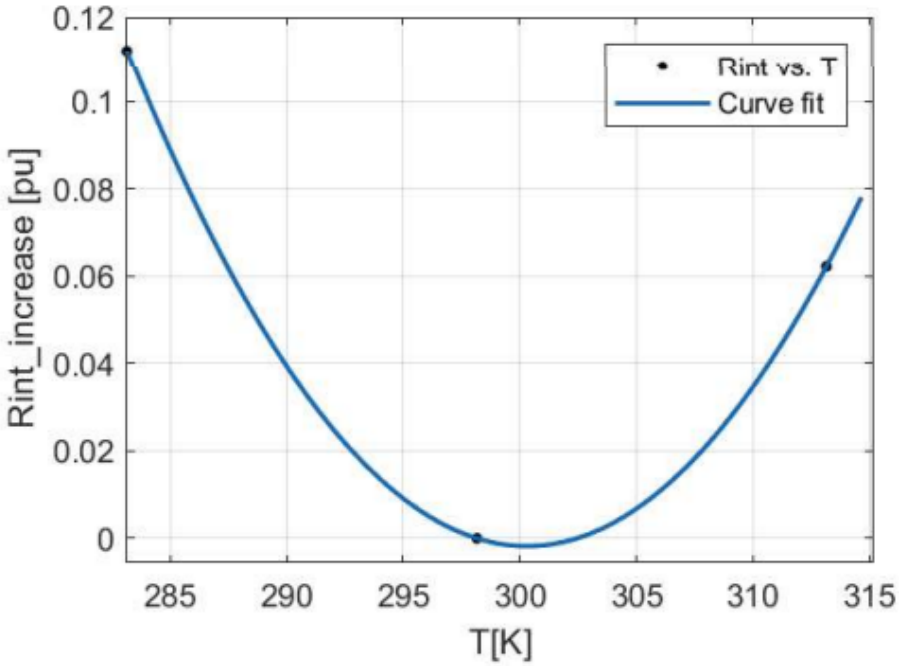

Figure 5 *Curve fitting increase in Rint as a function of the temperature of a Li-ion battery*

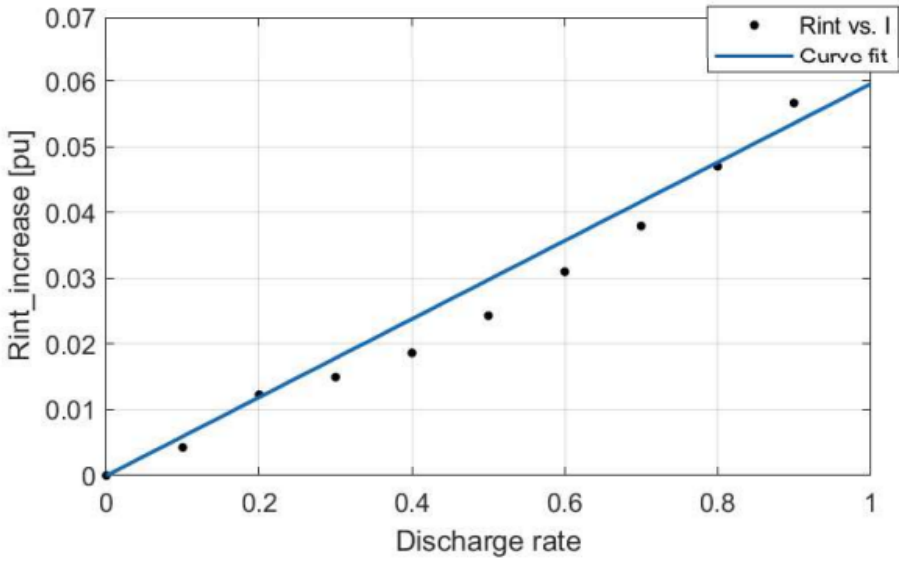

Figure 6 *Curve fitting increase in Rint as a function of discharge rate of a Li-ion battery*

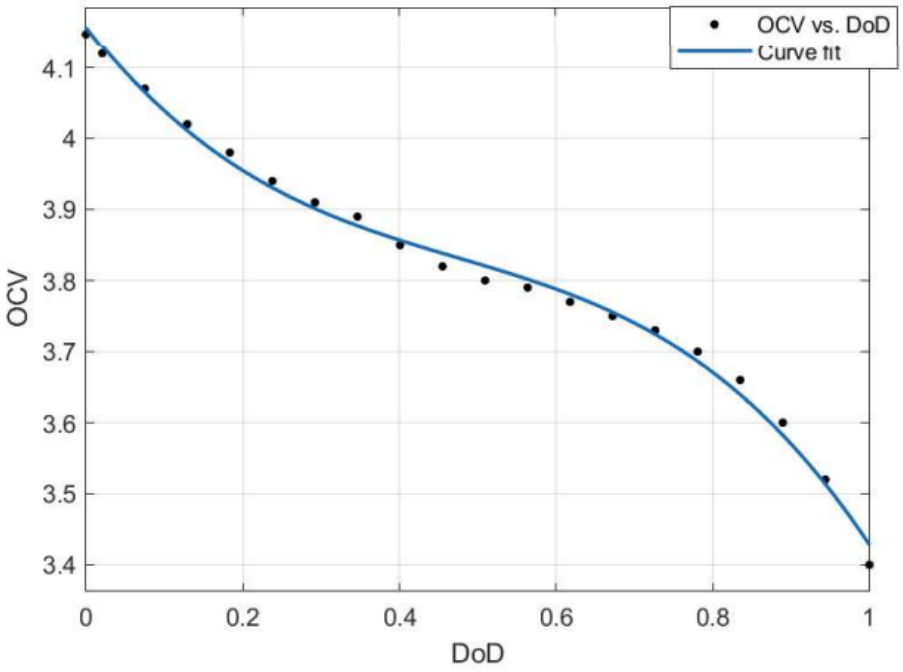

Figure 7 *OCV-DoD curve fitting of Samsung SDI NMC battery cell*

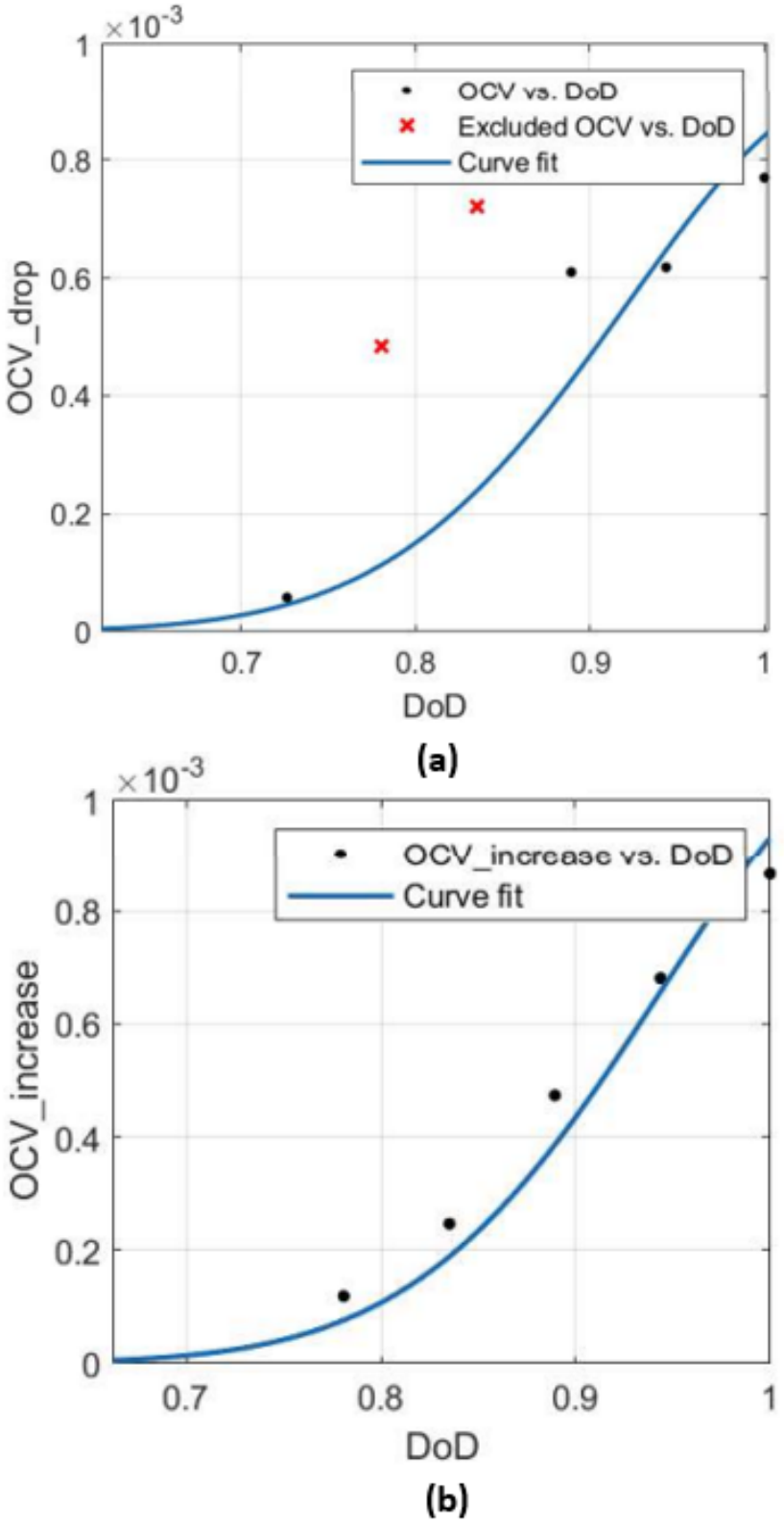

Figure 8 *OCV-DoD curve fitting of Samsung SDI NMC battery cell: temperature effect*

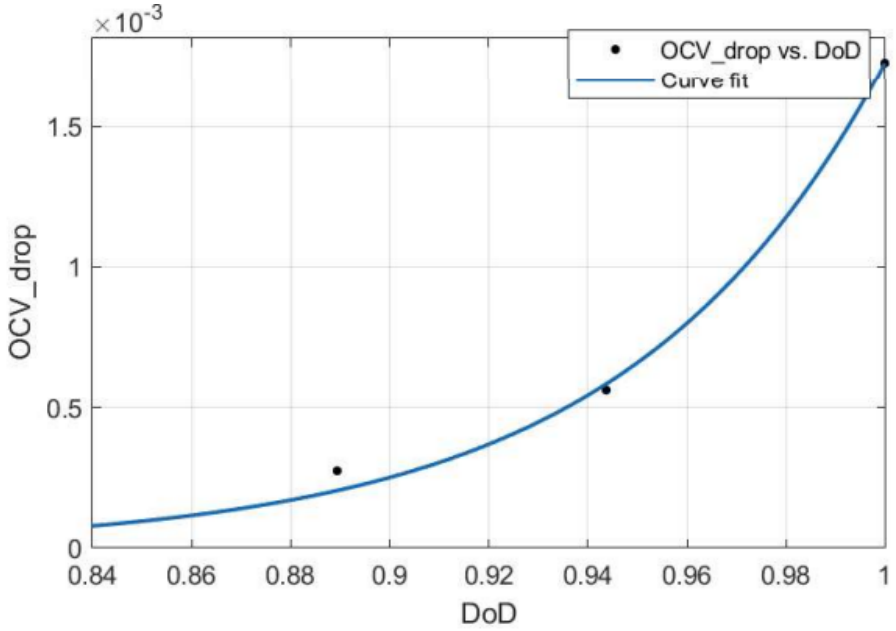

Figure 9 *OCV-DoD curve fitting of Samsung SDI NMC battery cell: SoH effect*

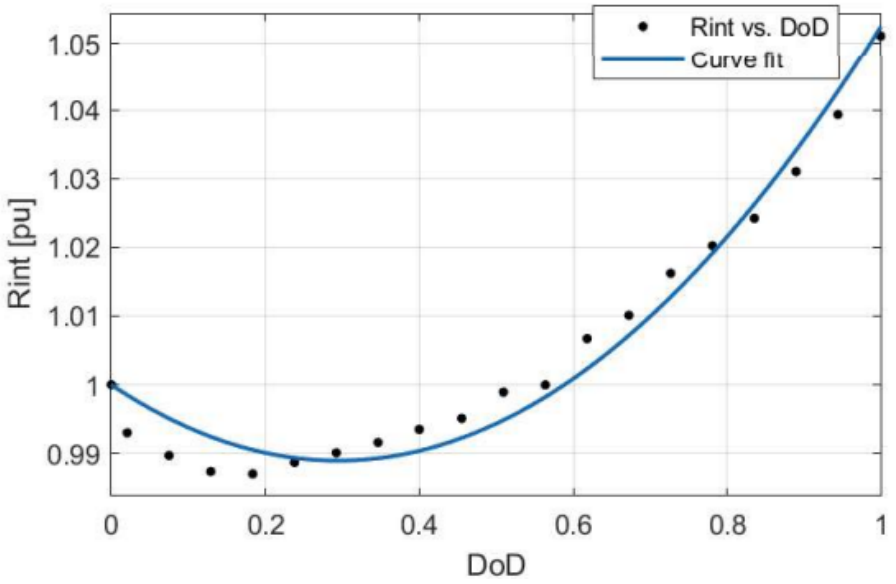

Figure 10 *Curve fitting Rint-DoD curve of Samsung SDI NMC battery cell*